OCS Study
BOEM 2020-034

Investigation of an Ancient Bald Cypress Forest in the Northern Gulf of Mexico

U.S. Department of the Interior
Bureau of Ocean Energy Management
New Orleans Office

BOEM
Bureau of Ocean Energy Management

OCS Study
BOEM 2020-034

Investigation of an Ancient Bald Cypress Forest in the Northern Gulf of Mexico

Authors

Kristine L. DeLong
Samuel J. Bentley, Sr.
Kehui Xu
Grant L. Harley
Carl Andy Reese
Jeffrey B. Obelcz
Suyapa Gonzalez
Jonathan T. Troung

Prepared under BOEM Award
M15AC00016
by
Louisiana State University
227 Howe-Russell-Kniffen Geoscience Complex
Baton Rouge, LA 70803

Published by

U.S. Department of the Interior
Bureau of Ocean Energy Management
New Orleans Office

New Orleans, LA
June 2020

DISCLAIMER

Study collaboration and funding were provided by the US Department of the Interior, Bureau of Ocean Energy Management (BOEM), Environmental Studies Program, Washington, DC, under Agreement Number M15AC00016. This report has been technically reviewed by BOEM, and it has been approved for publication. The views and conclusions contained in this document are those of the authors and should not be interpreted as representing the opinions or policies of BOEM, nor does mention of trade names or commercial products constitute endorsement or recommendation for use.

REPORT AVAILABILITY

To download a PDF file of this report, go to the US Department of the Interior, Bureau of Ocean Energy Management Data and Information Systems webpage (http://www.boem.gov/Environmental-Studies-EnvData/), click on the link for the Environmental Studies Program Information System (ESPIS) and search on 2020-034.

CITATION

DeLong KL, Bentley Sr SJ, Xu K, Harely GL, Reese CA, Obelcz J, Gonzalez S, Truong JT. 2020. Investigation of an ancient bald cypress forest in the Northern Gulf of Mexico. New Orleans (LA): US Department of the Interior, Bureau of Ocean Energy Management. 108 p. Agreement No.: M15AC00016. Report No.: 2020-034

ABOUT THE COVER

The cover photo is LeFleur's Bluff State Park in Mississippi on December 8, 2017 by Abby Braman of Peace Riverkeepers; used with permission.

Acknowledgments

Funding for this study was provided by the US Department of the Interior, Bureau of Ocean Energy Management (BOEM), Washington, DC, under Coastal Marine Institute Cooperative Agreement Number M15AC00016. We are deeply thankful to BOEM Program Officer Alicia Caporaso for her guidance, insight, and participation in this project.

This project would not be possible without our wonderful students who participated in many aspects of this project. Jeffery Obelcz, Suyapa Gonzalez, and Jonathan Truong are acknowledged for their achievements in this project as part of the research program for their degrees at Louisiana State University (LSU). We thank students Rodney Stieffel, Brianna Crenshaw, Jeff Duxbury, Haoran Liu, Patrick Robichaux, Johnny Ryu, and Robin Cobb for their help during fieldwork and Kaleb Robertson for his lab work with the seeds in the sediment cores. We thank Clay Tucker for his help with tree samples, his work on the modern flood analogs, and discussions on the bald cypress analyses.

We also like to thank the crew of the R/V *Coastal Profiler*, Captain Chris Cleaver and First Mate Charlie Sibley, as well as Bill Gibson and support staff of the Coastal Studies Institute at Louisiana State University. The LSU Museum of Natural History: Section of Fossil Protists and Invertebrates for the use of their foraminiferal collection.

This project benefited from the expertise of many colleagues on the different aspects of this project, and we thank them all. Tom Guilderson of the Center for Accelerator Mass Spectrometry, Lawrence Livermore National Laboratory for his help with radiocarbon dating analysis and interpretations. Zhixiong Shen of Coastal Carolina University for his help with OSL dating. Beth Middleton of the US Geological Survey in Lafayette, Louisiana. for her expertise with seed samples. James Flocks of the US Geological Survey in St. Petersburg, Florida is thanked for providing vintage seismic data that aided CHIRP data interpretation. We thank Mike Ewing for his help with the pollen diagram as well as for useful discussion on pollen results. We thank River Shen and Hsun Ming for their work on U-Th dating the wood samples. We thank the University of Southern Mississippi Department of Marine Science, in particular Davin Wallace, for his insights and knowledge of the study area, and David Dodd and Monty Graham for their initial geophysical survey of the site in 2012.

Last, we thank the people for whom this project would not have been possible. Ben Raines for his local expertise on the ancient tree site, for his public outreach efforts, and the “The Underwater Forest” documentary. Chas Broughton for his diving expertise and local knowledge on the site. We thank the Wallace Foundation for providing the initial seed money to start this project allowing us to conduct the first dives on the site, for the initial radiocarbon dating of the wood, and fieldwork with the R/V *Coastal Profiler*.

Contents

List of Figures

List of Tables

Abbreviations and Acronyms

Short Form	Long Form
AMS	accelerator mass spectrometry
~	approximately
BP	Before Present (defined as 1950)
BOEM	Bureau of Ocean Energy Management
cal	calendar years
^{14}C	carbon-14 (radiocarbon)
$\delta^{13}C$	carbon stable isotopic ratio
CAMS	Center for Accelerator Mass Spectrometry
cm	centimeters
CE	Common Era
DO	Dansgaard Oeschger Event
DOG	derivative of Gaussian
ºC	degrees Celsius
DEM	digital elevation model
DF	Drowned Forest
ENSO	El Niño-Southern Oscillation
g	grams
Gy	Grays Equivalent dose of radiation
Gulf	Gulf of Mexico
ha	hectare
HE	Heinrich Event
HS	Holocene sand
HISM	Holocene interbedded sand and mud
IGSN	International Geo Sample Number
ITRDB	International Tree-ring Data Bank
kHz	kiloHertz
km	kilometers
ka	kiloannus
LGM	Last Glacial Maximum
LPIMP	Late Pleistocene Interbedded Mud and Peat
LPISM	Late Pleistocene Interbedded Sand and Mud
LPP	Late Pleistocene Paleosol
LOI	loss on ignition
LSU	Louisiana State University
MIS	marine isotope stage
m	meters
masl	meters above sea level

Short Form	Long Form
mbsl	meters below sea level
µm	micrometers
mm	millmeters
MS	Mississippi
MAFLA	Mississippi-Alabama-Florida
MSCL	Multi-sensor core logger
MC-ICP-MS	Multi-Collector Inductively Coupled Plasma Mass Spectrometer
NOAA	National Oceanic and Atmospheric Administration
OSL	Optically stimulated luminescence
OCS	Outer continental shelf
PASC	Pascagoula tree-ring chronology
%	percentage
PI	Principal Investigator
ppm	parts per million
p	probability
s	second
sp.	species
spp.	multiple species
SFC	Submerged Forest tree-ring chronology
SESAR	System for Earth Sample Registration
3-D	three-dimensional
2-D	two-dimensional
U1	Unit 1
U2	Unit 2
USGS	US Geological Survey
UI	University of Idaho
USM	University of Southern Mississippi
U-Th	uranium-thorium

1 Introduction

In 2004, shortly after Hurricane Ivan had made landfall in Gulf Shores, Alabama, a fisherman found a location about 13 km offshore with abundant fish; he continued to fish at that location for the next several years. The fisherman asked a local dive shop owner to dive the site to see why so many fish were there. That diver descended to 18 m and discovered that the seafloor was covered with tree stumps rooted in their growth position (Raines 2017). Subsequently, in October 2012, an initial geophysical survey of the location was conducted by the University of Southern Mississippi (USM); it found an elongated depression in the seafloor (Figure 1). Members of this initial project dove the site in October 2013; they found several previously buried logs and tree stumps emerging from a dark peat sediment ledge and numerous fish swimming among the tree stumps. The divers counted more than 50 tree stumps, some up to 2 m in diameter, with visible buttresses and knees common to bald cypress trees (Figure 2a). The divers recovered several pieces of wood, and closer examination found the primary cellulose structure intact with no visible indications of permineralization or fossilization by replacement of cellulose with minerals, i.e., the first step in petrifying wood. The majority of the wood specimens retrieved by the divers in 2013 were identified as bald cypress (*Taxodium distichum* [L.] Rich.), which is a long-lived tree species (up to 2,624 years) (Stahle et al. 2019) that is commonly found in coastal and riparian ecosystems from Texas to Delaware.

In the marine and freshwater environments, wood rapidly decomposes due to bacteria, fungi, and wood-boring organisms; finding a grove of tree stumps offshore was unexpected. Yet the preservation of woody material is possible in anoxic sediments and waters that limit biological organisms and so reduces decomposition. Ancient wood has been found in anoxic peat bogs in freshwater environments (Ramil-Rego et al. 1998, Stoll et al. 1994, Szumigalski and Bayley 1996, Wheeler and Proctor 2000) but wood is rarely preserved in the marine environment unless it is buried (e.g., Fojutowski et al. 2014) or in anoxic waters (e.g., Brennan et al. 2011). The pieces of wood recovered from the site have good preservation and smelled like freshly cut cypress when samples were removed for dating (see Figure 2b). Wood specimens that were fully exposed on the seafloor contain more marine boring organisms than those recovered from inside the sediment ledge. Some wood pieces recovered from the sediments still had bark and beetle chambers intact, suggesting quick burial and excellent preservation (Figure 2b). Initial radiocarbon dating of wood specimens collected by divers found that the trees were radiocarbon dead, that is, more than 50,000 years old (i.e., the limit of radiocarbon dating). This suggests that these trees were alive when global sea level was lower than today, during the previous ice age 18,000 to 100,000 years ago when the northern Gulf of Mexico (Gulf) coastline was farther south than it is today (Figure 3).

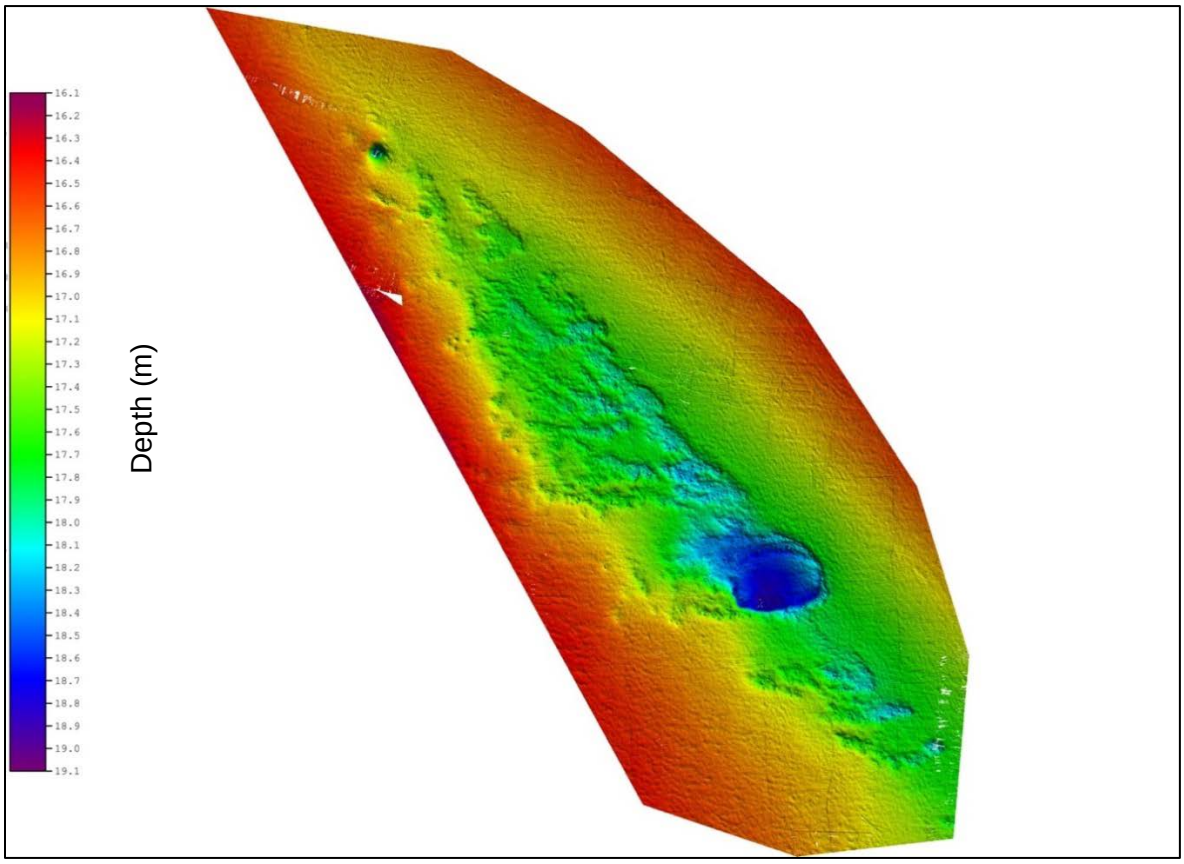

Figure 1. Preliminary multi-beam bathymetry image of the site.

Elevation scaled to 1:10.

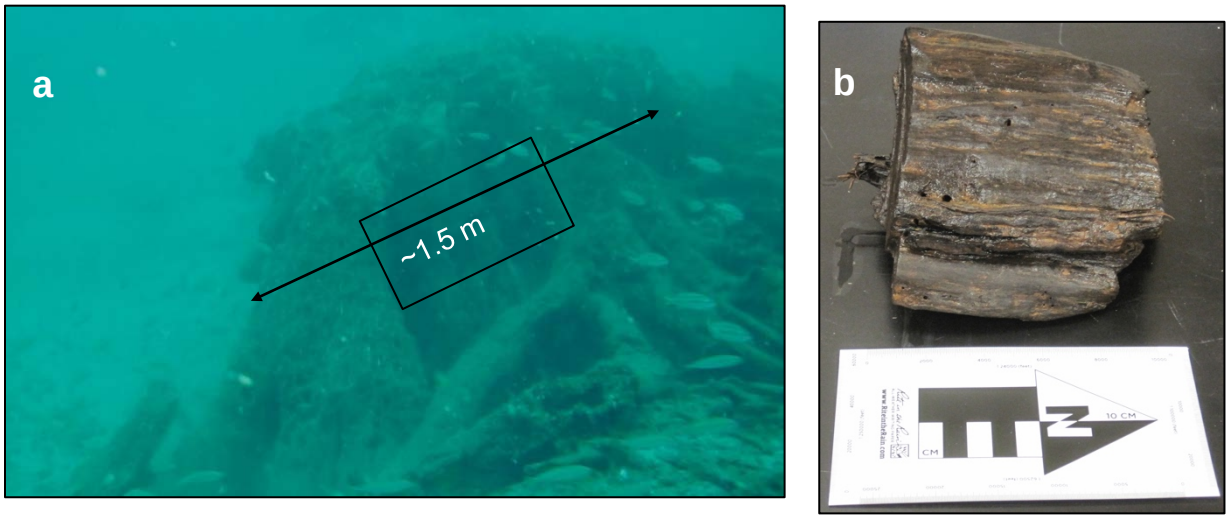

Figure 2. Underwater tree stump exposed in the study site.

(a) Underwater photograph of a bald cypress stump emerging from the sediments, taken by Ben Raines on October 2013. (b) Well-preserved wood with bark intact recovered by divers in 2013.

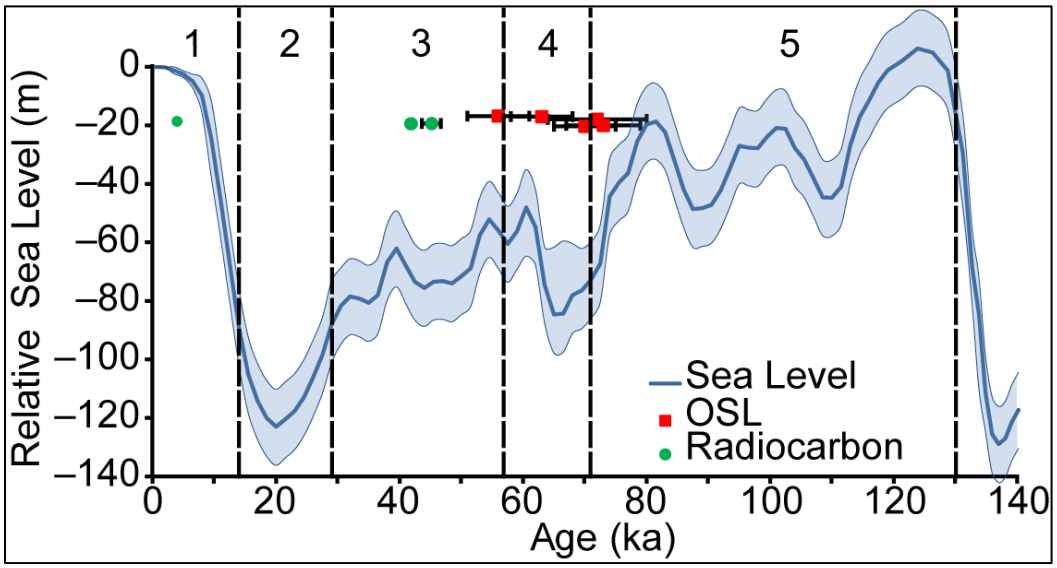

Figure 3. Global sea-level variations for the last glacial interval.

Relative sea-level estimates below modern sea level (0 m) shown as a blue line with shaded area for minimum and maximum global sea level (Waelbroeck et al. 2002). Green circles and red squares are ages from radiocarbon and optically stimulated luminescence (OSL) dating (1σ error bars), respectively, for this study (Tables 2–3) with respect to dating sample depth below modern sea level. Marine Isotope Stage (MIS) numbers (Lisiecki and Raymo 2005) appear along top.

Sedimentary strata exposed during long periods of lower sea level are commonly lost due to weathering and erosion. As a result, knowledge about glacial age sediments, geomorphology, climatic and environmental conditions, including sea-level fluctuations, are limited, particularly for the Gulf region because of the rarity of archives being preserved in such erosional settings. Therefore, preservation of this particular terrestrial deposit, preserved through a glacial cycle with more than 40,000 years of terrestrial erosive activity, represents a stratigraphic puzzle. Previous geological surveys of the area did not reveal any evidence of buried forests (Flocks et al. 2011), yet technological advances with geophysical data collection should provide evidence of the buried trees in the study area. Furthermore, geomorphology of the site and the sequence of events that needed to occur to preserve the wood and their coeval terrestrial sediments need to be defined and assessed. Also, this offshore forest discovery offers a unique opportunity to develop information on past environmental and climatic conditions in the Northern Gulf region during the last glacial interval.

1.1 The Location and Its History

The study site is located 13.5 km south of Gulf Shores, Alabama; the area encompasses ~30,000 m^2 of the northeastern Gulf continental shelf (Figure 4). The site is bounded to the north by the Alabama barrier islands, to the west by the St. Bernard Lobe of the Mississippi River Delta system and the Chandeleur Islands, to the east by the carbonate-ramp platform of the Florida Peninsula, and to the southeast by DeSoto Canyon. The width of the continental shelf thins from 200 km near the Chandeleur Islands to 50 km near the Florida panhandle. The shelf south of Alabama receives a modest supply of terrigenous sediment mostly from nearby Mobile Bay and coastal barrier islands and spits (Otvos 1985). The site is located in water depths between 18 and 20 m and is near the transition between Transitional-Inner Shelf and Middle Shelf (Witrock et al. 2003) within the Mississippi-Alabama-Florida (MAFLA) sand sheet province of the Northern Gulf (Doyle and Sparks 1980; Mazzullo and Peterson 1989, McBride et al. 1999). The MAFLA sand sheet was deposited over the seafloor in this area during the Holocene Epoch and exhibits a northwest-southeast shore-oblique ridge and trough morphology with relief up to 5 m (McBride et al. 1999). Below the MAFLA sand sheet is the Last Glacial Maximum (LGM) lowstand deeply incised valley carved out by the Mobile-Tensaw River system (Figure 5) (Anderson et al. 2004, Bartek et al. 2004). The Northern Gulf Coast is microtidal with frequent tropical cyclones that can shift sediments on the shelf (Teague et al. 2006, Wang et al. 2005). In 2004, Hurricane Ivan was a Category 4 hurricane in the Gulf producing extreme wave heights (largest was 27.7 m), resulting in substantial bottom scour (Teague et al. 2006; Wang et al. 2005) before making landfall in Gulf Shores (Figure 4). Because the study site was discovered soon after Ivan made landfall, it is assumed that the hurricane removed the overburden sand and exposed the Pleistocene Epoch sediments containing the stumps and wood.

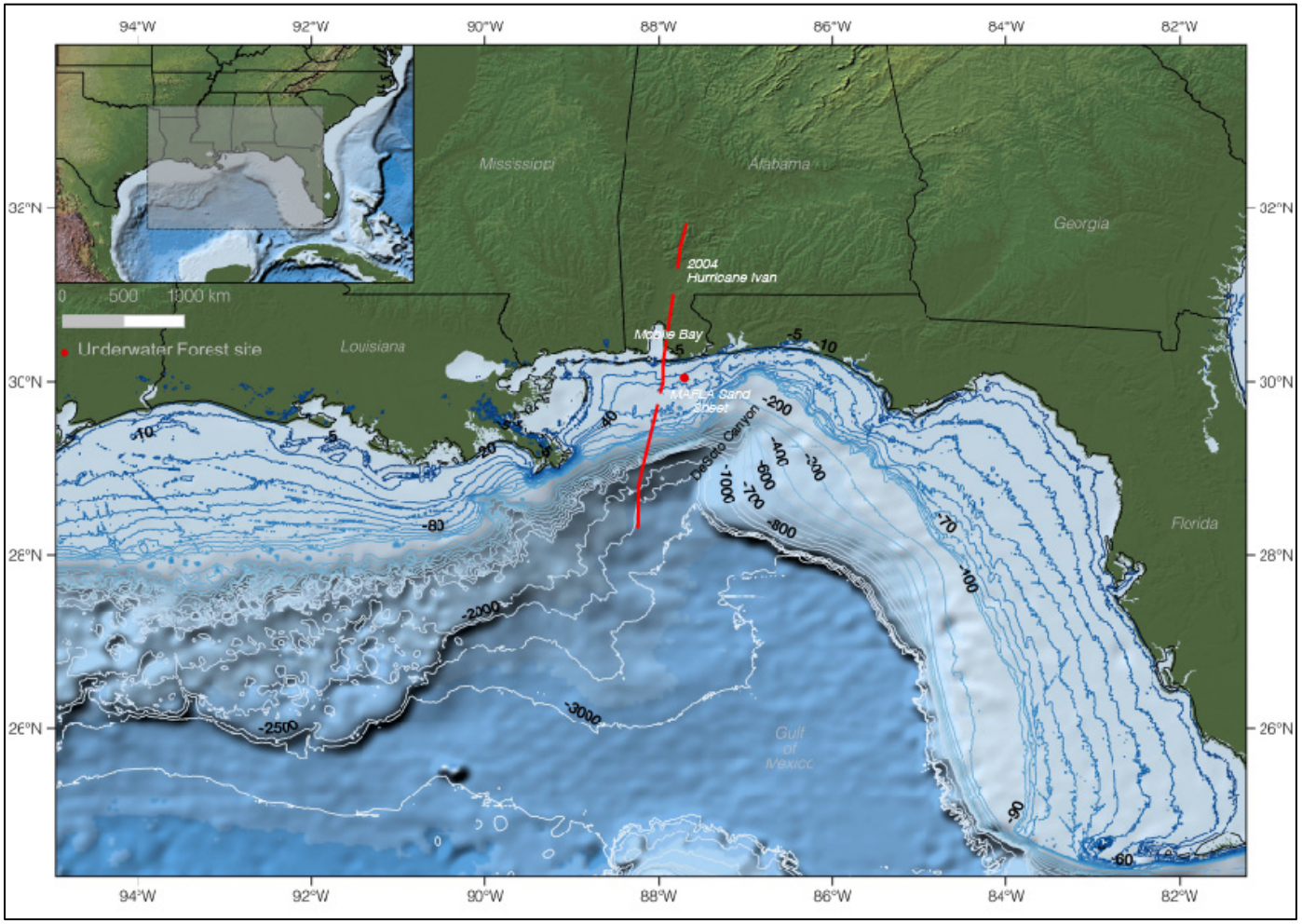

Figure 4. Northern Gulf continental shelf and study site location.

Location of the bald cypress stumps (red dot) is offshore of Alabama at ~18 m depth along the Northern Gulf of Mexico (Gulf); to protect the site, the exact location of stump exposure is not given. Bathymetric contours acquired from the Bureau of Ocean Energy Management (BOEM) with the path of Hurricane Ivan (red line) (Landsea and Franklin 2013) that passed within 10 km of the study site.

The Northern Gulf along the Alabama coast is described as a slowly subsiding, passive continental margin (Sydow and Roberts 1994). Glacio-isostatic uplift and subsidence rates are not known for the study site but are likely to be on the order of ±2 m during the last glacial interval (Blum et al. 2008). Global sea levels fell below the modern water depth of the study site during the interval from ~80 ka to 10 ka (Figure 3), which is a much higher range (>100 m) than concurrent glacio-isostatic motions (Blum et al. 2008). This time interval represents a period when it was possible for the bald cypress forest to be alive as sea levels dropped (Figure 3), exposing the continental shelf as land, which is broad in the Northern Gulf, allowing terrestrial ecosystems to become established.

During the Pleistocene Epoch, the Gulf experienced multiple global glacioeustatic cycles driven by Milankovitch orbital modulations (Hays et al. 1976, Lobo and Ridente 2014) that caused global sea levels to fall by ~120 m compared to present (Donoghue 2011; Waelbroeck et al. 2002) (Figure 3). Extensive portions of the continental shelves were subaerially exposed at various times during the Pleistocene as sea levels responded to the growth of large continental ice sheets in North America, Europe, and Asia. Along the Northern Gulf coast, the combined effects of worldwide sea-level changes and collapse of the Laurentide ice sheet forebulge resulted in a series of marine shoreline advances and retreats. Offshore of Alabama, the most prominent geological features are the paleovalleys incised by the Pascagoula (west) and Mobile (east) rivers during glacial intervals (Figure 5) (Bartek et al. 2004). These valleys were initially carved during Marine Isotope Stage (MIS) 6 or 8 and were reoccupied by their respective rivers during the LGM (MIS 2) ~21,000 years ago (Bartek et al. 2004). The study site straddles the lateral boundary between the Mobile paleovalley and its western interfluve (Figure 5). There is no surficial expression of the paleovalleys today since they were infilled during and possibly after sea level transgression with a combination of deltaic, estuarine, and marine sediments (Kindinger et al. 1994). From MIS 5 to 2, sea level fell and allowed the ancestral Mobile-Tensaw River system to further incise and shape valley complexes (Bartek et al. 2004) (Figures 3, 5). As incision occurred during falling sea levels, the interfluve vegetation established on the newly exposed continental shelf landward from the basinward-shifting shoreline. This floodplain environment and its associated peat accumulations responded directly to base level change (Anderson et al. 2016, Fisk 1960, Shen et al. 2012). Modern swamps found in the southeastern US are dominated by *T. distichum* and *Nyssa aquatica* (tupelo-gum tree), and these wetlands frequently inhabit inland freshwater floodplains behind levees of distributary systems (Middleton and McKee 2004, Reese and Liu 2001).

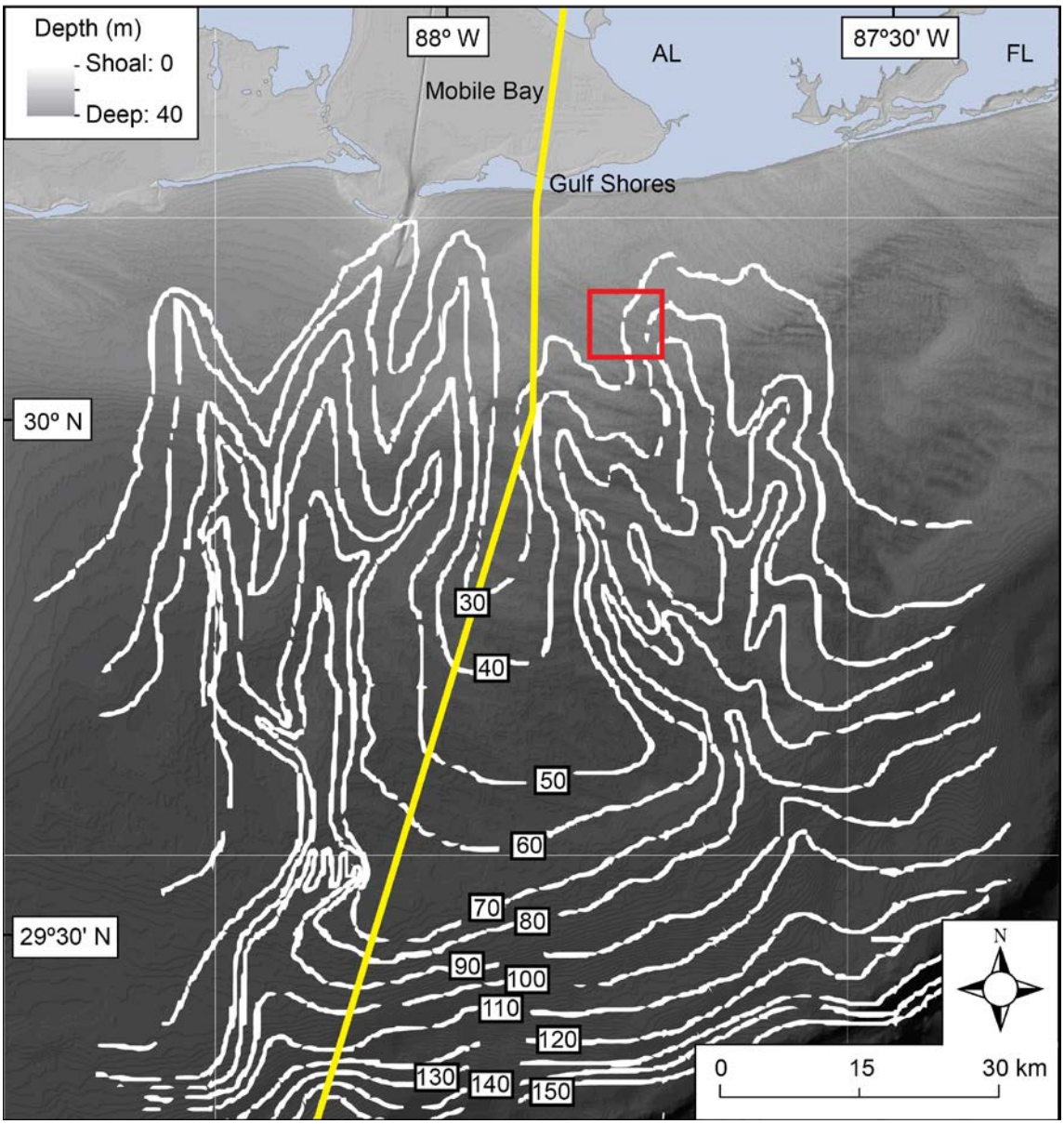

Figure 5. Map of Alabama inner continental shelf.

Bathymetry shown (shaded area) is a modern seafloor with northwest-southeast trending ridge and trough complexes. White contours are isopachs, modified from Bartek et al. (2004), showing the acoustic two-way travel time (in milliseconds) to the erosional base of the MIS 2 low stand that reveals the location of the Pascagoula and Mobile paleovalleys that crossed the shelf during the Last Glacial Maximum (LGM). Yellow line shows the path of Hurricane Ivan, which passed within 10 km west of the study site (red square).

Many Northern Gulf stratigraphic studies have focused on the Holocene evolution of Mobile Bay (e.g., Mars et al. 1992, Osterman and Smith 2012) but only a few have studied the Pleistocene-Holocene evolution of the MAFLA area (Bartek et al. 2004, McBride et al. 1999). Regional stratigraphy of the northeastern Gulf outer continental shelf (OCS) consists of Holocene sands with abundant shells, underlain by estuarine and other coastal deposits from the Holocene to Pleistocene (Bartek et al. 2004, McBride et al. 1999, McBride and Byrnes 1995, McBride et al. 1996). Those studies described seven environmental facies (sand sheet, lower shoreface, central estuary or open bay, bay beach, lower bay shoreface, and two Pleistocene soil horizons) alongside two local erosional unconformities due to bay and

shoreface ravinement. The study of McBride et al. (1999) identified four primary and eight secondary foraminiferal assemblages and interpreted environmental affiliations through multivariate analysis for the MAFLA region (see Table 1 in McBride et al. [1999]). The sand facies become finer (medium to fine) upwards in the sediments and westward across the MAFLA sand sheet (McBride et al. 1999). The Quaternary evolution of the MAFLA is largely tied to retention of sandy sediment discharged by small rivers, including the Pearl, Mobile, and Apalachicola rivers (Anderson et al. 2004). During sea-level high stands, these rivers' sediment discharge was mostly confined to bays and the inner continental shelf. During glacial intervals, the depocenters shifted seaward with falling sea levels.

Preliminary analysis of a sediment core and geophysical data collected in 2012 and 2013 shows that the local stratigraphy is consistent with previous regional shelf-stratigraphic studies, consisting of a surface layer of Holocene sands overlying Pleistocene terrestrial and coastal deposits. However, the Pleistocene-aged, wood-bearing section of the cores recovered from the ancient forest site is composed of river-derived, back swamp, and deltaic plain muds, which differ considerably in both depositional environment and degree of environmental preservation, compared to previous studies (Bartek et al. 2004, McBride et al. 1999). Previous geological surveys of the general site area did not reveal any evidence of this buried bald cypress forest or any other types of buried forest (Bartek et al. 2004, McBride et al. 1999). This study examined and reconstructed the series of events that took place to allow the preservation of this unique Pleistocene-aged deposit and remnant forest.

1.2 Biogeography of Bald Cypress

Bald cypress (*T. distichum*) is found in riverine and swamp environments in seasonally inundated floodplains of the humid subtropics in the southeastern US where there is high precipitation (Conner and Toliver 1990, Doyle et al. 2015, Kennedy 1972, Little 1971, Wilhite and Toliver 1990). Bald cypress is an indicator species for coastal wetlands and swamps. It generally grows in areas less than 50 m above sea level (Doyle et al. 2015, Little 1971) but does occur at elevations up to 120 m in Texas and the along the Mississippi River (Figure 6). Bald cypress is not found in brackish or saline waters but is able to withstand modest short pulses of saltwater, thus these trees are subject to the effects of sea-level rise and increases in coastal flooding and salinity (Conner and Toliver 1990, Hook 1984, Middleton and McKee 2004). Pond cypress (*Taxodium ascendens*) is considered a variety of *T. distichum* by some botanists; it grows at altitudes up to 30 m in still blackwater rivers, ponds, and swamps without silt-rich flood deposits (Figure 6).

Based on the preferred habitats for bald cypress (low elevation freshwater floodplains), time frames can be identified for when this forest may have been alive by examining Holocene and Pleistocene global sea-level variations (Figure 2). Glacio-isostatic subsidence and uplift rates are not known for the study site but are likely to be on the order of ±2 m during the last glacial interval (Blum et al. 2008). Global sea levels fell below the modern water depth of the study site (18 m) during the interval from ~115 ka to 82 ka, and ~80 ka to 10 ka, which has a range much greater (>100 m) than concurrent glacio-isostatic motions (Blum et al. 2008). Thus, these time intervals are possible intervals during which the glacial bald cypress forest may have been alive.

Bald cypress has been used for climate and environmental reconstructions through dendrochronology, the study of the annual growth rings in trees (Keim and Amos 2012, Stahle et al. 2012). Wood samples collected from exposed stumps by divers in 2013 have good preservation with cellular structure intact and smell like freshly cut cypress when sanded. The excellent condition of the recovered wood suggests that the forest was buried quickly and preserved in oxygen-free sediments for millennia, before the recent exhumation. These wood samples provide useful information about the climate and environment these trees lived in during the last glacial interval.

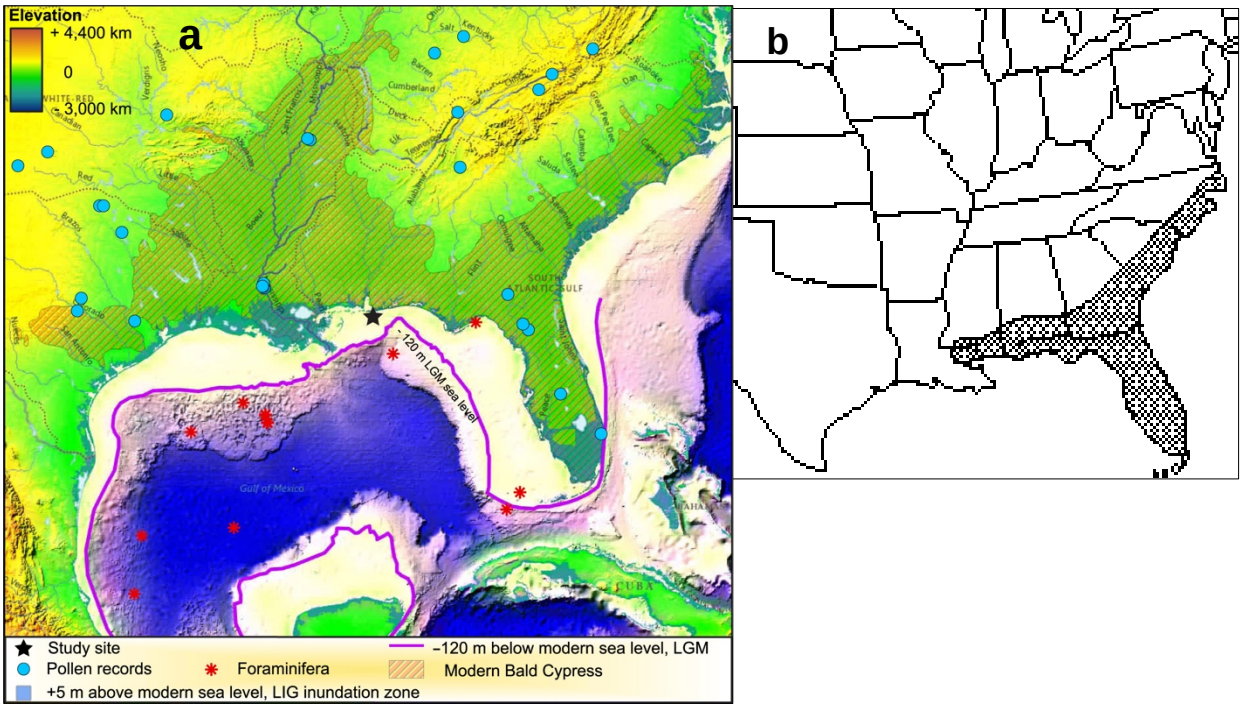

Figure 6. Biogeography of *Taxodium*

(a) Modern *T. distichum* tree distribution, modified from Doyle et al. (2015) based on Little (1971). Locations of MIS 1–5 pollen and foraminifer reconstructions from NOAA Paleoclimate and Neotoma databases noted. The study site is 13 km off the Alabama coast (black star). (b) Modern pond cypress (*T. ascendens*) distribution is 0–30 m in elevation in the southeastern range of *T. distichum* from Watson (1985) and Flora of North America Editorial Committee (1982).

1.3 An Archive of Past Environmental and Climatic Change

Trees, plants, plankton, and other organisms have specific temperatures, precipitation, and salinity requirements that are useful in biostratigraphy and paleontology, as well as for providing information about past environmental and climatic conditions. This information about the past is usually conveyed through pollen and planktonic remains because some combination of aerobic-anaerobic decomposition, early diagenesis, subaerial erosion, and sea-level transgressions generally result in the physical and chemical degradation of organic material. Pollen-based records and climate models conflict with each other with regard to the type of trees growing in the southeastern US during the last glacial interval (Webb et al. 1998). Preliminary wood, pollen, and sediment analyses of a sediment core collected at the site by divers in 2013 revealed that the site was once a wetland habitat with a vegetation community consisting of *T. distichum* and tupelo (*Nyssa aquatic*) trees, similar to current wetlands in the southeastern US.

There are few paleoclimatic and paleoenvironmental records preceding the LGM (MIS 3–5) for the northern Gulf coastal region and the southeastern US. This limits our understanding of glacial oceanic-atmospheric interactions in this region during colder glacial conditions and how they may have shaped the past coastal environments. A climate model study of the MIS 4 found winter atmospheric circulation remained unchanged, but summers were influenced by the topography of the ice-sheets (Lofverstrom et al. 2014). Climatic shifts are known as Dansgaard-Oeschger (DO) events (Dansgaard et al. 1993); these are abrupt and repeated warming climate shifts occurring during colder glacial intervals. Some of the colder glacial intervals are associated with ice-rafted debris in the North Atlantic known as Heinrich Events (HE) (Heinrich 1988), which caused extensive amounts of freshwater to be released from the

continental ice sheets into the North Atlantic. There is limited knowledge of DO-HE events in the southeastern US and how these fluctuations influenced coastal Gulf landscapes and climate because proxy records for the recent glacial interval are rare (e.g., Donders et al. 2011, Montero-Serrano et al. 2011, Nürnberg et al. 2008, Ziegler et al. 2008).

1.4 Project Goals

In recent decades, the Bureau of Ocean Energy Management (BOEM) has devoted considerable resources to carrying out its responsibilities to protect the nation's natural, cultural, and heritage resources from bureau-permitted activities as per the National Historic Preservation Act of 1966 and the National Environmental Policy Act of 1969. However, there is a gap in understanding how the presence of preserved landscapes–such as buried wetland forests and marshlands, which contain valuable information of past ecosystems, climate, and physical geology and geography–fit within this realm and how the geological and geophysical characteristics of these formerly terrestrial habitats interplay with BOEM's OCS management needs and objectives. Information that the project gathered and refined about the geological, geophysical, ecological, and paleo-environmental characteristics of this glacial-age forest preserved on the OCS is valuable to BOEM for making responsible environmental decisions for proposed oil, gas, and other activities on the OCS (e.g., Research Planning Inc. 2004). The project's overarching goal was to document the well-preserved bald cypress forest buried in the sediments in the Northern Gulf continental shelf and to develop a model for other potential sites that could contain preserved wood on millennial and longer time scales. This study aimed to provide valuable information on Northern Gulf coastal geomorphology, sediment preservation of macro- and micro botanicals, and the glacial age environment. By placing the site within the sedimentological context of the Northern Gulf, the main goals of this study included:

(1) Determine the preservation characteristics of the site;

(2) Provide a better understanding of the depositional and geomorphic layout of the site; and

(3) Develop a model to predict other preserved paleo-forest sites in the Northern Gulf and OCS.

To address these goals and further explore this unique site, we pursued the following objectives:

Objective 1: Establish a method for identifying buried tree stumps in submerged sediments;

Objective 2: Map the exposed submerged tree site and adjacent areas;

Objective 3: Document and characterize the sediment and depositional environment encompassing the tree remains;

Objective 4: Establish a chronology for the age and formation of the site;

Objective 5: Provide information on the depositional history and geomorphology of the site;

Objective 6: Develop a model to predict other buried forest sites on the OCS;

Objective 7: Catalog and determine the potential for ecological and archaeological resource preservation at this site type; and

Objective 8: Place the submerged forest landscape in the context of the Northern Gulf shelf evolution with changes in sea level.

1.5 Study Approach

The research was conducted by an interdisciplinary team consisting of two geological oceanographers (Kehui Xu and Samuel Bentley) with expertise in geoacoustics, coastal geological oceanography, and coastal sediment dynamics, three paleoclimatologists (Kristine DeLong, Grant Harley, and Andy Reese) with expertise in the coastal Gulf region, tree-rings, and pollen used to reconstruct past vegetation and climate, and one marine archaeologist (Alicia Caporaso). The Principal Investigator (PI) team supervised graduate and undergraduate students working on different aspects of the project, including Jeffrey Obelcz, Suyapa Gonzalez, Jonathan Truong, Johnny Ryu, Clay Tucker, and Caroline Miles. The project resulted in one undergraduate honors thesis, two master's theses, and one doctoral dissertation by the students working on the project. Zhixiong Shen of Coastal Carolina University performed the OSL dating. Beth Middleton of the US Geological Survey (USGS) in Lafayette, Louisiana aided with seed samples found in the sediments. Ben Raines, a local reporter and diver with extensive knowledge on the site and has led the site conservation efforts for the past nine years, provided additional local expertise.

Previous geological surveys of the Northern Gulf of Mexico OCS did not reveal any evidence of buried forests (Flocks et al. 2011). This may have been due to the survey methods and technology used. However, technological advances with geophysical instrumentation could provide the technology needed to map the buried trees in the study area. The study of Plets et al. (2009) used a sub-bottom profiler to successfully image buried wooden shipwrecks using a 1.5 to 13 kHz linearly swept acoustic pulse, which is similar to the frequency of the Edgetech 2000 system used in this study. Field methods included conducting geophysical surveys and collecting new sediment cores from the site area. Field operations were conducted in August 2015 and July 2016. The 2015 fieldwork concentrated at the main site where trees were exposed in the depression while the 2016 fieldwork focused on the finer scale geophysical surveys at the main site and areas to the east and south of the tree exposure site. Sediment cores were collected in and adjacent to the main site area in 2015, and replicate cores for OSL dating were collected in 2016. The cores were analyzed to characterize the sediments at the site, build stratigraphic relationships with the samples dating using radiometric and OSL methods, and to understand paleoenvironmental conditions.

Laboratory methods included core logging and descriptions, organic content determinations (loss on ignition), and pollen, and microfossil analyses. Wood samples collected from the site were shared between Louisiana State University (LSU), USM, and the University of Idaho (UI) for analysis. Geophysical data collected during field operations were processed and analyzed by PIs Xu and Bentley and their students. Sediment cores were analyzed by PIs Bentley, Xu, DeLong, and Reese and their students for core logging, and analysis of sediment, pollen, seeds, and microfossils.

The project resulted in two publications submitted to peer-reviewed journals for publication. The first publication described the longest sediment core collected in 2015 that contains the wood-bearing sediments (Gonzalez et al. 2017) and the second paper described the pollen results from that core (Reese et al. 2018). A paper detailing the dendrochronology results is in preparation. A second paper combining the theses and dissertation work from the three students (Obelcz; Truong; Gonzalez) on the microfossil assemblages, the stratigraphy of cores 15DF1 and 15DF3, dating results, the sedimentological analysis of the other 17 sediment cores collected, and a hypothesis for the site's evolution is also in preparation. The results from these papers are summarized in this final report. Additional data analyses and information not included in one of the above publications are presented and discussed in this report.

1.6 Team Organization

The organization of the study team from LSU, USM, and UI consisted of the following key personnel fulfilling the listed roles:

Kristine L. DeLong, Department of Geography and Anthropology and Coastal Studies Institute, LSU. Principal investigator with expertise in the coastal Gulf paleoclimate, and lead author of the final report.

Kehui Xu, Department of Oceanography and Coastal Sciences, and Coastal Studies Institute, LSU. Co-Principal investigator leading geophysical data collection and processing, and co-author of the final report.

Samuel J. Bentley, Sr., Vice President, Office of Research and Economic Development, Department of Geology and Geophysics and Coastal Studies Institute, LSU. Co-Principal investigator leading coring, grain size analysis, core logging, and stratigraphy, and co-author of the final report.

Grant L. Harley, Department of Geography and Geology, USM, now at the UI Department of Geography. Co-Principal investigator leading dendrochronology, paleoclimate, and biogeography, and co-author of the final report.

Carl Andy Reese, Department of Geography and Geology, USM. Co-Principal investigator leading palynology, paleoclimate, and paleoenvironments, and co-author of the final report.

Jeffrey B. Obelcz, PhD student, Department of Oceanography and Coastal Sciences, advised by Xu, now at the US Naval Research Laboratory, Stennis Space Center, Mississippi. Collaborator with expertise in geophysical methods and coastal geology, and co-author of the final report.

Suyapa Gonzalez, Undergraduate and Master's degree student, Department of Geology and Geophysics, advised by Bentley. Collaborator with expertise in sediment core descriptions and coastal geology, and co-author of the final report.

Jonathan T. Truong, Master's degree student, Department of Geology and Geophysics, advised by Bentley and DeLong. Collaborator with expertise in microfossils, Petrel software, and co-author of the final report.

2. Field and Laboratory Methods

2.1 Previous Fieldwork

In November 2012, initial survey with multi-beam and side-scan sonar were arranged by Ben Raines and conducted by the University of Southern Mississippi (USM) Department of Marine Science with DeLong on board (Figure 1). That survey revealed that the site contained a 1.2 m deep depression and a 408-m-long channel. The initial side-scan sonar and multi-beam survey provided a view of the site bathymetry, but individual tree stumps were difficult to identify.

In October 2013, DeLong and Harley conducted diving operations for two days. This fieldwork was funded by a private grant from the Wallace Research Foundation. The Weeks Bay Foundation, Ben Raines, and Chas Broughton provided diver expertise at the site and additional divers to support fieldwork efforts. This fieldwork was documented by Ben Raines and appeared in his documentary "The Underwater Forest" (Raines 2017).

During the 2013 fieldwork, DeLong and Harley recovered 23 specimens of wood from the site and a push core near the ledge where the wood was exposed. That core contained grayish-brown clays with remnant wood. The sediment ledge was not consolidated and was easily eroded. The divers who found the site have reported some shifts in the ledge to the east, indicating ongoing erosion. The outlines of several bald cypress stumps were observed in the flat portion of the seafloor adjacent to the ledge and are neither exposed vertically nor resolved in the 2012 geophysical survey. These stumps are assumed to be well preserved because only the tops of the stumps are partially exposed and covered with a thin layer of sand. One tree core was recovered using an increment borer on a stump partially exposed from the sediment ledge in its original growth position. This core was bagged on the boat to prevent contamination. To ensure the acquisition of intact subfossil segments, specimens were collected that exhibited the least amount of visible degradation. Wood specimens were sent to the surface in buckets with air-lift bags, tagged with a unique identification number, submerged in deionized water to prohibit desiccation and subsequent degradation, and transported back to the laboratory at USM. Some wood specimens were cut into smaller pieces and those subsections were transported to Louisiana State University (LSU). Unburied wood recovered from the base of the hole contained numerous marine wood-boring organisms whereas buried wood extracted from the sediment ledge had little evidence of marine decomposition and wood-boring organisms. Some wood specimens recovered from the sediments still had intact bark (Figure 2b) with clear branching nodes and evidence of beetle chambers, suggesting quick burial and preservation in anoxic sediments. The large wood specimens were cut, producing the characteristic odor of fresh-cut cypress—a sensory confirmation of well-preserved and unaltered wood. The Lawrence Livermore National Laboratory Center for Accelerator Mass Spectrometer conducted radiocarbon analysis in August 2014 of 12 wood subsamples including the tree core recovered from the in situ stump.

2.2 Field Methods

The primary objective of the fieldwork was to collect geophysical data and sediment cores from the stump exposure depression and adjacent areas. All fieldwork was conducted in 2015 and 2016 from the R/V *Coastal Profiler*, owned by LSU's Coastal Studies Institute. In both years, geophysical surveys were completed on the first day, and coring operations on the second day after review of the geophysical survey's preliminary results. Ben Raines filmed the 2015 fieldwork for his documentary.

2.2.1 Geophysical Surveys

Geophysical data collected during fieldwork used an Edgetech 512i CHIRP sub-bottom sonar, side-scan sonar, and sub-bottom profiler (~0.3 m vertical resolution, 1–2 m horizontal resolution), Edgetech 4600 multibeam and side-scan sonar (~2.5 mm vertical resolution, 1 m^2 horizontal resolution with a 540-kHz transducer), Edgetech DS2000 combined CHIRP sub-bottom and side-scan unit (in 2016 only), Valeport sound velocity profiler, Hemisphere Differential GPS/SMC motion compensation system, and a Geometrics G882 magnetometer (Figure 7). The Edgetech 4600 produces high-resolution three-dimensional (3-D) maps of the seafloor while providing co-registered simultaneous side-scan (backscatter) data. The vertical sub-bottom resolution of the Edgetech DS2000 is approximately 0.1 m, more than ten times smaller than the 2-m x 1-m tree stumps. A magnetometer was used to detect any potential metal or ferrous objects in the area. Ultimately, neither the Edgetech DS2000 data nor the magnetometer data was used in this study, but a pipeline and a metal object were detected by magnetometer and side-scan sonar in the eastern survey area.

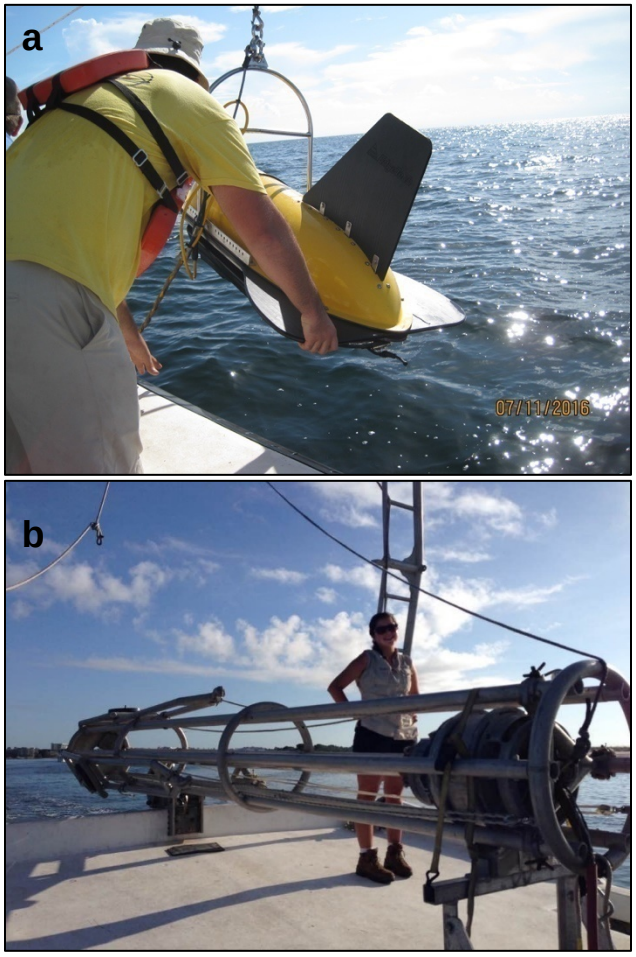

Figure 7. Fieldwork on the R/V *Coastal Profiler*.

The Edgetech DS2000 being deployed (a) and the submersible vibracorer during transit (b).

Survey line of 75 m and 100 m in strike and dip orientation, respectively, provided ~50 to 100% swath overlap of the bathymetric data. This survey methodology yielded continuously generated bathymetric digital elevation models (DEMs), backscatter maps, and a dense grid of two-dimensional (2-D) seismic reflection profiles imaging the top 10 to 20 m of the seafloor subsurface. Perpendicular survey lines

provided different approach directions, which is helpful in buried object identification. In 2016, three sites were surveyed: a return to the trough (2015 site) with tighter grid spacing for high resolution imagery, and two separate grids were surveyed to expand the surveying area further to the south and the east (Figure 8). The resurvey of the 2015 area used tighter line spacing, slower boat speed (<5 knots), and a high ping rate to maximize horizontal resolution of the trough.

Data were collected using Edgetech Discover software (side-scan and CHIRP) and Hypack Hysweep software (swath bathymetry). Surficial data (bathymetry, backscatter) were processed with Caris HIPS and SIPS version 9.0 and imported into ESRI ArcGIS® for analysis; sub-bottom data were processed using SIOSEIS version 2014.2.1 and imported into IHS Kingdom Suite and QPS Fledermaus for analysis and interpretation.

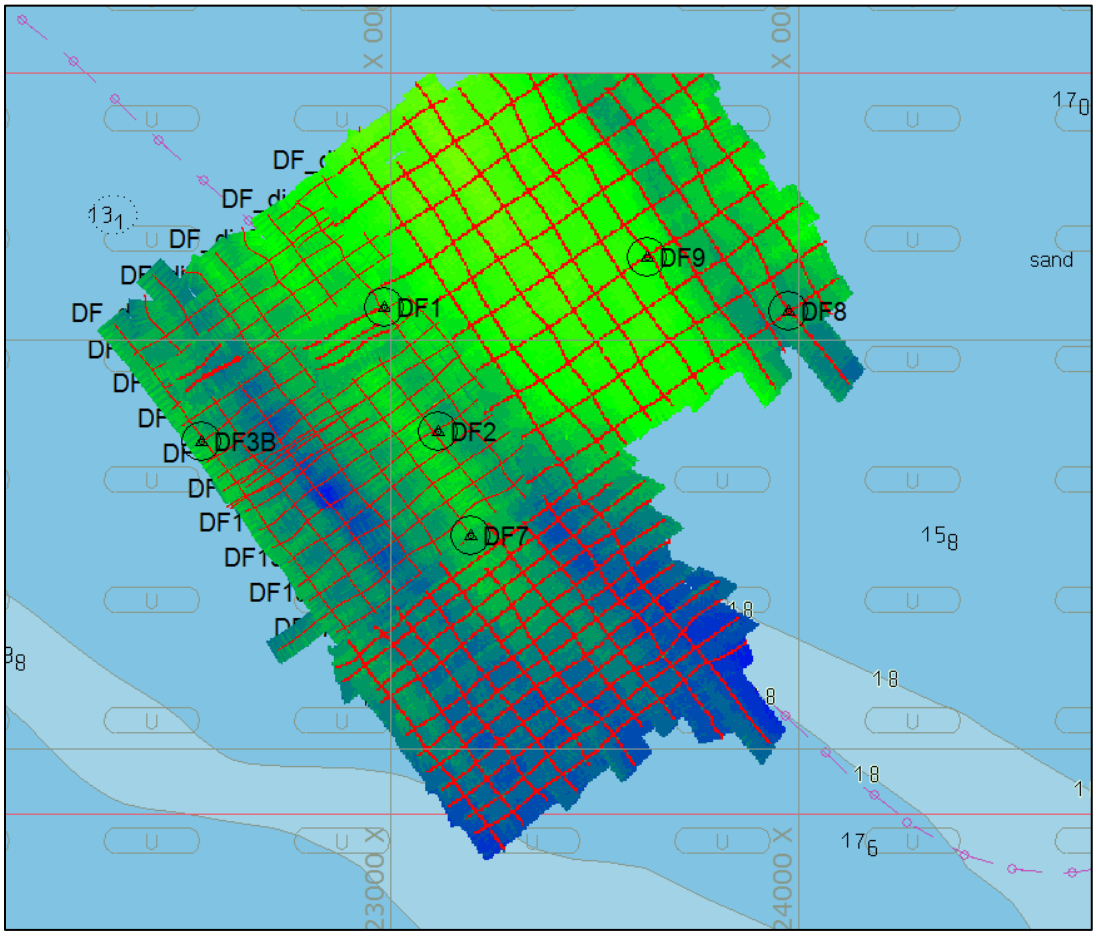

Figure 8. Field survey lines for 2016.

Red lines are actual survey lines shown on top of bathymetry and site map. Circles note locations of cores collected in 2016.

2.2.2 Vibracoring

Vibracores were collected using 6-m-long, 75-mm-diameter aluminum tubing attached to a vibrating head encapsulated within a steel tripod deployed from the R/V *Coastal Profiler* (Figure 7). The submersible vibracoring system was lowered onto the seafloor in water depths ranging from 14 m to 18 m and operated until subsurface penetration ceased. Sediment cores were collected at locations around the sediment ledge, inside the depression, and to the east and south of the ledge where modern sediments are present. Core sediment samples were collected to target specific features of interest (e.g., peat, stumps, and sediment ledge) while avoiding any identified stumps, wood, or pipelines. Locations for coring operations were determined in the field using real-time evaluation of geophysical data from the previous day and the USM multi-beam survey (Figure 1). Sediment cores were cut into up to 1.5-mm-long sections onboard, labeled, and sealed with tape for transport to LSU. In 2016, two cores were collected at each location (five locations in total), one core for the core scanner and the other core for optically stimulated luminescence (OSL) dating. All 2016 cores were wrapped in black plastic bags to limit sunlight penetration, which could affect OSL dating. Sediment trapped in core catchers was stored in Whirl Pak bags and retained for botanical and microfossil analysis. Field notes recorded core location, core length, and field observation of core sediments. Cores were transported back to LSU in the vertical position to preserve core integrity. All cores were registered in System for Earth Sample Registration (SESAR) and given an International Geo Sample Number (IGSN) (Table 1).

Table 1. Core Summary

Core ID [1]	Alternate core ID	Year collected	IGSN [2]	Depth (mbsl) [3]	Length (m)	Dating	# of sections
16DF1B	16DF-1-b	2016	IEADF161B	15.3	0.925		1
16DF1C	16DF-1-c	2016	IEADF161C	15.3	1.71		1
16DF1D	16DF1-d	2016	IEADF161D	15.3	3.97		4
16DF3A	16DF-3-a	2016	IEADF163A	16.8	2.32	OSL	2
16DF3B	16DF-3-b	2016	IEADF163B	16.8	1.03		1
16DF7A	DF-7-a	2016	IEADF167A	15.7	4.69	OSL	3
16DF7B	DF-7-b	2016	IEADF167B	15.7	4.78	OSL	4
16DF8A	DF-8-a	2016	IEADF168A	16.2	0.87	OSL	1
16DF8B	DF-8-b	2016	IEADF168B	16.2	0.75		1
16DF9A	DF-9-a	2016	IEADF169A	14.4	2.73	OSL	2
16DF9B	DF-9-b	2016	IEADF169B	14.4	2.39		2
15DF1	DF-1	2015	IEADF151A	15.3	4.90	^{14}C	4
15DF2	DF-2	2015	IEADF152A	15.8	3.30		3
15DF3A	DF-3-a	2015	IEADF153A	15.8	1.41		1
15DF3B	DF-3-b	2015	IEADF153B	15.8	4.53	^{14}C	4
15DF4	DF-4	2015	IEADF154A	16.3	1.99		2
15DF5	DF-5	2015	IEADF155A	17.1	1.23		1
15DF6	DF-6	2015	IEADF156A	16.7	0.94		1

[1] The first two numbers are for the year collected, DF is for drowned forest[1], and the number after DF is the core number in the order collected. Additional cores at the approximate same station have a letter following the core number.

[2] IGSN is International GeoSample Numbers cataloged in the SESAR (http://www.geosamples.org/).

[3] mbsl is meters below sea level.

Note: latitude and longitude for each core are not given to protect the site.

[1] "Drowned Forest" was the term used to describe the project site during the fieldwork.

2.3 Laboratory Methods

2.3.1 Geophysical Data Processing

Raw bathymetric and side-scan data were imported into Caris HIPS and SIPS, and SonarWiz software, respectively. Bathymetric data were cleaned for spurious pings, corrected for motion and sound velocity variations, and referenced to mean sea level of the closest National Oceanic and Atmospheric Administration (NOAA) tidal station (Dauphin Island, ID 8735180). The 2015 and 2016 point clouds were gridded into digital elevation models (DEM) at 25 m^2 resolution and merged into a single surface. The side-scan data were corrected for geometry (beam angle) and mosaicked at 0.2 m^2-resolution. Digital elevation models and side-scan mosaics were exported from processing programs as ASCII files and converted into rasters within the project Esri ArcGIS® geodatabase. Sub-bottom profiler data were converted from Edgetech JSF format to industry-standard *.sgy format, an open standard file format developed by the Society of Exploration Geophysicists for storing geophysical data. Processing, including swell filtering, water column muting, and secondary predictive deconvolution, were conducted in Sioseis software. Processed sub-bottom profiles were then loaded into IHS Kingdom Suite software for interpretation and Fledermaus software for 3-D visualization and analysis. The DEM, two seismically resolvable surfaces from 2-D sub-bottom surveys (interpreted in IHS Kingdom and exported as XYZ points), core imagery, and physical measurements were imported into Schlumberger's Petrel software. Acoustic impedance from density and p-wave velocities were used to create a time-depth relationship between core and seismic data. Interpretation of the geophysical data was aided by seismic data collected in the 1990s by the USGS for the MAFLA inner shelf region (Sanford et al. 2016).

2.3.2 Core, Sediment, and Microfossil Analyses

At LSU, the cores were stored in the refrigeration unit in the Department of Geology and Geophysics at 4ºC. The cores were logged using a Geotek Multi-Sensor Core Logger (MSCL) at LSU's Department of Geology and Geophysics for whole-core gamma density of sediments. All cores from 2015 were logged. For the 2016 cores, one of the cores from each location were logged while the other 2016 cores were retained for OSL dating. Next, cores were split in half longitudinally, and each section was placed inside plastic tubes for storage and further analyses. One half of each core was retained as an archive in the refrigeration unit in LSU Department of Geology and Geophysics. High-resolution images for each archive half was generated using the Geotek MSCL-XZ digital imaging system. The cores used for OSL dating were logged, scanned, and analyzed after OSL dating was complete if enough of the core remained.

Samples for grain size and organic analyses were collected at intervals of 20 mm for all cores. Granulometric analyses were conducted using a Beckman Coulter LS 13-320 Laser Diffraction Particle Analyzer, using methods specified in Hülse and Bentley (2012). Subsamples were wet-sieved at 850 μm to remove large particles, mostly shell debris that was not re-incorporated into size distribution, deflocculated in a 0.05% sodium metaphosphate solution to which 30% H_2O_2 was added to remove organic particulates and then samples were further diluted with sodium metaphosphate for analysis. Organic content was determined using loss on ignition (LOI) analysis using the methods of Heiri et al. (2001). Subsamples for core 15DF1were collected every 50 mm (Gonzalez 2017), later reduced to 20-mm intervals, for the remaining cores and 15DF1.

The micropaleontological analysis consisted of 28 samples from core 15DF1 (Figure 9) and three samples from cores 15DF3B, 16DF7B, and 16DF9B. Core 15DF1 is the longest of the cores and was collected approximately 420 m to the north-east of the trough with the exposed tree stumps on a slight ridge that is elevated roughly 3 m from the trough. A coarse sampling scheme was utilized through the Holocene sand facies in the upper part of core 15DF1. Samples from the transitional interbedded sand and mud facies were originally sampled at 100-mm intervals and then resampled at 50-mm intervals due to lithological

variability. A 100-mm sampling scheme was employed through the forest-swamp facies for freshwater or terrestrial microfossils. Standard micropaleontological processing techniques outlined in Scott et al. (2001) were followed. Approximately 15000 mm^3 of sediment was collected for each sampling interval. Sediment was wet sieved with deionized water over 1 mm, 125 μm, and 63 μm sieves. The residue was transferred to a drying plate and left to dry at 50ºC in a lab oven. The residue was thinly spread over a picking tray, and >300 foraminifera were picked from the 1 mm to 125 μm fraction under a binocular stereo microscope, identified, and stored on micropaleontological assemblage slides. The >1 mm fraction was screened for Soritids and Peneroplids on a presence basis only. The >125 μm fraction was used to eliminate small, hard to identify foraminifera. Foraminiferal abundance (counted foraminifera per weight of dry sediment picked) was calculated for all samples.

Samples used for micropaleontology were collected directly above and below inferred erosional surfaces in three other cores (15DF3, 16DF7B, and 16DF9B) to improve stratigraphic interpretations. The previously mentioned methods were used for processing. Residue dispersed over one picking tray was examined from each core on a presence basis only. In the context of stratigraphy, foraminifera are essential for determining the chronological development of the site. Coastal foraminifera could have only occupied the site during the late Holocene or previous highstands due to the bathymetric depth of the site (18 m) and sea-level elevations (Figure 3). This study used the framework of McBride et al. (1999), alongside other Gulf foraminifera ecology studies to interpret the results.

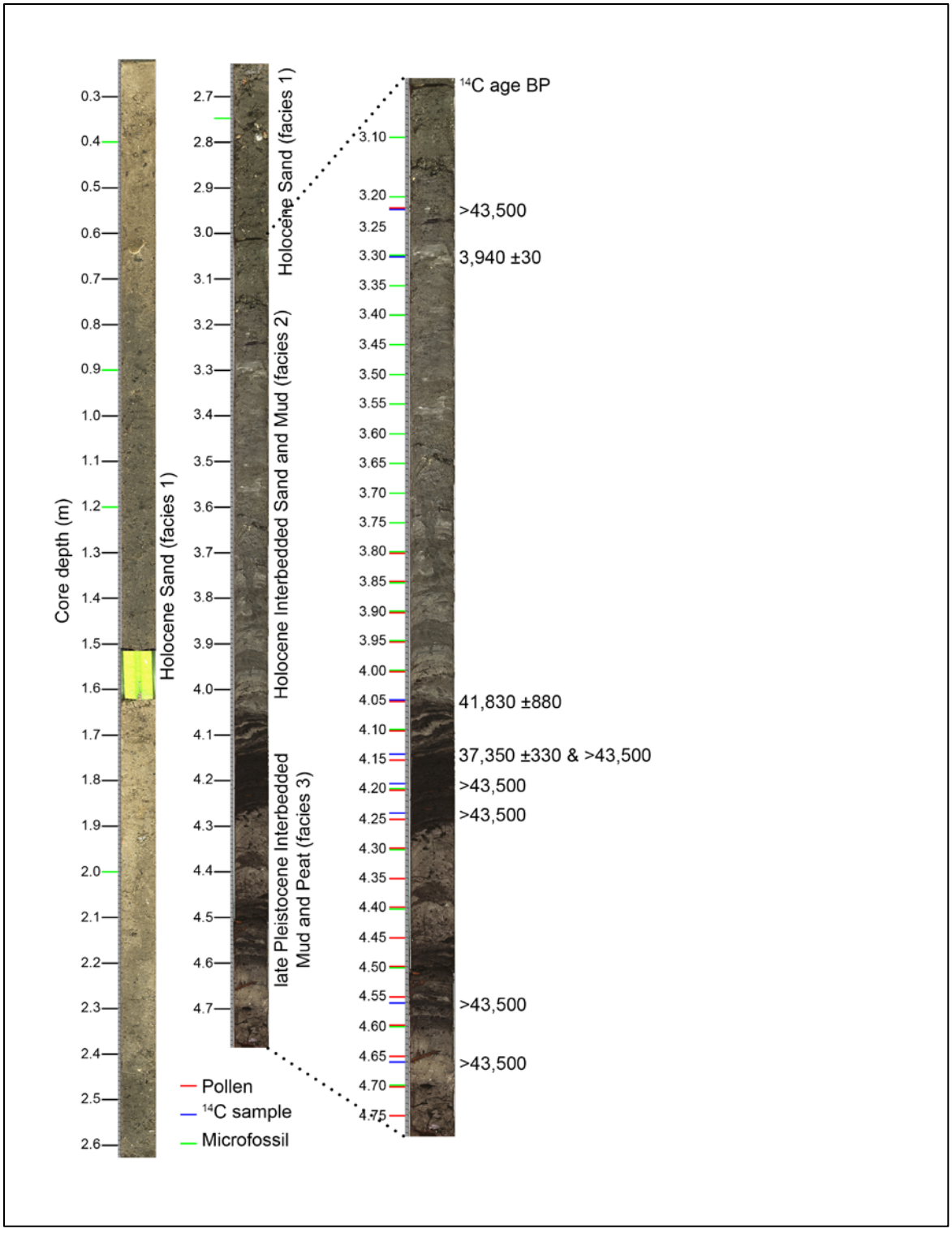

Figure 9. Micropaleontological and radiocarbon sample locations for core 15DF1.

Core images with expanded section (3.0–4.78 m) to the right. Pollen, microfossil (including seeds), and radiocarbon sampling locations are noted on the left (m) and radiocarbon ages (BP) (Table 2) are shown on the right. Seeds were also recovered from the core catcher sample from this core.

Pollen analysis focused on the lower 0.7 m of core 15DF1 where interbedded mud and terrestrial peat were found consisting of dark gray and tan brown to dark brown muds. This section had higher percentages of organic material, and lower bulk density and woody macrofossils are present. Samples were collected for pollen analysis every 50 mm in core 15DF1 (4.05–4.75 m) (Figure 9). One sample was also collected from a small disjunct layer of peat at the 3.23 m level in the core. At each sample location, 600 mm^3 of the material was extracted for pollen analysis. Before processing began, 1 Lycopodium tablet (Lund University, batch 483216, count 18,583) was added to the sample to aid in the calculation of pollen concentration (Stockmarr 1971). Standard pollen processing procedures were followed (Faegri and Iversen 1989). Each sample was subjected to HCl (removal of carbonates), KOH (deflocculates the sample and breaks down organics), HF (removal of clays), and acetolysis solution (removal of cellulose). The residue was stained with safranin, suspended in silicone oil, and mounted onto slides.

All pollen and spores were counted under a light microscope (400x magnification) until minimums of 300 were obtained (including indeterminable grains). North American pollen references (McAndrews et al. 1973, McAndrews and King 1976) were used to help with identification. Tilia software was used to calculate pollen percentages and concentrations, and to present the results graphically (Grimm 1991). The percentage of indeterminable grains was calculated as a proxy for preservation (condition). Indeterminable grains were defined as grains that were degraded, folded, compressed, or damaged to the point that identification was impossible. Samples with over 10% indeterminable grains were interpreted as having poor preservation.

2.3.3 Macro Botanical Analysis

In the laboratory, wood specimens collected by divers in 2013 were placed in a fume hood and allowed to dry slowly to reduce cracking and checking. The dried wood was sliced using a microtome to make the thin sections and to view cellular structure. Harley and paleobotanist Renee Breedlovestrout at UI identified the species of the wood collected by divers in 2013. The identification of wood in the sediment cores is saved for future analysis.

After drying, samples were mounted and sanded using progressively finer sandpaper and processed using standard dendrochronological methods (Speer 2010, Stokes and Smiley 1968). These laboratory methods ensured that all wood surfaces were prepared so that cellular features can be discerned under a light microscope. Because the exact calendar year of growth rings within the wood specimens was unknown, the innermost complete ring on each sample was assigned the relative year "1" and each subsequent 10^{th} ring was marked with an "X" under the microscope. Each sample was scanned with an EPSON Expression 10000XL scanner, and all tree-ring widths were measured to 0.001 mm accuracy using coupled WinDendro (Regents, Inc., ver. 2016c) software. The computer program COFECHA was used, which uses segmented time-series correlation techniques to assist in crossdating of undated tree-ring time series (Holmes 1983), to help match and cross date each sample relative to one other. Forty-year time segments lagged by 20 years were tested to suggest possible temporal placements of all samples and used a minimum correlation value of 0.40 (typically $p < 0.001$) as a statistical standard of convincing agreement between measured series. After considering the suggested temporal placement made by COFECHA, each series was visually compared. Internal cross-dating (or crossmatching) resulted in a set of measured series that were aligned temporally with each other "floating" in time but were not absolutely dated. The computer ARSTAN program was used to standardize each tree-ring series with a smoothing spline with a 50% frequency response cutoff equal to two-thirds the length of each series. This level of detrending preserves low-frequency variance in each series suitable for analysis of multidecadal climate trends. Interactive detrending on each measured series was used to ensure that the applied standardization spline was accurately capturing the ends of the series and not over- or under-predicting the raw values.

To understand how the trees at the offshore glacial-age site responded to the climate before becoming inundated by sea-level rise and subsequent marine burial, the floating chronology was compared with the closest tree-ring chronology within the Gulf Coast region. A *T. distichum* (TADI) collection was located from Pascagoula, Mississippi (30.58ºN, 88.02ºW) available on the International Tree-Ring Data Bank (IRTDB) (MS002 contributed by D.W. Stahle, M.D. Therrell, and M.K. Cleaveland). The Pascagoula River *T. distichum* chronology spanned 484 calendar years from 1466 to 1992 CE. To update the existing MS002 chronology, Harley and others relocated the cypress stand from which the original cores were collected and collected new increment cores in October 2015 (referred to here as PASC). Two cores were extracted from 23 *T. distichum* trees following standard dendrochronology field methods (Stokes and Smiley 1968). Telescoping ladders were used to get above the lower buttress swell of individual trees. Tree cores were prepared and cross dated using methods standard to the field of dendrochronology (Stokes and Smiley 1968).

A suite of techniques and analyses were used to compare the floating Submerged Forest tree-ring Chronology (SFC) with other bald cypress chronologies that are anchored in time. To assess the inequality in the paleo record (SFC) compared to reference chronologies, the Gini coefficient (Biondi and Qeadan 2008)—an all-lag measure of ring-width variability within each time series—was calculated using all bald cypress tree-ring chronologies within the species geographic range available on the ITRDB (n = 39, including Pascagoula River). The redfit function in dplR software package in R (Bunn 2008) was used to investigate the frequency domain and spectral aspects of the SFC and PASC. Spectral analysis was complemented with wavelet analysis using a Morlet and derivative of Gaussian (DOG) mother wavelets to examine how the modes of variability change over time within the reconstruction time series (Torrence and Compo 1998).

An examination of sediments in the core catchers by Beth Middleton of the USGS, an expert of botanicals in the Southeast US, found several well-preserved seeds. Middleton provided DeLong with seed type samples of common seeds in the Lower Mississippi Valley for seed identification. During microfossil analysis of core 15DF1, seeds and seed fragments were separated from the sediments and identified to genus and/or species level using a dissecting microscope. Seeds were saved for future analysis.

2.3.4 Dating of Sediments and Wood

Stratigraphy and radiometric dating methods were used to establish the relative age range for the site with previously buried trees. Smaller samples were cut from the larger diver-collected wood specimens for radiocarbon (^{14}C) dating at the Center for Accelerator Mass Spectrometry (CAMS) at Lawrence Livermore National Laboratory in 2013 and 2014. In 2016 and 2017, additional samples were sent to the Beta Analytic Testing Laboratory for radiocarbon dating ^{14}C dating, including eight bulk sediment samples extracted from the floodplain facies in core 15DF1 (Figure 9) and one sample from core 15DF3B. Samples were pretreated, rinsed over a 150-μm sieve and examined under a microscope to ensure the residue was woody debris. Only this woody debris was used for ^{14}C dating. No marine reservoir correction was used for woody samples because they had initially been terrestrial. In 2017, a 4.0-mg sample made up of mixed genera benthic foraminifera was collected from the deepest section of core 15DF1 (3.30 m), where there was sufficient carbonate material for ^{14}C dating (Figure 9), and sent to Beta Analytic. The date for the foraminifera was corrected for the marine reservoir effect using MARINE 13 (Reimer et al. 2013). Measured radiocarbon ages were corrected for isotope fractionation to conventional radiocarbon ages based on separate determinations or assumed values for δ^{13}C.

Because many of the ^{14}C dates were radiocarbon dead, OSL dating was used to obtain the age of the sediment in the cores. Cores collected in 2015 were analyzed using MSCL and were “reset” by the cesium-137 radiation, so OSL dating was not advised on these cores. New cores were collected in 2016, with two cores extracted from each location, one for stratigraphy and one for OSL dating, (Table 1). Zhixiong Shen, an OSL expert at Coastal Carolina University, performed OSL dating of five core sections

collected in 2016 following the method of Shen Z et al. (2012). Technology and methods have drastically improved the reliability and precision of OSL dating with reliable age measurements up to 200 ka (Murray and Wintle 2003, Rhodes 2011). To help refine the chronology of the site, all 2016 cores were examined for their potential for OSL dating. Five sections (0.2–0.43 m in length) from cores 16DF3A, 16DF9A, 16DF7B, 16DF7A, and 16DF8A were selected for OSL dating at the Luminescence Dating Laboratory at the University of Liverpool. Cores were sampled at the deepest depth identified below a prominent erosional surface in each core. Silt-sized quartz (4–15 µm) were the dominant datable particles in all OSL samples. They have been used to date coastal deposits in the northern Gulf back to ~200 ka (Shen Z et al. 2012). OSL ages were obtained for all the five samples. Sand-sized quartz (180–250 µm) extracted from the sample from core 16DF7B was also dated to corroborate the silt-sized ages. OSL measurement was done using the single-aliquot regenerative-dose protocol of Murray and Wintle (2003) with a preheat at 240ºC for 10 s, a cut-heat at 180ºC, and a blue light stimulation at 280ºC for 40 s at the end of each single-aliquot regenerative-dose run. The equivalent dose (D_e) of each aliquot was calculated using an early background subtraction method (Ballarini et al. 2007). Dose recovery tests with a given dose ranging between 100 and 200 Gy on 16 aliquots produced a recovered/given dose ratio of 1.02 ±0.06.

Natural radioactivity of all the samples was measured using a high-resolution, low background gamma spectrometer at the University of Liverpool and converted to natural dose rate using the conversion factors by Guérin et al. (2011). Water content measured in the lab for each sample, an a-value of 0.03 (Mauz et al. 2006) for silt-sized quartz, an internal dose rate of 0.03 ±0.02 Gy/ka for sand-sized quartz, and the attenuation of beta irradiation following Mejdahl (1979) were also used for natural dose rate calculation. For cosmogenic radiation calculations, it was assumed that the samples were underneath 20 m of water for 15% of their burial time and subaerially exposed for the remainder. An uncertainty of 10% is introduced to cosmogenic radiation calculations. The samples from cores 16DF3A and 16DF9A were collected from close to major lithologic boundaries, and their gamma radiation heterogeneity was accounted for following Aitken (1985).

Wood is not typically dated with uranium-thorium (U-Th) methods, but because the wood was too old to be dated using radiocarbon methods, it was decided to try U-Th dating. Previous studies have demonstrated that trees can uptake uranium (Edmands et al. 2001, Ma et al. 2000), so U-Th dating may be feasible, as demonstrated in buried wood from Hudson Bay (Allard et al. 2012) and tested in western Siberia (Maksimov et al. 2015). DeLong contacted a colleague at National Taiwan University, River Shen, an expert with U-Th dating in carbonates. DeLong's student, who worked in Shen's lab for a semester in 2015, transported wood samples from three core catchers and diver-collected wood to Taiwan for dating in September 2015. U-Th chemistry (Shen et al. 2003, Shen et al. 2008) was performed in October 2017 on a Thermo Electron Neptune multi-collector inductively coupled plasma mass spectrometer (MC-ICP-MS) (Frohlich et al. 2009, Shen et al. 2012) at the High-Precision Mass Spectrometry and Environment Change Laboratory in the Department of Geosciences, National Taiwan University. Replicate U-Th analyses were performed on all samples. The coral U-Th dating method (Shen et al. 2008) was modified for the analysis of wood samples dissolved in 5% nitric acid.

3. Results

3.1 Geophysical

Bathymetry around the exposed forest region is similar to that described in previous regional studies (Dufrene et al. 2003, McBride et al. 1999); the most prominent features are a series of northwest-southeast trending ridges and troughs with 2–5 m vertical relief and ~0.5 km wavelength (Figure 10). The tree stumps are located within and around a hole in the seafloor (~1 m relief, ~100 m long, <10º walls) nested in a trough (Figure 10). Seafloor backscatter is uniformly lower within the troughs compared to the ridges (Figure 11a) and particularly low within the hole where tree stumps are exposed. Individual tree stumps can be identified by side-scan sonar and appear to have lower reflectivity than the surrounding seafloor (Figure 11b). Buried stumps could not be confidently identified in the subsurface through CHIRP sub-bottom profiling, even with tighter line spacing (Figure 8) and slower surveying speeds (<5 knots) in the 2016 survey.

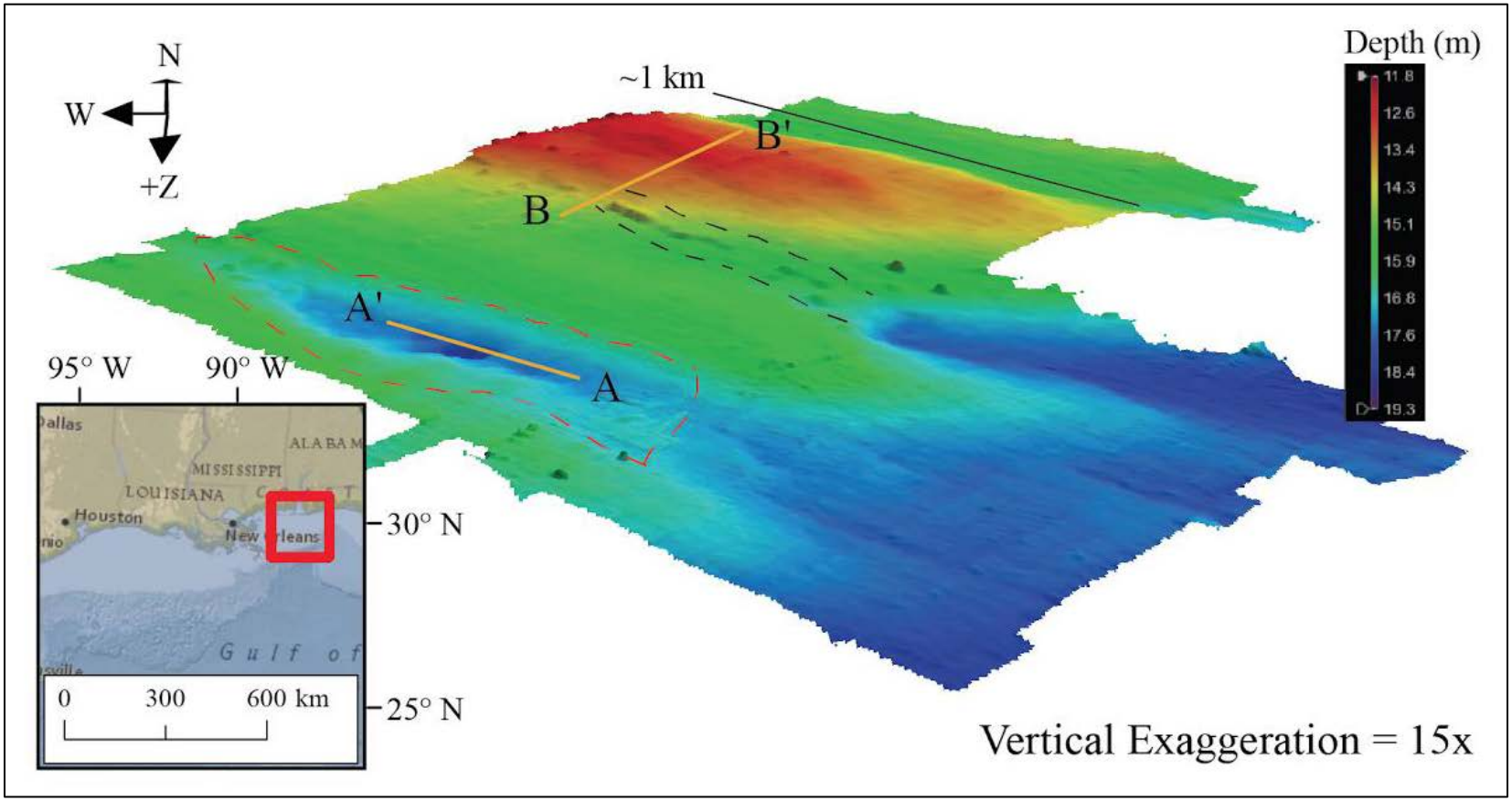

Figure 10. Three-dimensional digital elevation model of 2015 and 2016 bathymetric data.

The red dashed line outlines the depression where tree stumps are exposed. Black dashed lines bracket an artifact of merging the 2015 and 2016 data sets. Data were smoothed to a 1 m grid. A-A' is referred to in Figure 13 and B-B' in Figure 26.

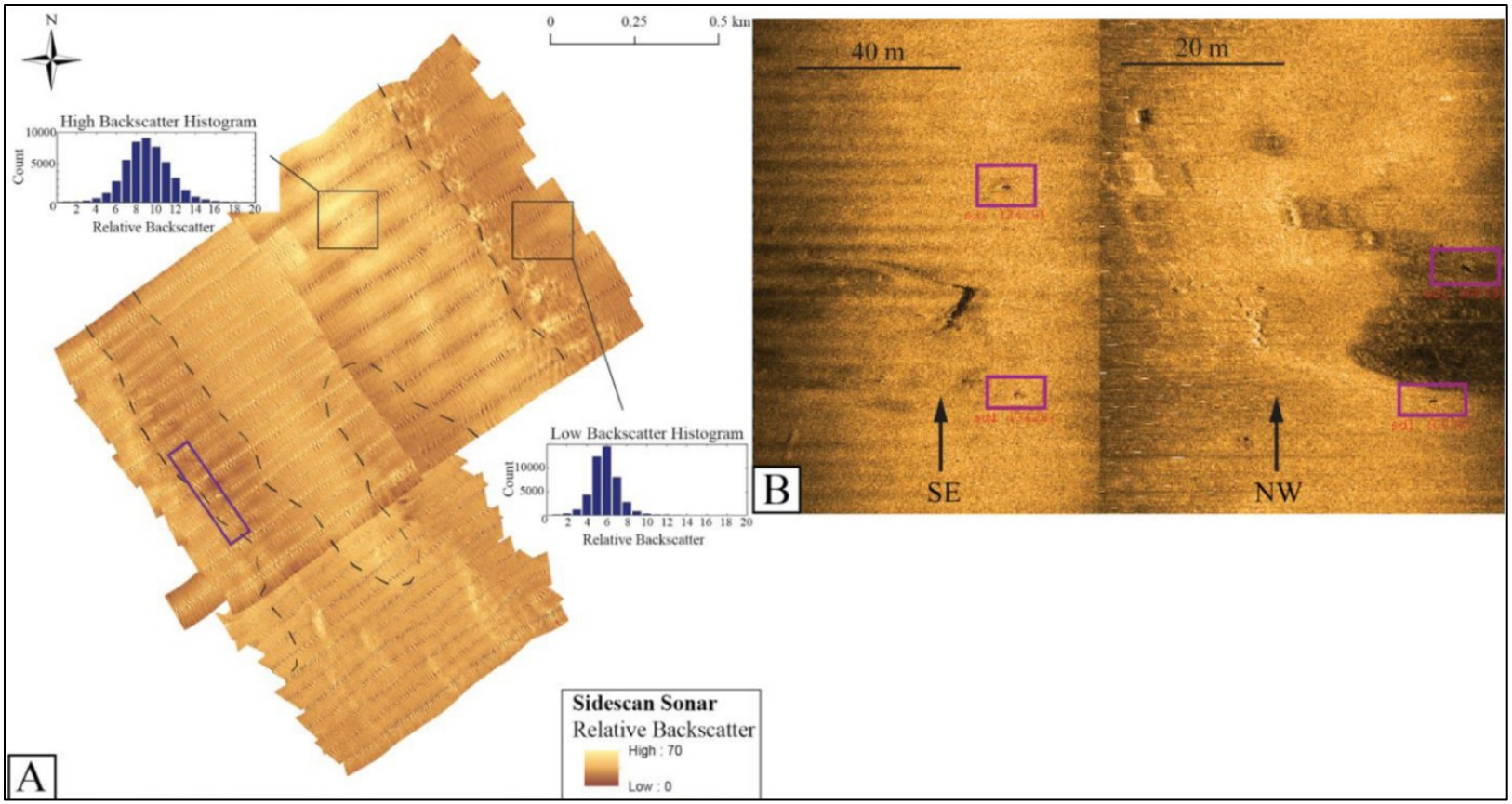

Figure 11. Side-scan sonar mosaic illustrating seafloor sediment texture variation.

(A) Light and dark colors indicate higher (coarser sediment) and lower (finer sediment) backscatter, respectively. Backscatter is lowest between ridges (dashed black lines) and particularly where trees and Pleistocene swamp sediments are exposed (purple box). (B) Side-scan sonographs of trees exposed to the seafloor (purple boxes). Left and right panels are from the same approximate area (purple box in A) but acquired on adjacent track lines.

The uppermost stratigraphic layer present across the entire survey site is a sand sheet, except where the tree stumps are exposed. Lithology indicates this layer is a predominantly well-sorted medium to fine sand and shell hash (Gonzalez et al. 2017). The sand varies in thickness between 0 and 5 m, is thickest on ridges, and thinnest or absent in troughs (Figure 12). Bathymetry and sand sheet thickness generally correlate well. This indicates that strata underneath the sand sheet are relatively flat, and sand distribution is not controlled by precedent stratigraphy.

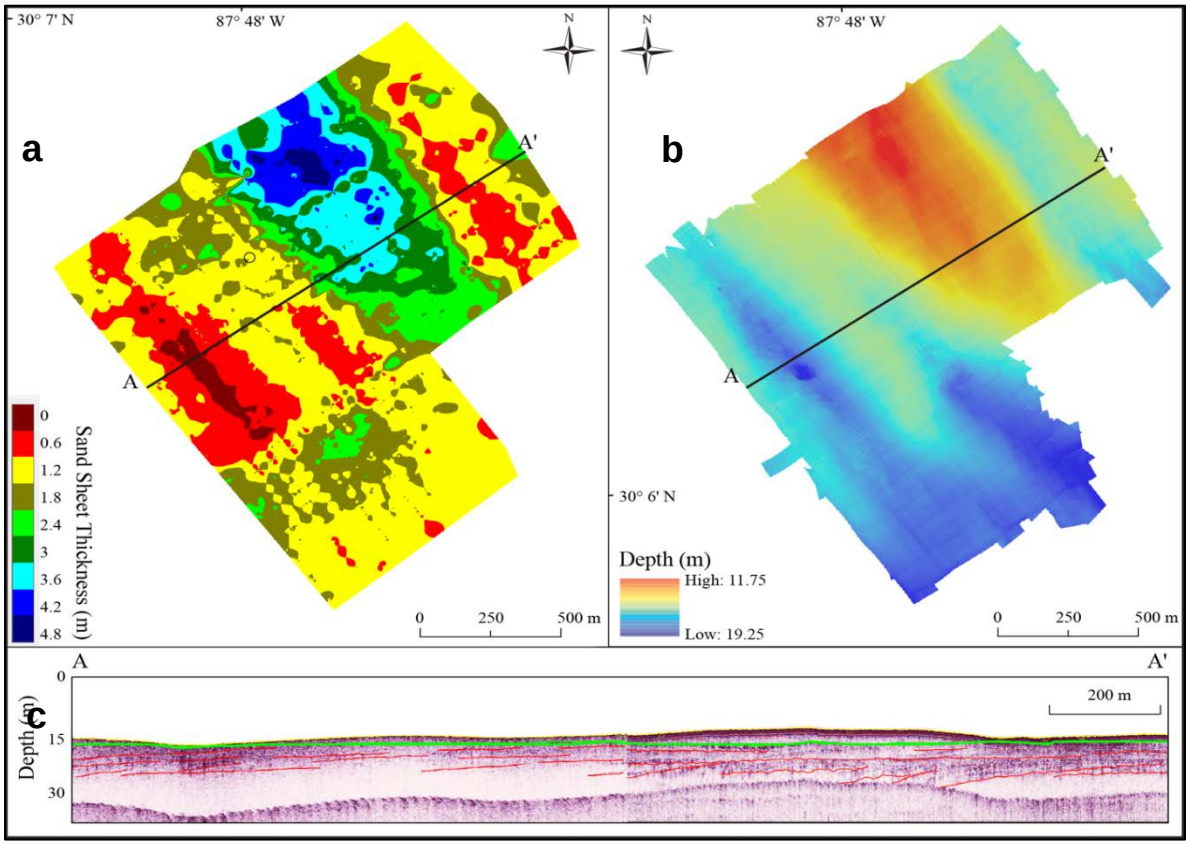

Figure 12. The thickness of Holocene sand sheet in the study area.

(a) Isopach map of sand sheet thickness derived from CHIRP seismic data. Reds indicate a relatively thin or absent layer; blues indicate thickest sand deposits. The thickness of the sand sheet scales with relief from the seafloor, where seafloor depressions have thin or absent sand cover, and seafloor ridges have thick (~5 m) deposits. (b) 2015–16 bathymetry, which demonstrates that the Holocene sand sheet is not primarily influenced by precedent stratigraphy. (c) Sub-bottom profile of transect A-A' (upper left and right); the green line indicates the base of the Holocene sand sheet; red lines indicate Pleistocene surfaces. Vertical exaggeration 10x.

The dense CHIRP sub-bottom grid can be projected into three-dimensional space and viewed as a fence diagram to aid analysis and interpretation (Figure 13). The CHIRP data, in general, provides higher vertical resolution than previous surveys but does not resolve strata >30 m below the seabed surface, likely due to the acoustically reflective surficial sand sheet (Figure 11). Based on seismic facies and stratal geometry, the subsurface is divided into two units, Unit 1 and Unit 2, from deepest to shallowest.

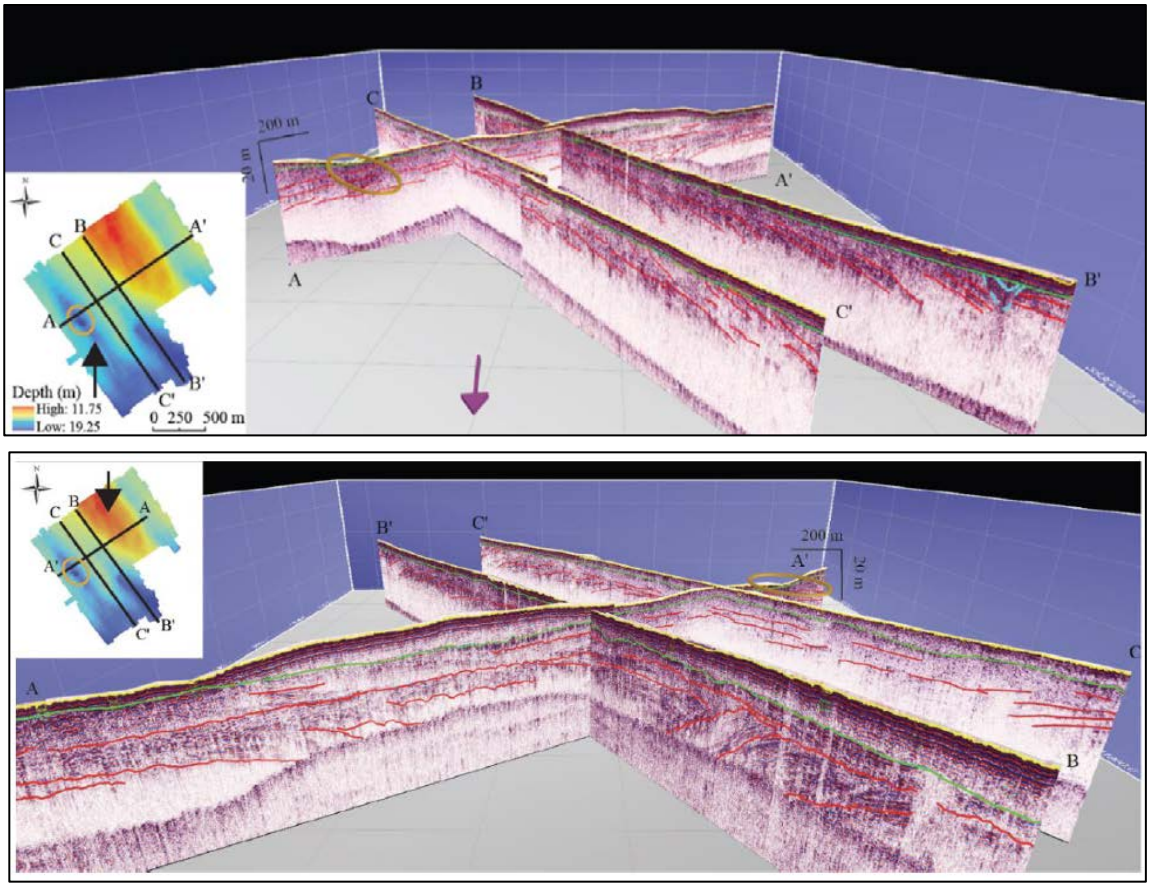

Figure 13. Three-dimensional fence diagrams of interpreted CHIRP data.

(a) Aspect is looking north, and (b) Aspect is looking south. Vertical exaggeration is ten times. The gold ellipse represents an area where tree stumps are subaqueously exposed. Annotated reflectors are water bottom (yellow), base of Holocene sand sheet (green), paleochannels (blue) and Pleistocene surfaces (red). Pleistocene strata generally dip to the south-southeast with dip angle decreasing both east-west (reflectors in the stump area are relatively flat-lying) and deep-shallow. (a) Pleistocene reflectors are incised by paleochannels and are truncated by the base of the Holocene sand sheet. (b) Steeply dipping clinoform geometry of Pleistocene reflectors in the northeast quadrant of the survey area, as compared to relatively flat-lying western reflectors in the stump area.

Unit 1 (red annotation, upper bounded by green horizon in Figure 13) extends from the deepest resolvable reflectors to 0–5 m below the seafloor, and is characterized by concordant, subparallel reflectors that dip south-southwest. The dip angle of these reflectors generally decreases from east to west (particularly flat-lying reflectors underlying the exposed trees), with deepest resolvable reflectors in the east displaying sigmoidal geometry. Localized crosscutting is apparent within Unit 1 (blue annotation in Figure 13) and regional but discontinuous unconformities truncate dipping strata from overlying flat-lying reflectors. Unit 2 (bounded below by green horizon and above by yellow horizon in Figure 13) varies in thickness between 0 and 5 m and overlies a strong and laterally continuous reflector. Unit 2 has no internal reflectors and is acoustically homogeneous.

The geophysical results (Obelcz 2017) aid in the interpretation of the core stratigraphy and define the paleo-geomorphology of the region around the exposed stumps. Figure 14 displays the CHIRP sub-bottom profile (both interpreted and uninterpreted) crossing over the trough where stumps are exposed, with the surficial sandy unit found on either side of the trough (near A–A′ in Figure 15), along with a gamma-density profile of core 15DF6 illustrating the physical properties that are related to the acoustic properties. In this profile, four seismic units are identified: (top, pink) a surficial sand sheet separated

from subjacent deposits by a reflector that occurs near the same depth as the sand-mud boundary in the density profile of core 15DF6 and is likely the Holocene ravinement surface also identified by Kindinger et al. (1994) and McBride et al. (1999); (laterally contiguous, yellow) undifferentiated deposits below the sand sheet with horizontal reflectors; (adjacent, green) more strongly reflective deposits below the trough; and (deepest, blue) deposits with steeply dipping reflectors. This deepest unit is comparable to seismic strata interpreted by Kindinger et al. (1994) to be bay-head deltas of late Pleistocene age.

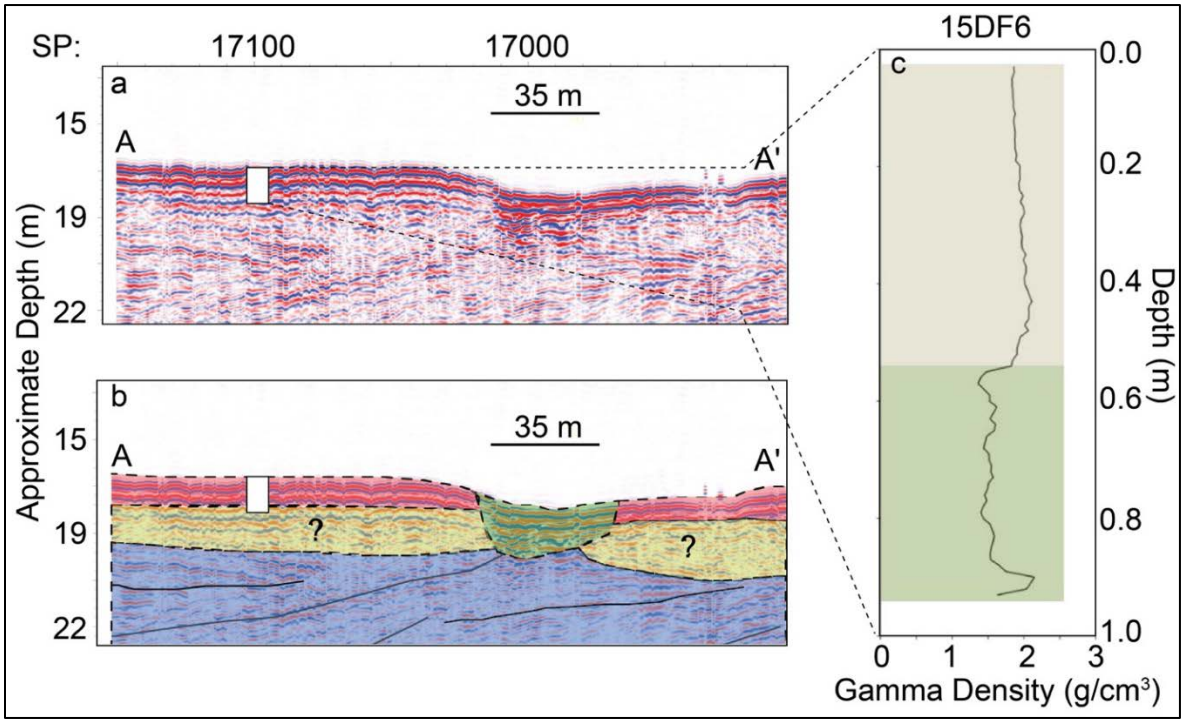

Figure 14. CHIRP sub-bottom profile along trough where wood was found.

Uninterpreted (a) and interpreted (b) CHIRP sub-bottom profile dip-oriented across the subaqueously exposed tree stumps (see Figure 10 for location of A-A′). Holocene sand (red) is thin or absent near the late Pleistocene interbedded mud and peat (green) where the stumps are located. The stump area presents as a negative amplitude anomaly, but individual trees cannot be identified likely due to being at or below the horizontal resolution threshold of the system. Below the sand sheet is undifferentiated late Pleistocene terrestrial deposits, which may include swamp, paleosol, or floodplain facies (yellow), and below that bay-head delta facies with clinoform dipping directions (solid black lines). (c) Gamma density profile of core 15DF6, which was acquired in the vicinity of the trough (see Figure 15 for core location).

3.2 Physical Properties of the Sediments

A total of 18 vibracores were collected in 2015 and 2016, spanning multiple sediment types, both inside and outside of the depression that contains exposed stumps (Figure 15 and Table 1). In August 2015, a linear total of 17.08 m of cores were collected, and on July 2016, 26.16 m were collected. Excellent preservation of organic materials was observed in the peat sections of the cores including large pieces of wood, roots, seeds, pollen, and insects. The sand and mud sections directly above the peat sections yielded marine microfossils (foraminifera) with good preservation. The Holocene sand section contained whole and shell fragments including several olive shells (*Oliva* sp.) with glossy surfaces intact. Core and sediment analysis results were reported in Gonzalez et al. (2017) for core 15DF1 and the remaining cores in Gonzalez et al. (in review).

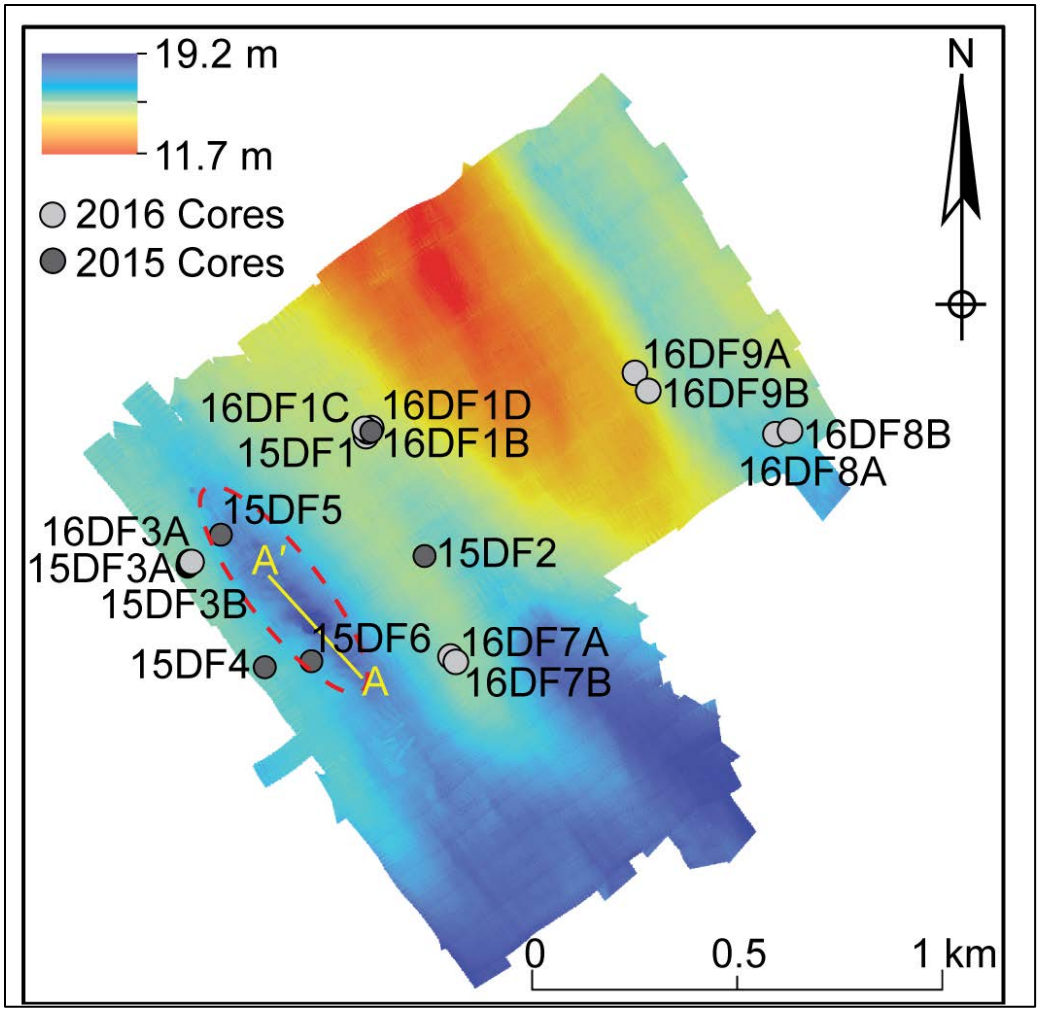

Figure 15 Bathymetric map of study site with core locations.

Red dashed line encircles the trough where stumps are exposed. Core locations are gray circles with core labels (Table 1). Exact latitude and longitude are not shown to protect the site. A-A′ is the cross-section shown in Figure 14.

Grain size-frequency contour plots were generated using the results obtained from the laser-diffraction analysis of the cores (Figure 16). Distinct grain size changes and distribution are evident in the down section in each core. Surficial units of each core (up to ~3 m thick) are generally >95% sand. Core 16DF1C is dominantly sand of uniform grain size throughout. Core 16DF3B is also sandy, but fines gradually downward, with some depth intervals of siltier sediment. Core 16DF8B has a sandy uppermost 0.10 m, below which grain size is primarily silt, except for an additional sandy interval at 0.45–0.55 m depth. Below the surficial sandy unit, interbedded sand and mud are evident in some cores (0.30–0.405 mm in core 15DF1 and 0.60–2.96 m in 15DF3B). Below units of interbedded sand and mud, the dominant modal grain size is in the silt range.

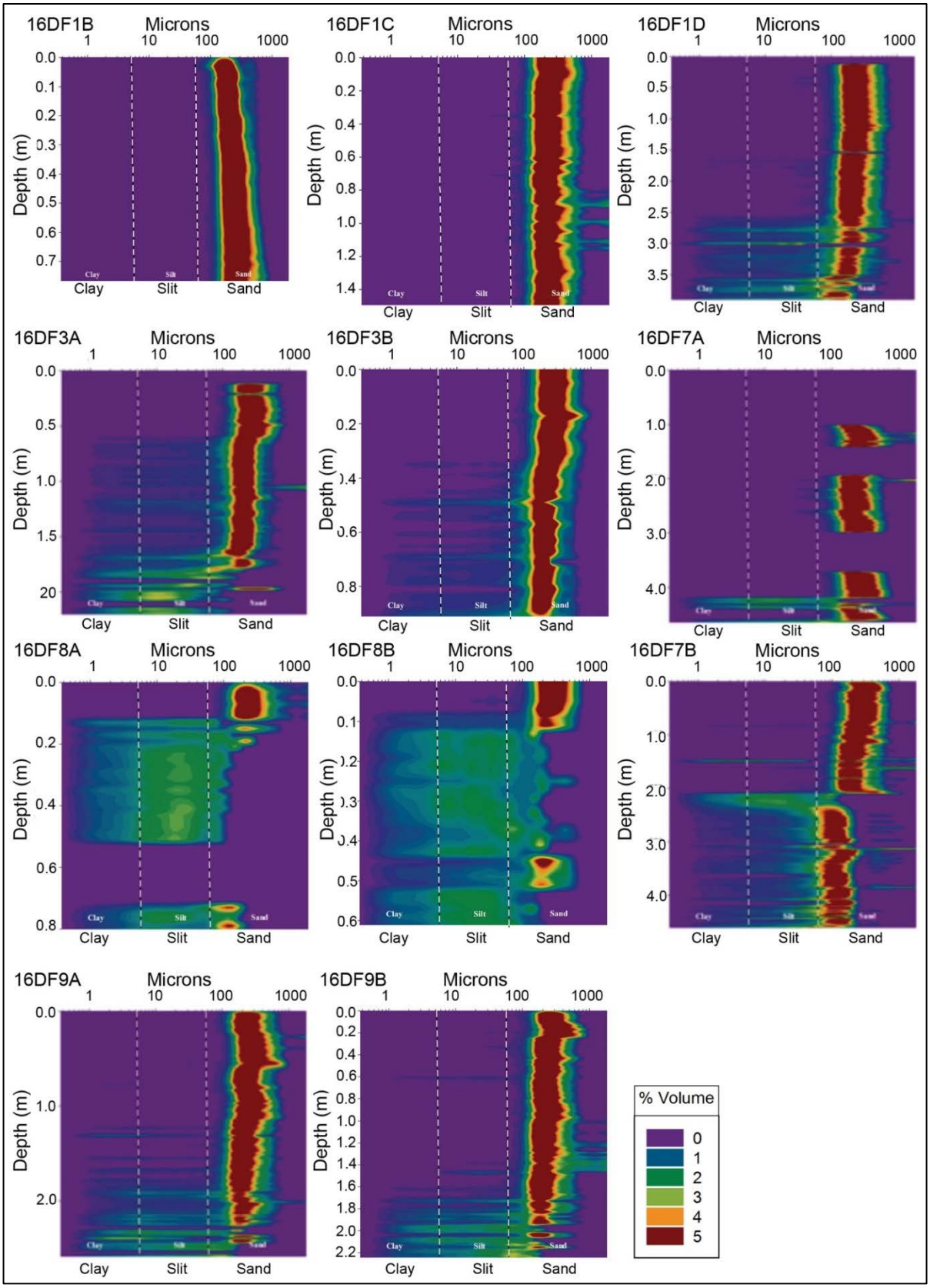
16DF1B
16DF1C
16DF1D
16DF3A
16DF3B
16DF7A
16DF8A
16DF8B
16DF7B
16DF9A
16DF9B
Microns
1
10
100
1000
Depth (m)
Clay
Silt
Sand
% Volume
0
1
2
3
4
5

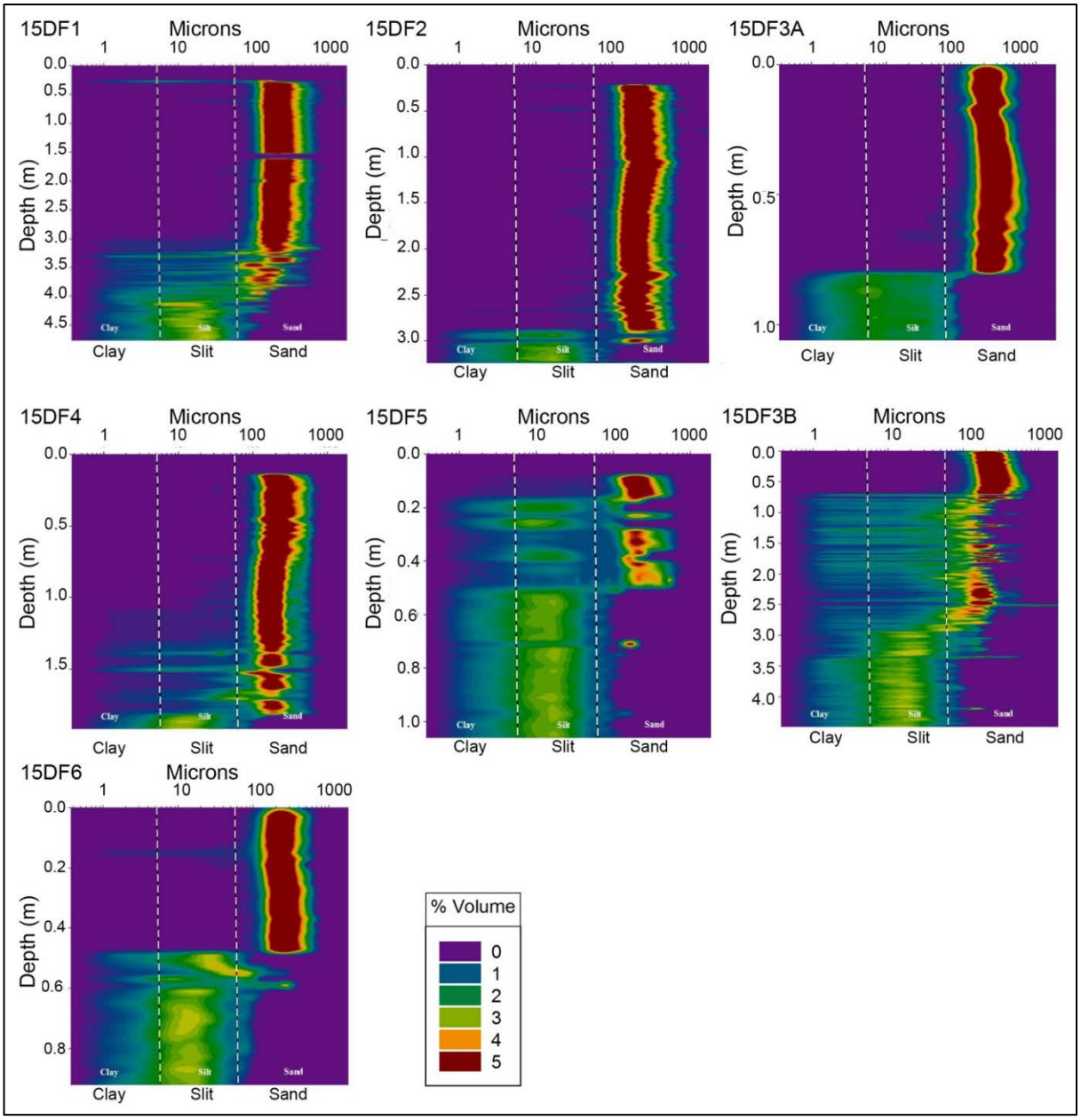

Figure 16. Grain size distributions for all cores.

Core grain size is shown as a color contour plot of % volume versus depth. Frequency contour plots with warm colors indicate the dominant grain size for that depth in microns.

Soon after collection, cores were logged using a Geotek MSCL for whole core gamma density of sediments. The combined loss on ignition (LOI), gamma density, and grain size were compiled into core comprehensive graphs (Figure 17), and these properties together define distinct lithologies for each core profile. The uppermost sandy unit in each core contains up to ~1% organic content (Figure 17). A slight increase in organic content is found in the interbedded sand and mud unit (1.3–2.6%). In the interbedded mud and peat unit, organic content was as high as 20.3%. A paleosol was found only in the base of cores 16DF8A and 16DF8B and displayed low organic content (0.6–3.8%). Overall, sandy units contained the lowest organic content, peaty units the highest, with intermediate values in muddy units.

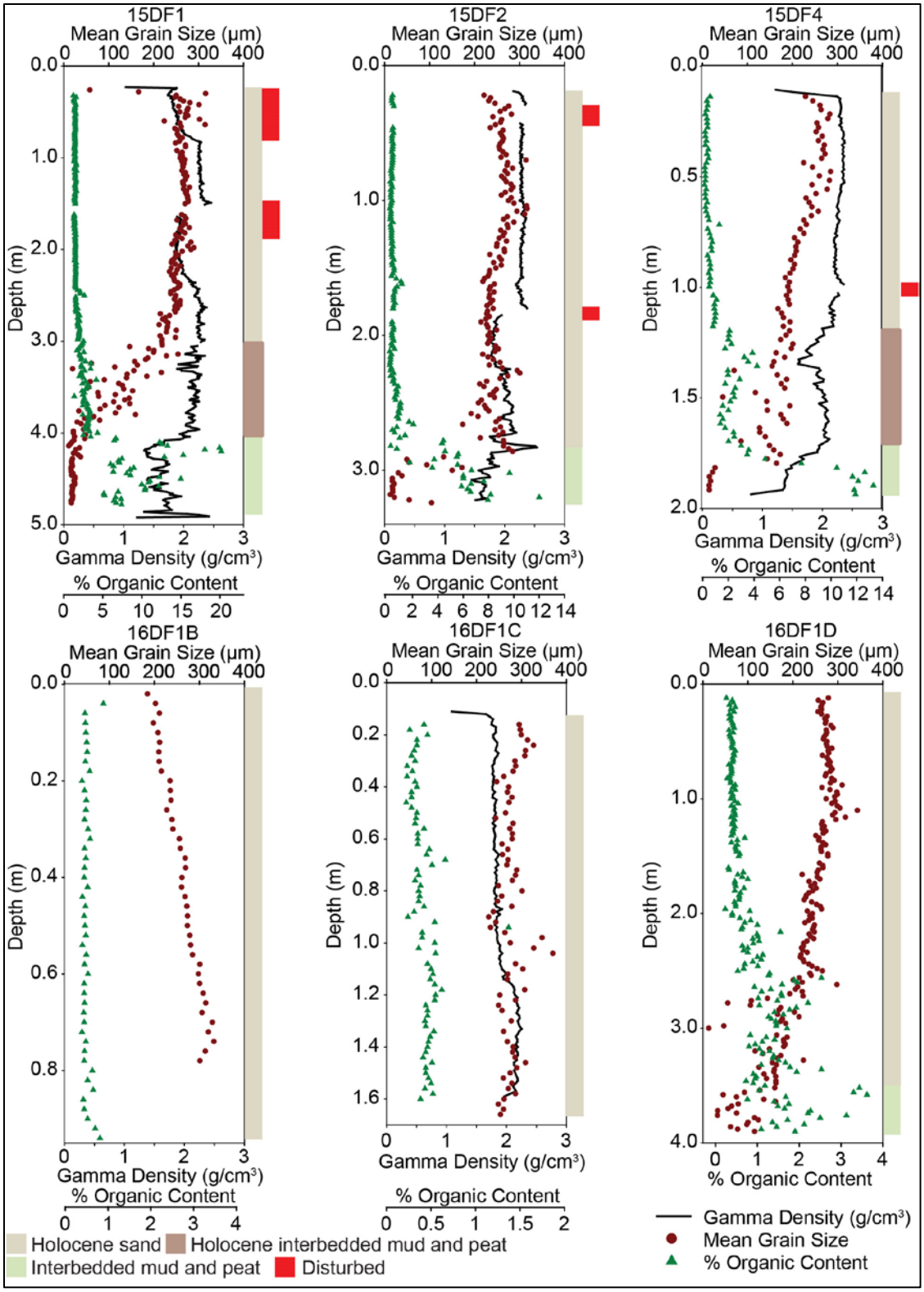
15DF1
Mean Grain Size (µm)
0 100 200 300 400
Depth (m)
Gamma Density (g/cm³)
% Organic Content
15DF2
Mean Grain Size (µm)
Depth (m)
Gamma Density (g/cm³)
% Organic Content
15DF4
Mean Grain Size (µm)
Depth (m)
Gamma Density (g/cm³)
% Organic Content
16DF1B
Mean Grain Size (µm)
Depth (m)
Gamma Density (g/cm³)
% Organic Content
16DF1C
Mean Grain Size (µm)
Depth (m)
Gamma Density (g/cm³)
% Organic Content
16DF1D
Mean Grain Size (µm)
Depth (m)
% Organic Content
Gamma Density (g/cm³)
Mean Grain Size
% Organic Content
Holocene sand
Holocene interbedded mud and peat
Interbedded mud and peat
Disturbed

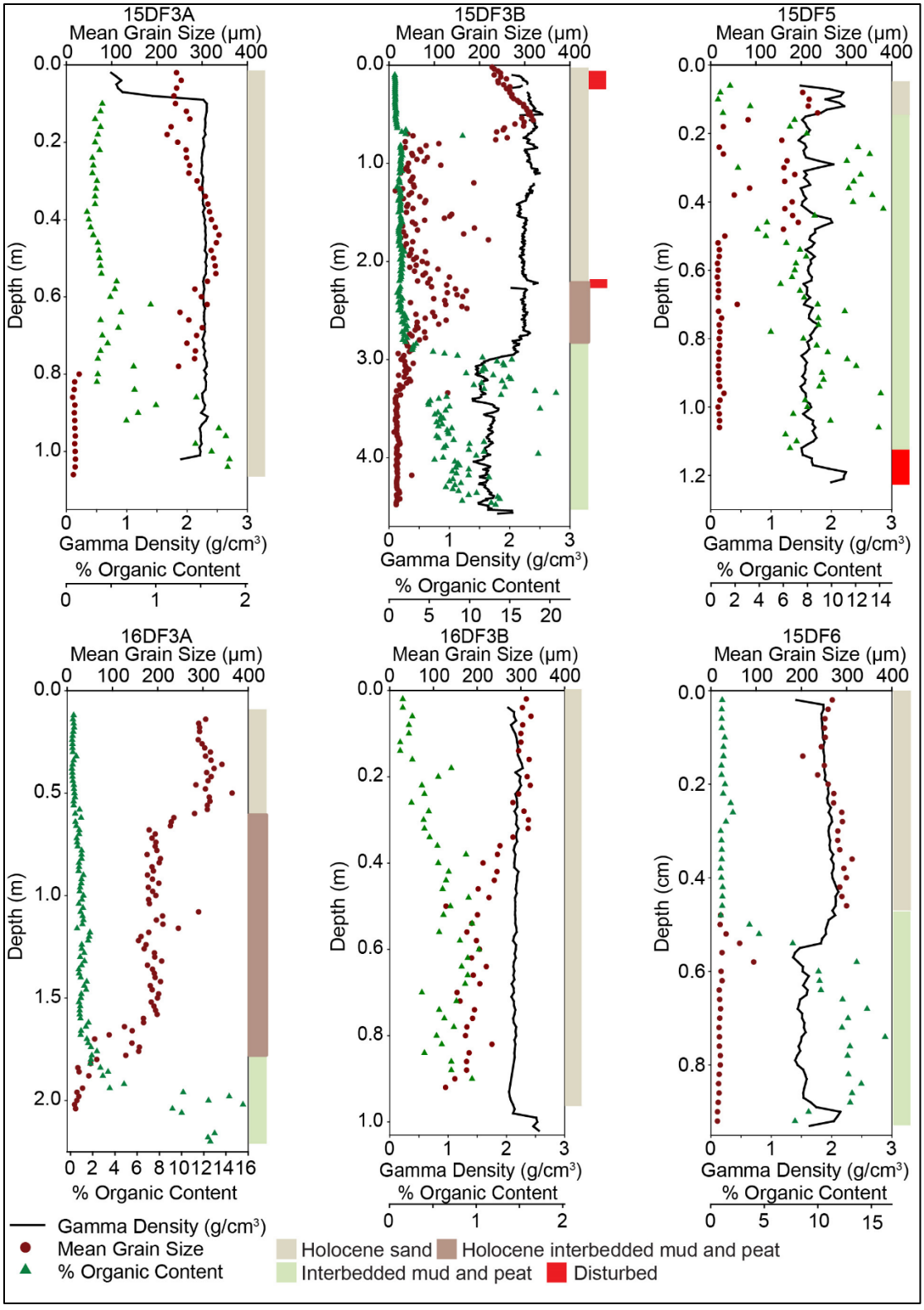
15DF3A
Mean Grain Size (µm)
0 100 200 300 400
Depth (m)
0.0 0.2 0.4 0.6 0.8 1.0
0 1 2 3
Gamma Density (g/cm³)
% Organic Content
0 1 2
15DF3B
Mean Grain Size (µm)
0 100 200 300 400
Depth (m)
0.0 1.0 2.0 3.0 4.0
0 1 2 3
Gamma Density (g/cm³)
% Organic Content
0 5 10 15 20
15DF5
Mean Grain Size (µm)
0 100 200 300 400
Depth (m)
0.0 0.2 0.4 0.6 0.8 1.0 1.2
0 1 2 3
Gamma Density (g/cm³)
% Organic Content
0 2 4 6 8 10 12 14
16DF3A
Mean Grain Size (µm)
0 100 200 300 400
Depth (m)
0.0 0.5 1.0 1.5 2.0
0 2 4 6 8 10 12 14 16
% Organic Content
16DF3B
Mean Grain Size (µm)
0 100 200 300 400
Depth (m)
0.0 0.2 0.4 0.6 0.8 1.0
0 1 2 3
Gamma Density (g/cm³)
% Organic Content
0 1 2
15DF6
Mean Grain Size (µm)
0 100 200 300 400
Depth (cm)
0.0 0.2 0.4 0.6 0.8
0 1 2 3
Gamma Density (g/cm³)
% Organic Content
0 5 10 15
Gamma Density (g/cm³)
Mean Grain Size
% Organic Content
Holocene sand
Holocene interbedded mud and peat
Interbedded mud and peat
Disturbed

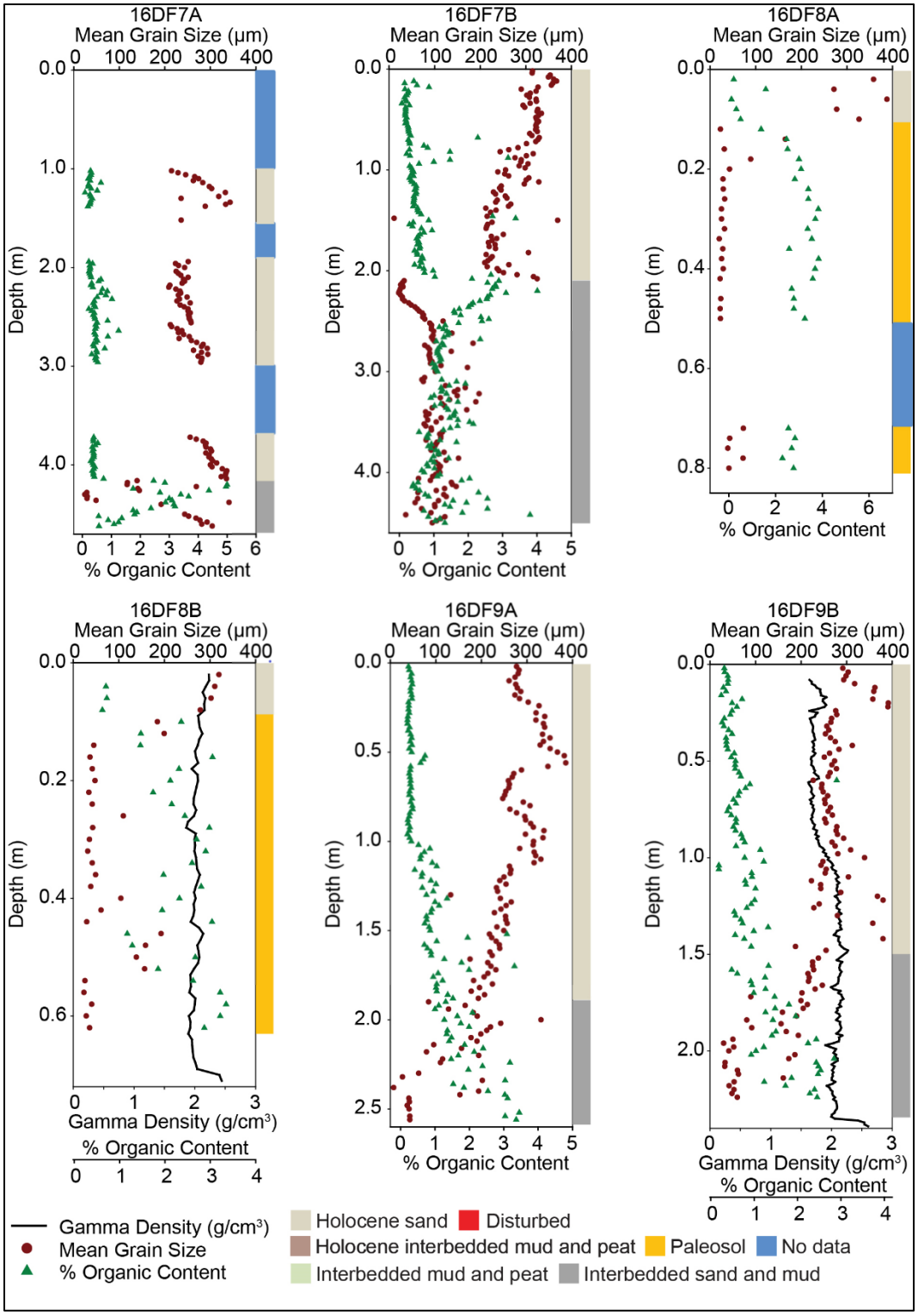

Figure 17. Comprehensive graphs for cores.

Percent organic content, mean grain size, and gamma density compared to depth profile are shown. Note: % organic content (horizontal axis) numbers were adjusted to show organic content variably throughout the core. Disturbed units are noted in red.

Gamma density profiles reveal distinctive variations down core that generally correspond to grain size and organic content: sandy units have the highest gamma density, peaty units the lowest, with muddy units having intermediate densities. Uppermost sands have high and relatively constant densities (~2.3–2.5 g/cm^3). Underlying interbedded mud and sand have intermediate densities (e.g., ~1.8–2.3 g/cm^3 for 3.1–4.05 m in core 15DF1). Interbedded muds and peaty muds have low and variable densities (e.g., 1.2–1.9 g/cm^3 for 4.05–4.78 m in core 15DF1). The last lithological unit was identified as a paleosol in one core (~0.1–0.6 m in 16DF8B), which showed gamma density readings of 1.9–2.4 g/cm^3. Some sandy sections were found to have settled during transport and storage creating gaps and disturbed units of sediment in cores and are thus noted in core profiles.

3.3 Dating

3.3.1 Radiocarbon Dating

Radiocarbon (^{14}C) ages (Table 2) for 18 out of 20 wood and sediment samples were inconclusive due to radiocarbon dating detection limits, i.e., radiocarbon dead (measured ^{14}C was not discernible from background levels thus older than ~50 ka) (Stuiver and Polach 1977). Woody debris samples collected from 4.05 m and 4.14 m downcore in core 15DF1 yielded conventional radiocarbon ages of 41,830 ±880 BP (calibrated age of 45,210 calendar years (cal) before present (BP), i.e., calendar years before 1950) and 37,350 ±330 BP (41,830 cal BP), respectively. Calibrated ages were calculated using IntCal13 (Reimer et al. 2013). A replicate sample (DF1-414-2 dup) had an infinite age; all of these radiocarbon dates should be interpreted with caution since they are close to the limitations of the radiocarbon dating method. Stratigraphic inversion, bulk dating methodology, and the limitations of radiocarbon dating have caused these ages from core 15DF1 to be cautiously treated as a minimum estimate of the forest's age. The sample of mixed genera benthic foraminifera had a conventional radiocarbon date of 3,940 ±30 BP (3,920 cal BP) thus providing a depositional age on the top of the interbedded sand and mud facies in core 15DF1.

Table 2. Radiocarbon Results

Sample [1]	Type [2]	Sample depth (m)	Facies	Lab analysis # [3]	$\delta^{13}C$ [4]	^{14}C age [5]	±	Cal BP [6]	Cal BP range [6]
ALAF C1	Wood		Seafloor	CAMS-160062	–25	51,700	2600		
ALAF C1 dup	Wood		Seafloor	CAMS-160064	–25	>52,500			
ALAF B1	Wood		Seafloor	CAMS-160063	–25	>49,600			
ALAF-B1 dup	Wood		Seafloor	CAMS-160128	–25	>51,200			
GOM 1A	Wood		Seafloor	CAMS-167083	–25	50,700	3100		
GOM 1B	Wood		Seafloor	CAMS-167084	–25	51,200	3400		
GOM 2A	Wood		Seafloor	CAMS-167085	–25	>51,400			
GOM 2B	Wood		Seafloor	CAMS-167086	–25	>52,600			
GOM 013A #1	Wood		Seafloor	CAMS-167087	–25	>48,600			
GOM #2	Wood		Seafloor	CAMS-167088	–25	52,400	3900		
GOM 005A	Wood		Seafloor	CAMS-167089	–25	>49,100			
15DF1-322	BWD	3.22	LPISM	Beta-433024	–30.1	>43,500			
15DF1-330	Foraminifera 7	3.30	LPISM	Beta-483831	–0.1	3,940	30	3,920	4,045–3,830
15DF1-405	BWD	4.05	LPIMP	Beta-433025	–28.8	41,830	880	45,210	46,690–43,625
15DF1-414	BWD	4.14	LPIMP	Beta-429909	–23.0	37,350	330	41,830	42,235–41,350
15DF1-414-2 dup	BWD	4.14	LPIMP	Beta-433026	–28.9	>43,500			
15DF1-419	BWD	4.19	LPIMP	Beta-433027	–28.7	>43,500			
15DF1-424	BWD	4.24	LPIMP	Beta-433028	–31.0	>43,500			
15DF1-456	BWD	4.56	LPIMP	Beta-433029	–27.4	>43,500			
15DF1-466	BWD	4.66	LPIMP	Beta-433030	–28.5	>43,500			
15DF3B-310	BWD	3.10	LPIMP	Beta-488002	–26.7	>43,500			

[1] "dup" is duplicate.

[2] BWD = Bulk woody debris

[3] CAMS samples were analyzed at the CAMS at Lawrence Livermore National Laboratory in California and samples labeled Beta were analyzed at Beta Analytic Radiocarbon Dating Laboratory in Miami, Florida. CAMS samples are wood samples collected by divers in 2013. Beta samples are from cores 15DF1, and

15DF3B collected in August 2015. CAMS sample preparation backgrounds were subtracted based on measurements of samples of ^{14}C-free wood. Backgrounds were scaled relative to sample size.

[4] CAMS carbon stable isotopic ratio ($\delta^{13}C$) values are the assumed values according to Stuiver and Polach (1977) when given without decimal places. Beta reported $\delta^{13}C$ values were measured separately in an isotope ratio mass spectrometer. They are not the AMS $\delta^{13}C$, which would include fractionation effects from natural, chemistry, and AMS induced sources. $\delta^{13}C$ values were calculated relative to the PDB-1 standard as per mil (‰).

[5] Quoted age is in radiocarbon years using the Libby half-life of 5568 years and following the conventions of Stuiver and Polach (1977). CAMS samples ALAF B, ALAF C1 dup, GOM 2A, GOM 2B, GOM 013A#1, and GOM 005A are reported as two sigma limits as per Stuiver and Polach (1977). Carbon-14 ages with an > before age are infinite ages and samples are radiocarbon dead, i.e., extremely low ^{14}C activity that is almost identical to the background signal.

[6] Calendar Years Before Present (cal BP; Present = AD 1950) determined using INTCAL13 (Reimer et al. 2013) with 2σ ranges given when appropriate. A calendar age is not reported for infinite dates (>) since calendar ages may imply a higher level of confidence than is appropriate.

[7] Foraminifera sample age determined using MARINE13 (Reimer et al. 2013) with no local reservoir correction.

LPIMP = late Pleistocene Interbedded Mud and Peat, LPISM = late Pleistocene Interbedded Sand and Mud.

3.3.2 Optically Stimulated Luminescence Dating

Four samples for optically stimulated luminescence (OSL) dating were collected from core depths with possibly undisturbed sediment overlying the forest-swamp facies, and one sample was collected from the paleosol found in the eastern section of the survey grid (Figure 15). The OSL dates range from 56 ka (16DF-8A-1) to 73 ka (16DF-7A-1) (Table 3) suggesting the forest age is between 56 and 74 ka or MIS 3–5 (Figure 3). The core with the paleosol (16DF-8A-1) dated to a younger OSL age than the other samples. This difference in age could be due to core 16DF-8A-1's location within a higher relief area (Figure 15). The age is still consistent with the hypothesis that the area exhibited variable relief. Some of the OSL cores penetrated more deeply than their duplicates, so there is incomplete stratigraphy of the area (see section 3.2).

3.3.3 Uranium-Thorium Dating of Wood

Initially, the wood cellulose did not dissolve in the nitric acid as quickly as desired, and it was decided to let it digest for a longer period before conducting U-Th dating and making further adjustments to the methodology. The age of the wood samples was all younger than the OSL and radiocarbon ages (Table 4). They are interpreted as apparent dates. Two different initial values were used for $^{230/232}$Th, 4 ±2 ppm (blue color, Table 4) and 2 ±2 ppm (green color, Table 4). The uncorrected ages should be the maxima age of these wood samples based on U-Th dates. The $^{230/232}$Th value of the soil surrounding the wood may be helpful for age correction. These ages are all deglacial and may represent a resetting of the U and Th concentrations in the wood as the terrestrial site became inundated by seawater as sea level rose.

Table 3. Optically Stimulated Luminescence Samples and Relevant Analytical Results

Core	Water/sample depth (m)	Facies	$^{238}U \pm 1\sigma$ (μg g^{-1})	$^{232}Th \pm 1\sigma$ (μg g^{-1})	$K_2O \pm 1\sigma$ (μg g^{-1})	Water content (%)	d_{cosmic} (Gy ka^{-1})[1]	Size fraction (μm)	$d_{natural} \pm 1\sigma$ (Gy ka^{-1})	De ±1σ (Gy)	OSL age ±1σ (ka)
16DF3A	15.8/2.12	LPIMP	2.96±0.09	11.61±0.34	1.37±0.04	0.57±0.10	0.15	4–15	1.48±0.17	106±3	72±8
16DF9A	14.4/2.57	LPISM	4.18±0.11	12.43±0.27	1.33±0.03	0.25±0.10	0.14	4–15	2.89±0.21	182±6	63±5
16DF7A	15.7/4.30	LPISM	3.52±0.09	12.63±0.28	1.34±0.03	0.27±0.10	0.12	4–15	2.64±0.22	193±5	73±6
16DF8A	16.2/0.60	Paleosol	4.96±0.13	17.02±0.35	1.52±0.04	0.20±0.10	0.18	4–15	3.81±0.29	214±10	56±5
16DF7B	15.7/4.58	LPISM	3.50±0.10	12.01±0.28	1.16±0.03	0.24±0.10	0.12	4–15	2.60±0.21	193±6	74±6
								180–250	2.25±0.20	138±10	61±7
										16DF7B weighted mean	70±5

[1] Cosmic dose rates were calculated with and without seawater at the coring site. The cosmic dose rates for age calculation were derived by assuming ~15% burial history with seawater of present-day depth at the coring sites, considering sample ages, water depth at the sites, and sea-level history.

LPIMP = late Pleistocene Interbedded Mud and Peat, LPISM = late Pleistocene Interbedded Sand and Mud.

Table 4. U-Th Isotopic Compositions and ^{230}Th Ages for Wood Samples

Sample ID	Weight (g)	^{238}U (ppb) [1]		^{232}Th (ppt)		δ^{234}U Measured [1]		[^{230}Th/^{238}U Activity [2]		^{230}Th/^{232}Th atomic (x 10^{-6})		Age (year ago) uncorrected		Age (year ago) corrected [3, 4]		Age (year BP) relative to 1950		$\delta^{234}U_{initial}$ corrected[4]	
W1	0.0154	41.42	± 0.50	11244	± 64	232	± 14	0.2025	± 0.0093	12.30	± 0.55	19,475	± 999	13,537	± 3193	13,471	± 3193	241	± 14
														16,549	± 3120	16,482	± 3120		
W2	0.0176	203.3	± 1.5	49006	± 462	194.8	± 9.2	0.1858	± 0.0097	12.71	± 0.67	18,344	± 1046	12,913	± 2959	12,846	± 2959	202.0	± 9.7
														15,664	± 2900	15,597	± 2900		
W3	0.0116	139.0	± 1.0	32578	± 257	238	± 11	0.1516	± 0.0070	10.66	± 0.49	14,188	± 707	9,090	± 2697	9,024	± 2697	244	± 12
														11,671	± 2639	11,604	± 2639		
W4	0.0171	116.72	± 0.38	15495	± 114	192.1	± 6.3	0.2035	± 0.0080	25.3	± 1.0	20,315	± 883	17,354	± 1730	17,288	± 1730	201.7	± 6.7
														18,845	± 1717	18,778	± 1717		

Analysis by MC-ICP-MS Thermo Electron Neptune at National Taiwan University. Analytical errors are 2σ of the mean.

[1] $[^{238}U] = [^{235}U] \times 137.818$ (±0.65‰) (Hiess et al. 2012); $\delta^{234}U = ([^{234}U/^{238}U]_{activity} - 1) \times 1000$.

[2] $[^{230}Th/^{238}U]_{activity} = 1 - e^{-\lambda 230 T} + (\delta^{234}U_{measured}/1000)[\lambda_{230}/(\lambda_{230} - \lambda_{234})](1 - e^{-(\lambda 230 - \lambda 234)T})$, where T is the age.

Decay constants are 9.1705×10^{-6} year^{-1} for ^{230}Th, 2.8221×10^{-6} year^{-1} for ^{234}U (Cheng et al. 2013), and 1.55125×10^{-10} year^{-1} for ^{238}U (Jaffey et al. 1971).

[3] Age corrections, relative to chemistry date in October 2017, were calculated using an estimated atomic ^{230}Th/^{232}Th ratio of $4 (\pm 2) \times 10^{-6}$.

Those are the values for a material at secular equilibrium, with the crustal ^{232}Th/^{238}U value of 3.8. The errors are arbitrarily assumed to be 50%.

[4] $\delta^{234}U_{initial}$ corrected was calculated based on ^{230}Th age (T), i.e., $\delta^{234}U_{initial} = \delta^{234}U_{measured} \times e^{\lambda 234 * T}$, and T is corrected age.

3.4 Micropaleontological Analyses

3.4.1 Pollen

Pollen results from core 15DF1 are reported in Reese et al. (2018) (Figure 18). Lowermost samples within the core (4.75–4.55 m) show high percentages of *Taxodium*, *Nyssa* (tupelo), and the family Cyperaceae (sedges). Minor components include typical bottomland hardwood species such as *Quercus* (oak), *Carya* (hickory), *Betula* (birch), *Ulmus* (elm), *Fraxinus* (ash), and *Liquidambar* (sweetgum). *Pinus* (pine) pollen is also prevalent, but < 20%, and is probably representative of the regional pollen rain transported from more upland sites. This pollen assemblage indicates a cypress-tupelo, backwater environment. At the 4.5-m level, however, a dramatic change is observed in the pollen assemblage. Percentages of cypress and tupelo decrease while Poaceae (grass) pollen is dominant in all but a few samples up to the top of the mud/peat section (at 4.05 m). Coeval with this change is the appearance of *Typha* (cattail) and the emergence of *Alnus* (alder). However, from 4.3 to 4.2 m, the grass percentage declines briefly. At this depth range, cypress spikes again, this time without tupelo. Alder remains a prominent pollen type and birch re-emergences. Above 4.2 m, cypress, birch, and alder decline, and grass again resume dominance up to the top of the mud-peat section.

We also examined pollen in a peat layer at 3.23 m separated from the lowermost mud/peat layer by a zone of interbedded sand and mud (Figure 9). Pollen preservation in this sample was particularly poor, with nearly 20% of the grains indeterminable. Pine, oak, hickory, and cypress are the prominent taxa, with birch, elm, and *Carpinus* (hornbeam) as minor components. The stratigraphic integrity of this layer does not appear to have been preserved. This section is probably reworked based on the foraminifera dating results at 3.3 m (Section 3.3.1), and the particularly poor preservation that is likely to be an artifact of bioturbation or mechanical mixing. A radiocarbon date for this material came back “dead.” In general, the pollen concentration shows an inverse relationship with the percentage of indeterminable pollen grains. Concentrations are highest in the lowermost zones, then decrease up the core, coeval with increased percentages of indeterminable pollen. It is important to note that throughout this section of the core, percentages of the organic matter remain constant, and do not decrease up the core. Thus, one hypothesis is that concentration is driven, at least in part, by pollen preservation and caution should be exercised against interpreting these changes in concentration with changes in actual pollen rain.

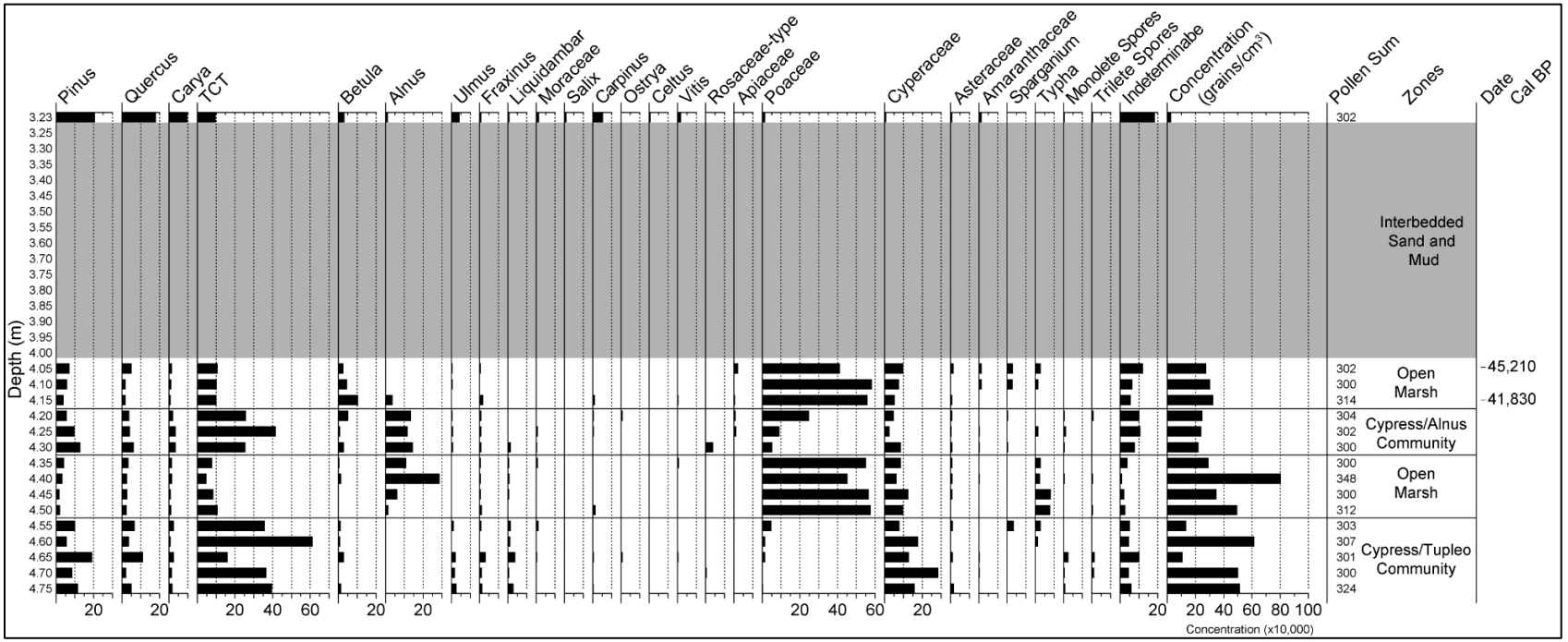

Figure 18. Pollen assemblages for core 15DF1.

Pollen results are shown as percentages. Four pollen zones were identified below 4.0 m. Above that is Holocene marine interbedded sand and mud.

3.4.2 Foraminifera

Marine microfossil results are reported in Troung et al. (in review) (Figure 19). Foraminifera identification to the genus level followed Loeblich and Tappan (1988), and to the species level, when possible, using Phleger and Parker (1951), Bandy (1954, 1956), Andersen (1961), Puckett (1992), and Poag (2015). Specimens were compared to samples housed at the LSU Natural Science Museum's Collection of Fossil Protists and Invertebrates. Paleoenvironmental interpretations were applied using foraminiferal distribution and environmental associations outlined in Phleger and Parker (1951), Bandy (1954, 1956), Murray (1991), Puckett (1992), Gangopadhyay et al. (1996), McBride et al. (1999), Scott et al. (2001), Kohl et al. (2004), and Poag (2015). *Triloculina* spp., *Nodobaculariella* sp., *Spiroloculina* sp., and *Miliolinella* sp. were grouped into "Other Miliolids." Indeterminate specimens were defined as being too small, degraded, or broken for positive identification. It is assumed that coastal foraminifera equate to Holocene sediments based on the depth of the site (18 m) and sea level elevations.

Foraminifera results from core 15DF1 (Figures 9, 19) indicate that *Rosalina* spp., *Hanzawaia concentrica, Elphidium* spp., *Cibicidoides* spp., and miliolid taxa account for >70% of all the genera in the top 3.30 m of core 15DF1 and are similar to the miliolid, *Rosalina*, and *Asterigerina carinata* assemblages from McBride et al. (1999). Soritids and Peneroplids are present in assemblages down to 3.2 m. Foraminiferal abundance in the core from 0.40 to 2.75 m is between 134 and 285 specimens/g and then significantly increases to 1625 specimens/g at 3.1 m. Organic content determined by LOI displays a subtle downwards increase within the top two facies (Gonzalez et al. 2017). The presence of preserved foraminifera is only found within the sandy sediments in the interbedded sand and mud facies. The number of shell fragments in samples decreases down the core, and no foraminifera was present from 3.35 to 3.55 m except one *Oolina* sp. at 3.5 m. A unit of coarser grain size and increased shell fragments corresponds with increase foraminiferal abundances similar to that observe within the Holocene sand assemblages at 3.6 m and 3.8 m. A distinguishing feature from the interbedded sand and mud facies is that porcelaneous taxa represent a much smaller percentage (<2%) of the assemblage from 3.6 to 3.8 m. An interval of no foraminifera is noted from 3.85 to 3.95 m with few shell fragments. Two broken and poorly preserved Textulariida tests were recovered from 4.0 m. Foraminiferal abundances from the interbedded sand and mud facies are much lower than throughout the Holocene sand and range from 0.7 to 73.10 specimens/g. Indeterminate specimens account for <2% of each sample. Samples from the interbedded mud and peat facies in core 15DF1 (4.05–4.78 m) are characterized by relatively high percentages of organic material (>4%), and no foraminifera or ostracoda were present (Figure 19).

Micropaleontological analysis of samples from cores 15DF3B, 16DF7B, and 16DF9B found *Ammonia parkinsoniana, Quinqueloculina* spp., *Rosalina* spp., *Elphidium* spp., *Asterigerina carinata,* and *Cibicidoides* spp. present in all samples that contained foraminifera. Microfossils are absent from sample depths of 2.25 m and 4.00 m in 16DF7B. From the detailed investigation of core 15DF1 age constraints, environmental associations, the depth of samples (16–20 mbsl), and sea-level reconstructions, these foraminiferal assemblages are determined to be Holocene in age and lie above the MIS 2 sequence boundary (Figures 3, 19).

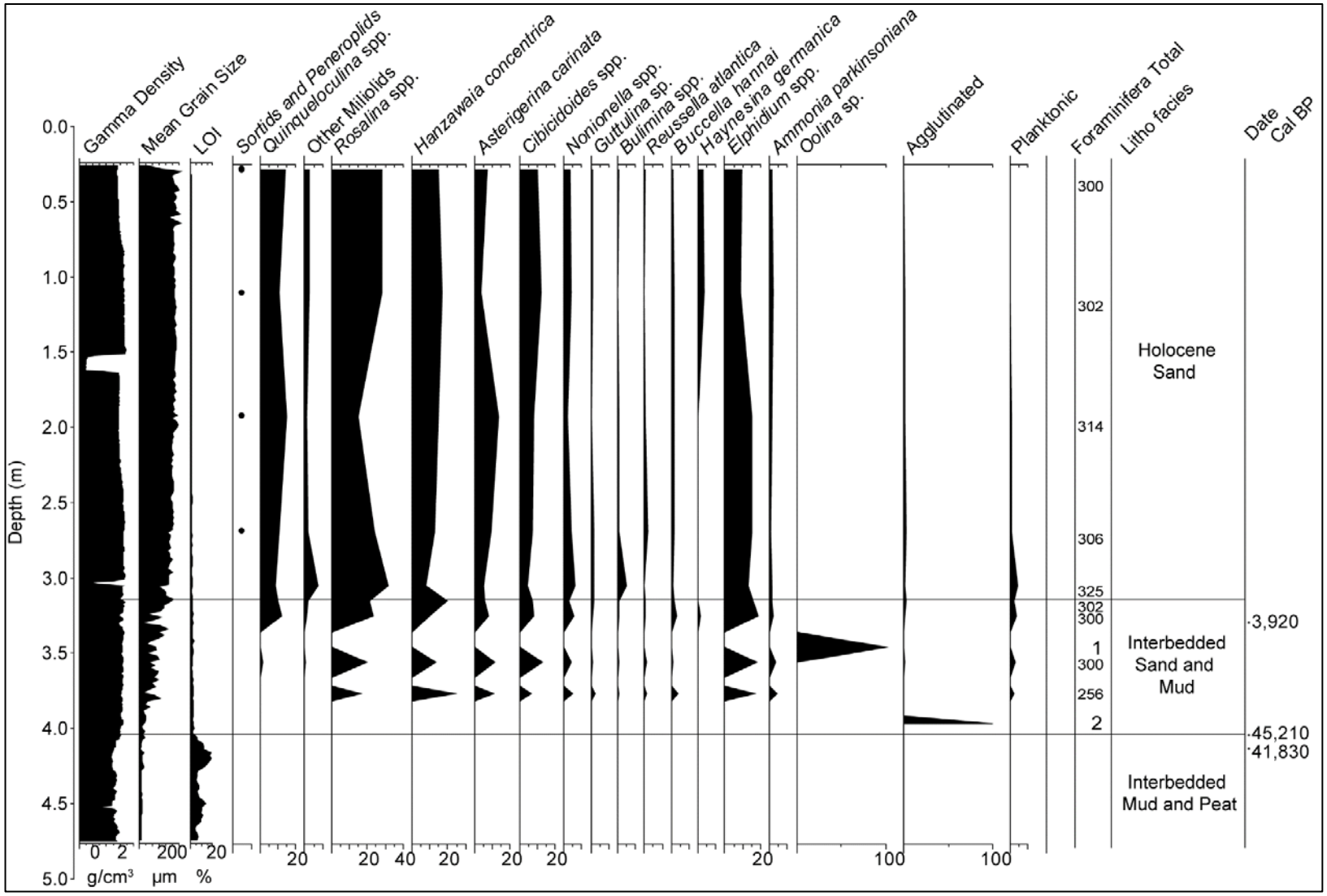

Figure 19. Foraminiferal assemblages for core 15DF1.

Foraminiferal percentages (%) for core 15DF1. Gamma density, mean grain size, and LOI analyses completed by Gonzalez et al. (2017).

3.4.3 Seeds

Intact preserved seeds (*T. distichum*, *Hibiscus lasiocarpas*, *Carex*, *Triadenum*, *Cephalanthus occidentalis*, *Liquidambar styraciflua*, and *Nyssa*) were found in peat and mud samples in core 15DF1 and identified using modern type samples (Figure 20). The preliminary analysis of seeds in core 15DF1 for presence only was completed (Table 5). Additionally, a small insect identified as a mite was found in the peat section; another example of the excellent preservation in the peat section of this core. The seeds were saved for future analysis.

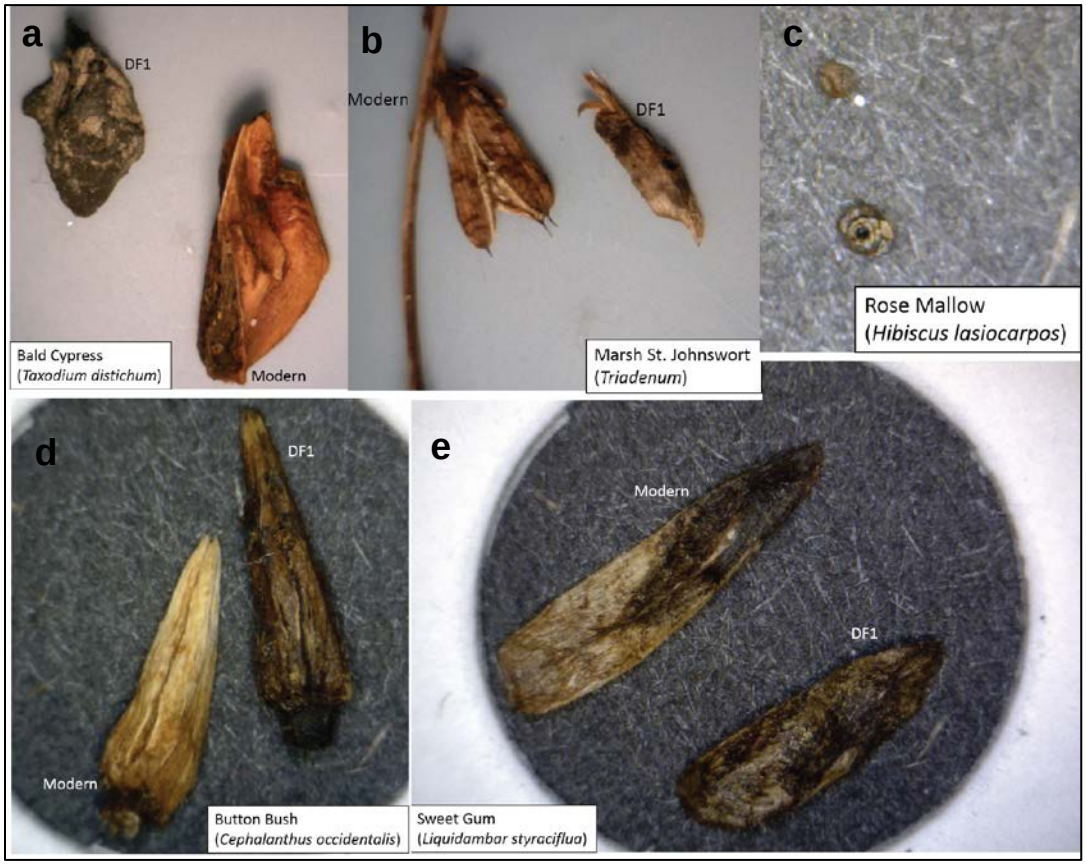

Figure 20. Seeds preserved in peat section.

Examples of seeds found in sediment core 15DF1 from 4.2 to 4.3 m shown with modern seeds for comparison. Clockwise from top left is bald cypress (*T. distichum),* marsh St. John's-wort *(Triadenum),* rose mallow (*Hibiscus lasiocarpos*), sweet gum (*Liquidambar styraciflua*), and button bush (*Cephalanthus accidentalis*).

Table 5. Preliminary Seeds Analysis in Core 15DF1

Core depth (m)	*Nyssa aquatic* (tupulo)	*T. distichum* (bald cypress)	*Cephalanthus occidentalis* (button bush)	Carex (Sedges)	Grass	Misc seeds	Notes
4.10–4.20	X	X	X	X	X	Poa	
4.30–4.40							None
4.40–4.50		X	X	X		Sedge	Many seeds
4.53		X		X		Juncus?	
4.60				X			Insect
4.70				X			

3.5 Wood and Dendrochronology

Dendrochronological and wood analyses results are summarized in Harley et al. (in review) and included here. Five of the diver-collected wood samples were sectioned with a microtome for microscopic analysis. All five were identified as bald cypress (*T. distichum*) (Figure 21). Not all of the wood specimens collected were microscopically identified since many of them were large enough to be visually identified as bald cypress. The wood samples were stored in deionized water for five years before thin sections were cut. As the wood had softened, it was difficult to make thin sections using the microtome, even when an epoxy was used to stabilize the wood. A change in cells and density from latewood and early wood boundaries can be observed. It is difficult to differentiate between Atlantic white cedar and bald cypress microscopically, but an indicator of bald cypress is the pinching of the annual rings that was observed in all wood specimens examined. Therefore, based on the ring anatomy and growth form, the specimens examined are most likely bald cypress. Additionally, these samples appear similar to modern bald cypress samples from Pascagoula, Mississippi. There are no observable differences at the cellular level between bald cypress and pond cypress (*T. ascendens*). No minerals deposition was observed; however, dissolution was observed in the wood some specimens. This could be due to storage of the specimens in deionized water for five years. Of the 23 wood specimens collected in 2013, one was identified in the field as a palm (Figure 22) and the another was very degraded, and both were discarded since they could not be used for dendroclimatology.

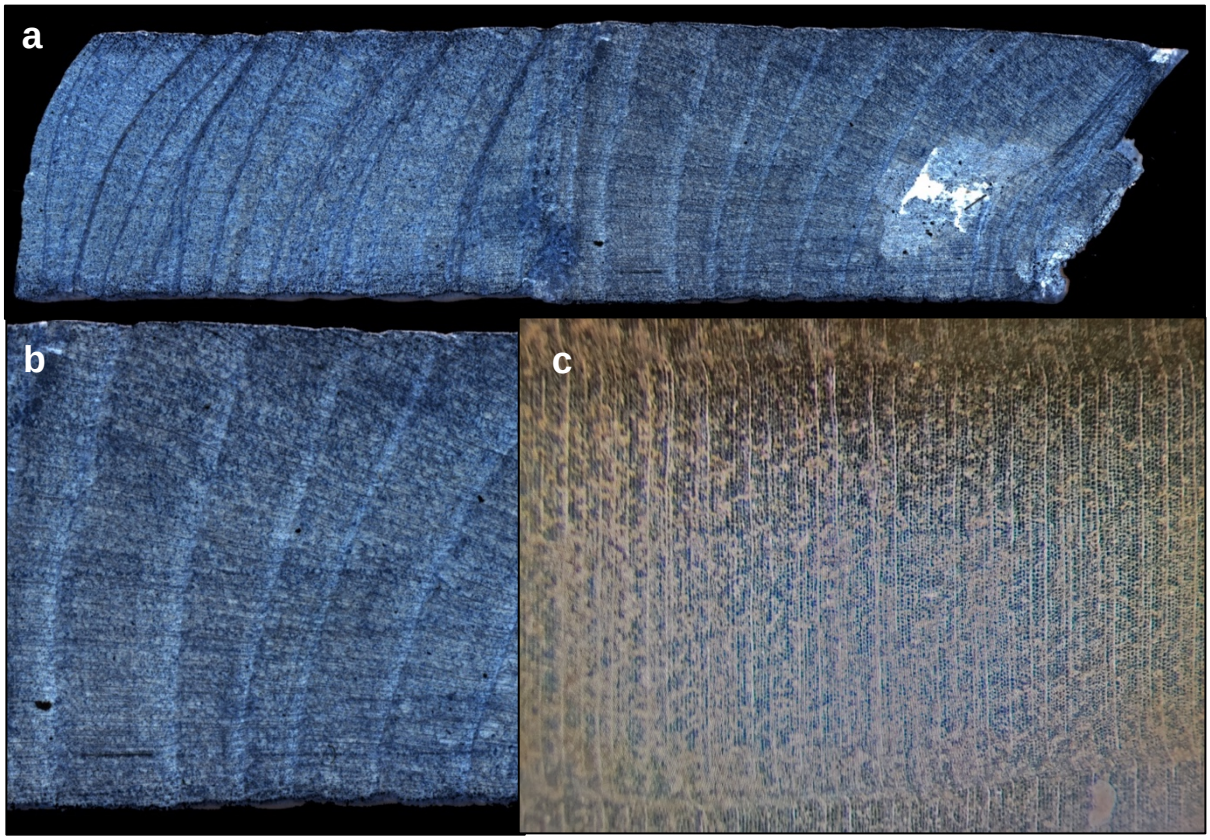

Figure 21. Example of bald cypress thin section.

Wood thin section (a); magnified view of (b); example of an annual growth ring in a bald cypress thin section (c).

Figure 22. Wood collected by divers in 2013.

Twenty-three wood specimens were recovered by divers (a-c) and processed on land for transportation (d–l) by cutting into smaller pieces to check for annual rings and preservation state. One was identified as palm (j–k) due to it fibrous texture and was discarded.

Of the 21 wood specimens extracted from the site by divers in 2013 and transported back to the laboratory, 12 were retained for dendrochronological processing and analysis (Figure 23). Samples that appeared to derive from roots or branches were excluded; only wood specimens collected from in situ stumps or large sections of stumps lying on the surface sands and sediments were retained. Two of the 12 specimens retained for dendrochronology could not be successfully cross dated due to issues with circuit uniformity and disturbance from wood-boring organisms.

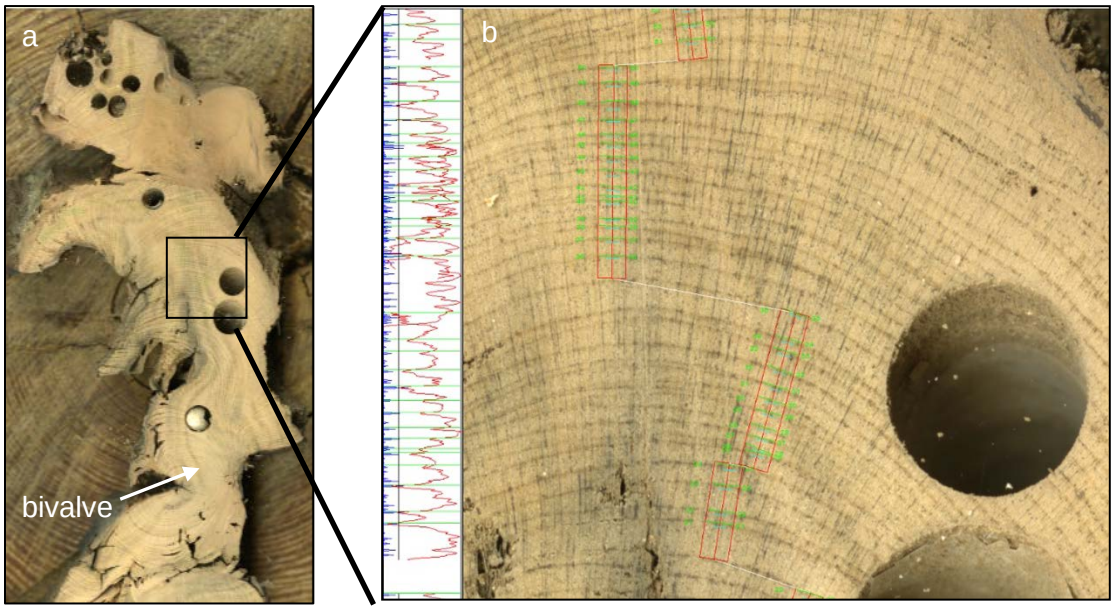

Figure 23. Bald cypress sample with ring width measurements.

This sample (ID: GOM100) was included in the tree-ring chronology. The full sample image is shown (a) with a zoomed inset displayed with the width measurement path (b). Large circular holes in wood are from shipworms and bivalves boring into the wood after being exposed to seawater.

A total of 10 samples were successfully crossdated against each other to develop a Submerged Forest tree-ring chronology (SFC) that was not anchored in time (e.g., "floating"). The SFC spans 489 years in length with an interseries correlation of 0.58 ($p < 0.001$) and mean tree age of 206 years (Figure 24). This chronology is floating in time because a confident radiocarbon date could not be attained for any of the wood specimens collected from the stumps (section 3.3.1), and the time series could not be crossdated against the Pascagoula *T. distichum* reference chronology (MS002; ITRDB) from the Gulf Coast region, which starts in 1466 CE. The radiocarbon and OSL results (section 3.3) suggest the age of the forest and the wood recovered from that site is between 41.8 and 74 ka.

The index of tree growth at the beginning of the SFC exhibited a high level of variability (years 0–97), but this is common in many tree-ring indices and is attributed to a low number of samples (<3) (Figure 24). Sample depth was low ($n = 1$) during the first 76 years of the chronology, but increases to four at year 98. This low sample depth precluded any growth trend interpretations until year 100. Years 100 to 350 are characterized by high-frequency growth variability until after which trees demonstrated a gradual decline in growth trend and year-to-year variability to year 430. A release (i.e., increase) in growth occurred during the period from year 430 to 482, after which is followed by a marked decline in growth to year 489. Year 489, the last complete ring in the chronology, is characterized by the narrowest growth ring in the entire time series. Further, eight of the ten samples contained the same outermost growth ring, which was characterized by a partial growth ring during year 490 of 6–10 rows of earlywood tracheids. Bark was not present on two of the samples, and this is evident in the drop in index growth about year 450 towards the end of the index chronology.

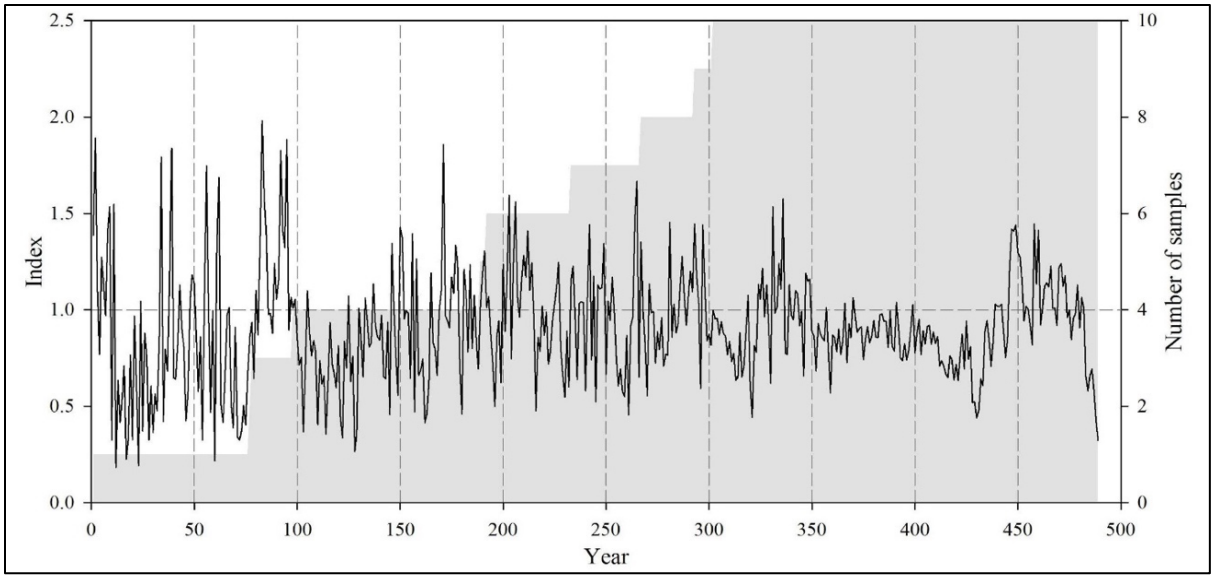

Figure 24. Tree-ring index from wood collected at the study site.

The master index chronology of tree-ring growth normalized to one (black) shown with the number of samples for each year (gray). The index is floating in time with the oldest year as 0 and the youngest as 489.

3.6 Facies

Based on gamma density, grain size, organic content, and sediment observations, five different lithologic units (i.e., lithofacies) characterize the sedimentary deposits found in the study area (Figure 25, Table 6). Lithofacies' names are generally considered to be age-independent (North American Commission on Stratigraphic Nomenclature 2005). Here, in order to provide more concise and practical litho- and chrono-stratigraphic descriptions, age and facies of strata identified in the cores are described together. Facies descriptions were initially derived for core 15DF1 in Gonzalez et al. (2017), which includes a high-resolution image of core 15DF1, and then applied to comparable lithologic units in the other 17 cores in this report. Two new facies classifications are added, a late Pleistocene interbedded sand and mud and a paleosol, which are found in five cores collected in 2016: 16DF8A and 16DF8B for the paleosol facies, and 16DF7A, 16DF7B, and 16DF9A for the late Pleistocene interbedded sand and mud facies. Facies' physical characteristics are consistent in all of the cores, but facies depth ranges are different for each core. Four of the facies (facies 1, 2, 3, and 5) are consistent with the lithologic descriptions of McBride et al. (1999).

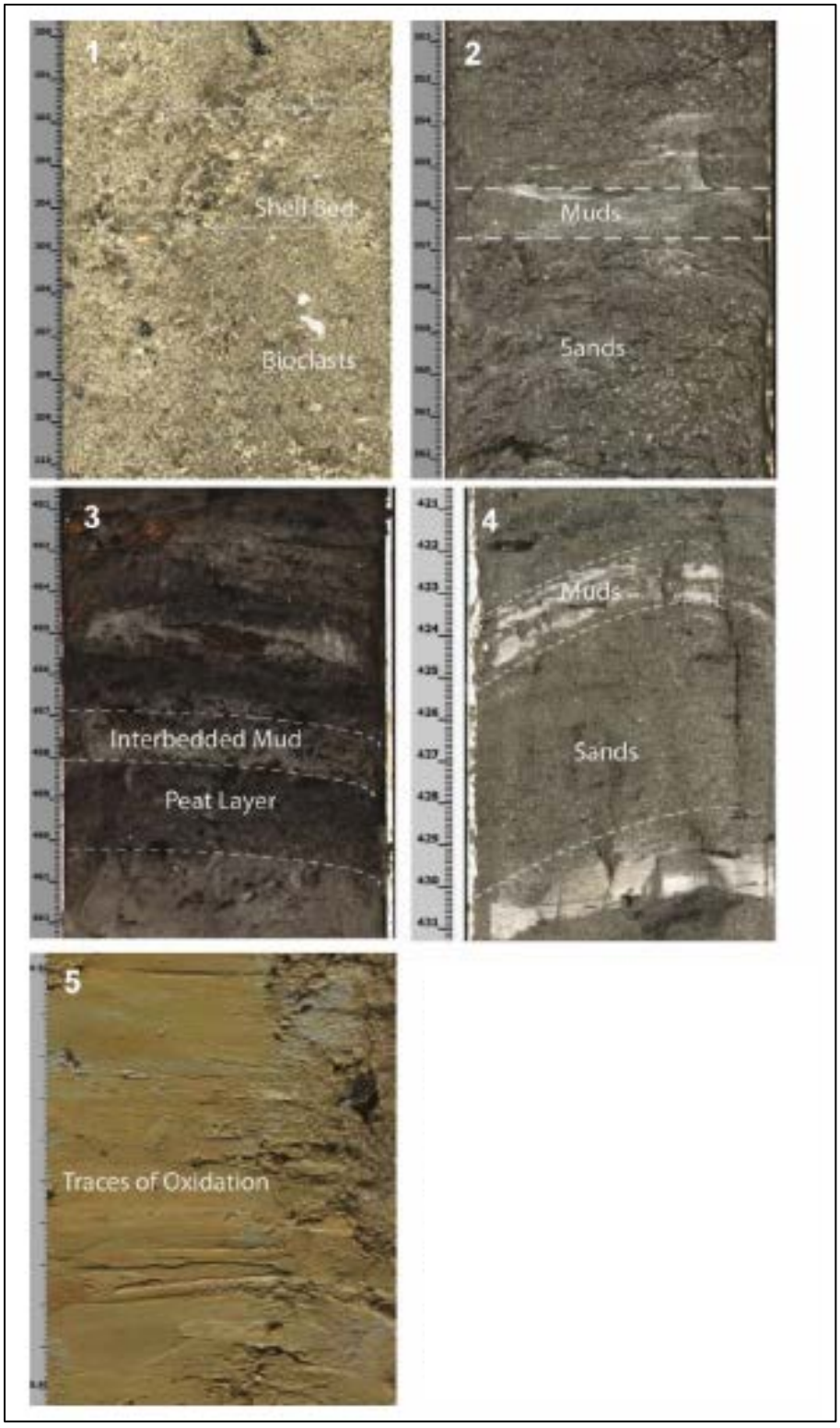

Figure 25. Examples of the five lithofacies.

Numbers indicate facies. Facies 1 is Holocene Sand (HS), facies 2 is Holocene Interbedded Sand and Mud (HISM), facies 3 is late Pleistocene Interbedded Mud and Peat (LPIMP), facies 4 is late Pleistocene Interbedded Sand and Mud (LPISM), and facies 5 is late Pleistocene Paleosol (LPP). See Table 6 for facies intervals.

Table 6. Facies Location and Depths for Sediment Cores

Core ID	Interval (m)	Facies	Date[2]
15DF1	0–3.10	HS	
	3.10–4.05	HISM	3,920 ^{14}C
	4.05–4.78	LPIMP	45,210 and 41,830 ^{14}C
15DF2	0–2.75	HS	
	2.75–3.30	LPIMP	
15DF3A	0–1.06	HS	
15DF3B	0–0.60	HS	
	0.60–2.96	HISM	
	2.96–4.53	LPIMP	
15DF4	0–1.20	HS	
	1.20–1.67	HISM	
	1.67–1.94	LPIMP	
15DF5	0–0.14	HS	
	0.14–1.12	LPIMP	
15DF6	0–0.47	HS	
	0.47–0.93	LPIMP	
16DF1B	0–0.94	HS	
16DF1C	0–1.66	HS	
16DF1D	0–3.64	HS	
	3.64–3.92	LPIMP	
16DF3A	0–0.62	HS	
	0.62–1.77	HISM	
	1.77–2.20	LPIMP	72 ±8 ka OSL
16DF3B	0–0.96	HS	
16DF7A	0–1.00	no sediments [3]	
	1.00–1.50	HS	
	1.50–1.93	no sediments [3]	
	1.93–3.0	HS	
	3.0–3.70	no sediments	
	3.70–4.05	HS	
	4.05–4.64	LPISM	73 ±6 ka OSL
16DF7B	0–2.06	HS	
	2.06–4.44	LPISM	
	4.50–4.72 [3]	LPISM	70 ±5 ka OSL
16DF8A	0–0.10	HS	
	0.10–0.80	LPP	56 ±5 ka OSL
16DF8B	0–0.10	HS	
	0.10–0.62	LPP	
16DF9A	0–1.86	HS	
	1.86–2.67	LPISM	63 ±5 ka OSL
16DF9B	0–1.75	HS	

[1] HS = Holocene Sand (facies 1), HISM = Holocene Interbedded Sand and Mud (facies 2), LPIMP = late Pleistocene Interbedded Mud and Peat (facies 3), LPISM = late Pleistocene Interbedded Sand and Mud (facies 4), and LPP = late Pleistocene Paleosol (facies 5). Facies examples are shown in Figure 24.

[2] Full dating results appear in Table 3. Radiocarbon dates are cal BP

[3] This core section was not imaged.

Facies 1: Holocene Sand. Facies 1 is characterized by light, beige to grey, fine- to medium-grained quartz sand containing abundant bioclasts and shell fragments (Figure 25, Table 6). Color becomes progressively lighter up section with some intervals slightly darker than others. Sediments are moderate to well-sorted, and minor planar bedding is present. The foraminiferal assemblage in cores 15DF1 and 15DF3 are consistent with a shallow marine environment (see section 3.4.2). Most of the bioclasts are highly

fragmented and vary in size. A prominent shell bed, 50 to 150 mm thick, is also found within this facies in some cores, typically at the base of the sand bed. This facies is consistent with facies five and six described by McBride et al. (1999) as primarily sand and shelly sand. These sand sheet deposits are thickest in the cores recovered from the ridges and thinnest or utterly absent in the cores recovered in the trough of the study site (Figures 12, 15–17). These facies are present in all cores.

Facies 2: Holocene Interbedded Sand and Mud. Facies 2 is characterized by light to medium-dark gray mud interbedded with very fine-grained sub-bioclastic sand and to some extent, shell fragments (Figure 25, Table 6). Fine-grained sand occurs in beds that are well-sorted and have no sedimentary structures present other than prominent sand-mud interbedding. Beds are mostly 10 to 30 mm thick where individual layers have relatively uniform thickness. At some intervals, the mud is more abundant than sand. This unit is present in cores 15DF1, 15DF3B, 15DF4, and 16DF3A. Bedding patterns are comparable to estuarine and middle-to-inner shelf interbedded mud and sand described by Bentley et al. (2002) and Keen et al. (2004) for the modern shelf and Mississippi Sound estuary 75 to 150 km west of the study area. Evaluation of microfossils suggests a shallow marine assemblage (see section 3.4.2). Foraminifera extracted from core 15DF1 at 3.3 m were radiocarbon dated to 3.9 ka cal BP. Global sea levels estimates for the Holocene puts this date at roughly 3 mbsl (Figure 3) or 0 to 1 mbsl from northern Gulf sea levels (Donoghue 2011). Collectively, these observations suggest that this facies is marine in origin and formed as coastal deposits during the Holocene transgression, but could likely be estuarine based on possible water depth. However, conditions on the lower shoreface of the shelf could also produce similar bedding. In addition, late Pleistocene ages have been determined for all units underlying this lithology, suggesting that the base of these facies (boundary between facies 2 and 3) defines a substantial unconformity.

Facies 3: Late Pleistocene Interbedded Mud and Peat. This facies is characterized by dark grey, tan to dark brown muds, and peats or peaty mud (Figure 25, Table 6). Some intervals are darker than others, especially where woody debris is found. Organic material and woody debris are abundant in this facies. Wood fragments are light brown in color and roughly 10 to 20 mm thick in the cores. No sedimentary structures are evident other than prominent bedding consisting of peat and mud layers. Woody debris visible in the cores correlate stratigraphically to the bald cypress stumps exposed in the scoured trough (Figures 15–17). This facies was not identified by McBride et al. (1999) but is present in nine cores in our study area (15DF1, 15DF2, 15DF3B, 15DF4, 15DF4, 15DF5, 15DF6, 16DF1D, and 16DF3A). This facies was sampled for radiocarbon dating in cores 15DF1 and15DF3B and for OSL dating in core 16DF3A (Tables 2–3). Radiocarbon dates from core 15DF1 ranged from ~41 ka to >50 ka (i.e., radiocarbon dead) suggesting an approximate time of MIS 3 or older (Figure 3). OSL dating results for this facies in core 16DF3A dated to 72 ±8 ka near the boundary between MIS 4 and 5.

Marine macro- and microfossils are absent in the samples studied from this facies (see section 3.4.2), but pollen is present and detailed for core 15DF1 (see section 3.4.1). Pollen assemblages are consistent with modern bald cypress-tupelo gum forest in the basal portion of this facies in core 15DF1 (4.45–4.75 m). This assemblage changes between 4.35 and 4.50 m where percentages of cypress and tupelo gum pollen decline sharply and are replaced by grass and sedge pollen. Reese et al. (2018) suggest this change is likely associated with a more open, possibly brackish environment as sea level increased during the transition out of marine isotope stage (MIS) 3 (Figure 3). However, from 4.30 to 4.20 m, the percentages of cypress increase again and are codominant with alder (*Alnus*). Furthermore, seeds were also found in this facies, and they generally align with pollen results (see section 3.4.3). Sediment properties of this unit are consistent with deposition in a bald cypress swamp producing peat and woody debris in a river floodplain that provides mud beds from episodic flooding (Heitmuller et al. 2017; Smith and Bentley 2015). Overall, there is a coarsening upwards in core 15DF1 where all three facies (Holocene sand, Holocene interbedded sand and mud, and late Pleistocene interbedded mud and peat) show some evidence of bioturbation such as mottling and truncated beds.

Facies 4: Late Pleistocene Interbedded Sand and Mud. This facies displays similar grain size and bedding patterns to facies 2 (Holocene interbedded sand and mud) although this unit contains more fine sand than facies 2, in which coarse grains are mostly fine sand (Figure 25, Table 6). Facies 4 also tends to be more consolidated (higher density), darker in color, has higher organic content (2–4% sometimes evident as woody fragments) than facies 2 (0–2%) (Figures 17–18), and generally contains no marine microfossils (only cores 15DF1 and 16DF7B were examined in detail [see section 3.4.2]). OSL dates from this facies are late Pleistocene in age when the study area would have been located well above sea level. Based on this information, this facies was likely deposited by a terrestrial, freshwater system during late MIS 4 to MIS 3. Such stratigraphy of interbedded sand and mud with woody organic debris produced by a terrestrial fluvial source has been observed in inland fluvial overbank deposits of the northern Gulf Coast, such as in the Atchafalaya Basin in Louisiana (Roberts et al. 1997).

Facies 5: Late Pleistocene Paleosol. This facies is characterized by light gray, yellowish, and orange-colored silt and clay-sized sediments and are only present in two cores: 16DF8A and 16DF8B (Figure 25, Table 6). This unit is identified by McBride et al. (1999) as their facies 1. Evidence of near subaerial exposure is confirmed by the clear traces of oxidation found in these sediments. Organic content determinations were low for this facies. The OSL age obtained from core 16DF8A is 56 ±5 ka (Table 3), which places this paleosol in the late Pleistocene near the boundary of MIS 3 and 4. Such a relatively young age for this core compared to the other cores dated using OSL suggests that this core location may have been elevated topographically, and unburied or exposed for a longer time than other core locations. Furthermore, age constraints from this facies and the overlying Holocene sand indicate the presence of an erosional unconformity between these two deposits (McBride et al. 1999). No macrofossils are evident in the archived core half or sieved samples in this facies (microfossil analysis was not performed).

3.7 Integrated Site Model

Bathymetry data captured characteristic ridge and trough morphology of the modern MAFLA province (Figure 15). Guided by background literature and core data from this project, Obelcz (2017) identified three seismically resolvable surfaces including the seafloor, a transgressive surface, and a basal surface truncating steeply dipping clinoform packages (Figure 26). Two seismic units are resolved from the three surfaces: Unit 1 (U1) is bounded above by the seafloor and below by a relatively flat-lying shoreface ravinement contact consisting of amalgamated shell hash and sand produced by Holocene marine transgression; Unit 2 (U2) is truncated above by the transgressive surface and below by the basal surface. U1 is interpreted to be the Holocene sand sheet (0–5 m thick) with age confirmed by the radiocarbon dating of foraminifera in core 15DF1 (Table 2). U2 is defined to be undifferentiated Pleistocene alluvial plain deposits (swamp/paleosol in the interbedded mud and peat facies) and interbedded sand and mud facies estimated to be 1 to 8 m thick. OSL and radiocarbon dating of these facies confirm the Pleistocene age between 42 and 73 ka (Tables 2–3). The dipping layers below U2 maybe point bar deposits, but Obelcz (2017) interprets them to be Pleistocene bayhead deltaic deposits due to geometry, literature, and constraint by the overlying swamp/terrestrial facies. These sequences are prograding, and generally, dip southwest with the incline increasing towards the east and with channel crosscutting apparent to the south.

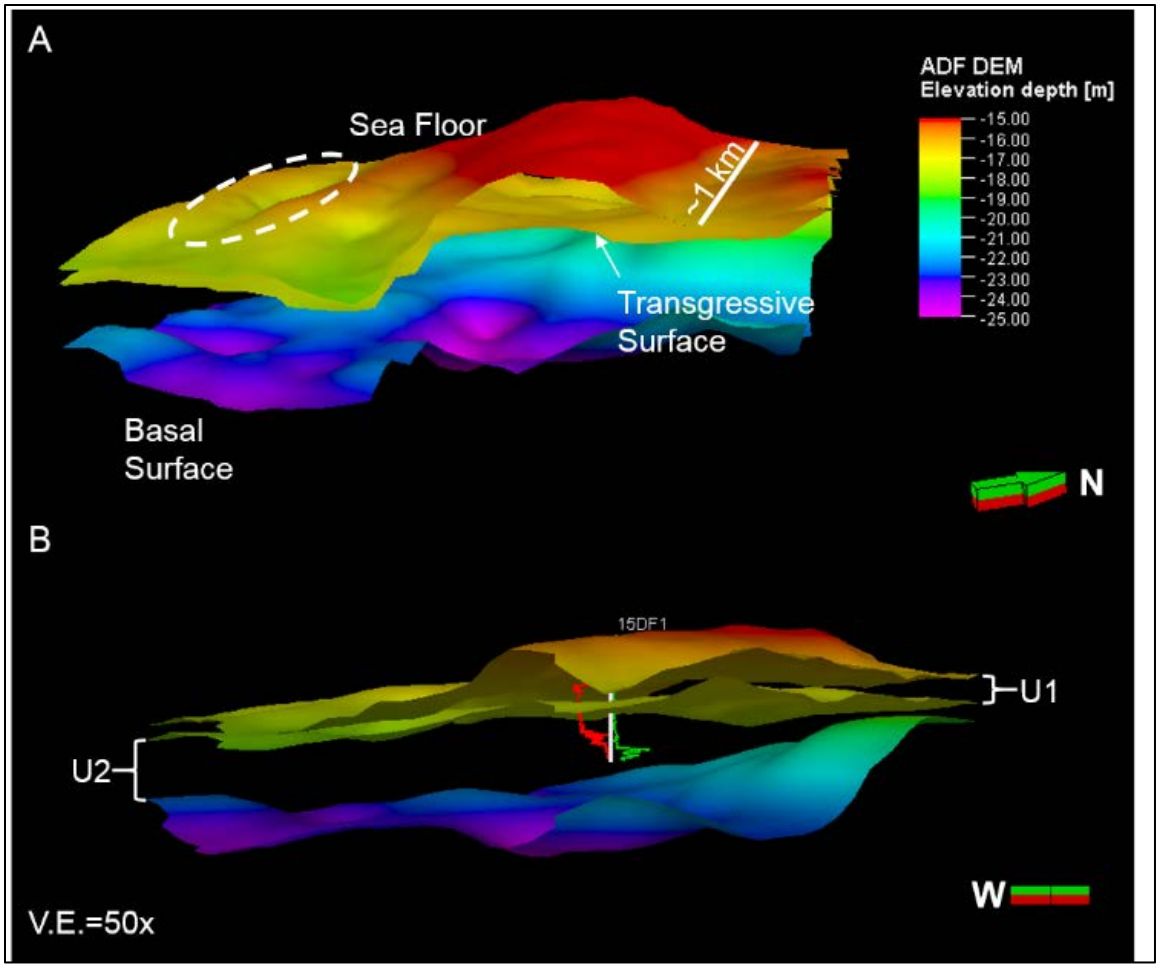

Figure 26. Three-dimensional subsurface model of the study area.

a) White dashed circle represents where stumps are exposed on the surface. b) Core data (15DF1) was imported to aid interpretations with grain size (red) and LOI (green) shown. The transgressive surface is relatively flat-lying while the basal surface geometry exhibits topographical highs. No cores penetrated the basal surface. Vertical exaggeration (V.E.) is 50x.

The base of U2 exhibits variable topography (Figures 26–27), and the presence of a paleosol (16DF8A) on top of one of these paleohighs suggests that there was paleorelief, which may have contributed to the preservation of the forest in a topographic depression. The thickness of the alluvial fill package (U2) is thickest in the central area of the study site and thinnest in the northeastern and southeastern corners where paleosols are present. The analysis shows that there was enough accommodation to allow at least 8 m of sediment accumulation (possibly in pulses) (Figure 27) before being eroded during lowstands and Holocene transgression.

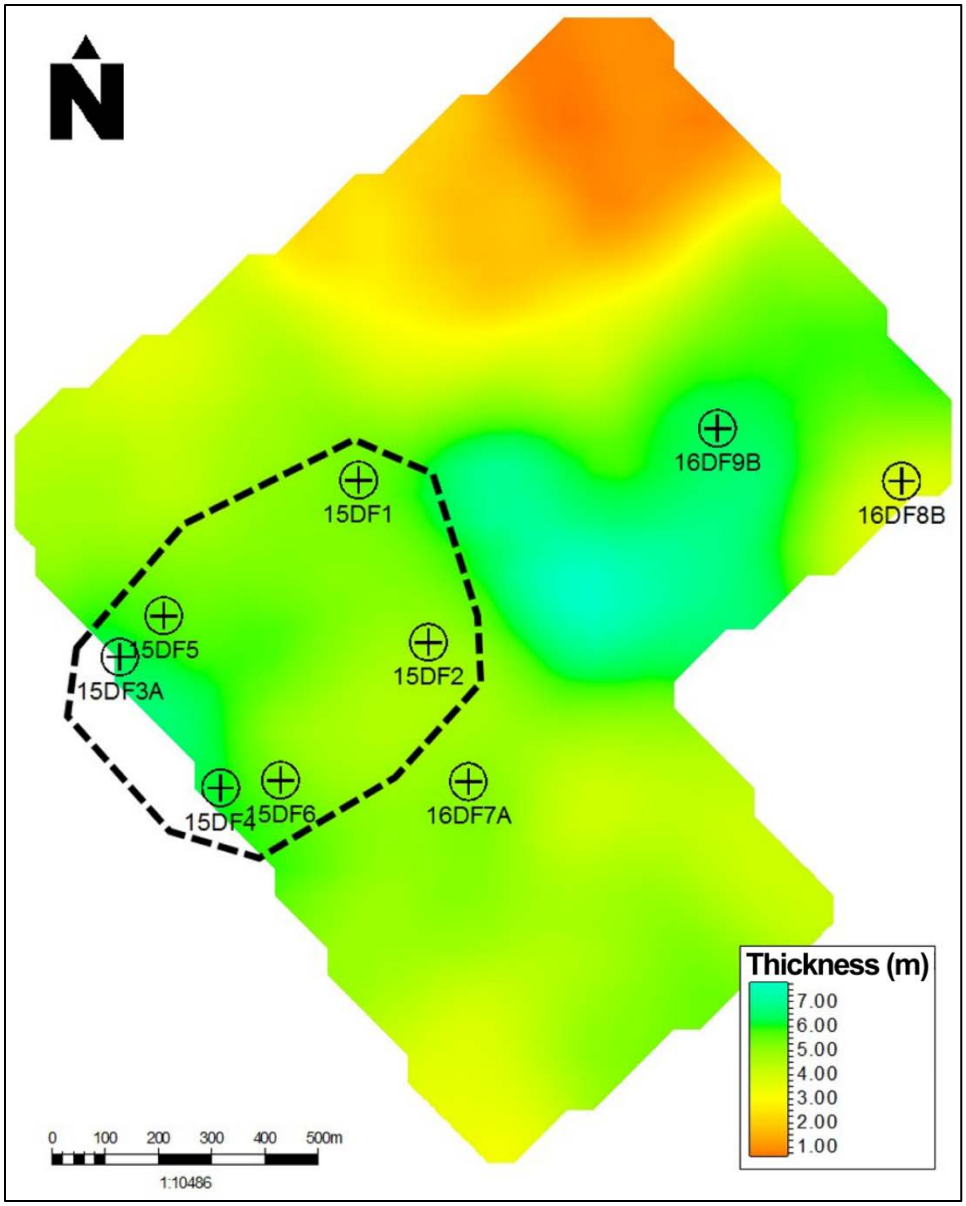

Figure 27. The thickness of U2 in the study area.

U2 is thickest in the central area of the study site. At least 8 m of sediment accumulated before being partially eroded during the sea level lowstand and Holocene transgression. U2 is thinnest in the northeast and southeast corners where paleosols formed (cores 16DF8A and 16DF8B)). The dashed line represents approximate area where peat and wood were observed in cores.

4. Discussion

Bartek et al. (2004) reconstructed the Mississippi and Alabama coastline from the marine isotope stage (MIS) 2–3 highstand approximately 35,000 years ago to the Holocene. The MIS 3–4 highstand may be similar to the interval when the ancient forest was growing; however, further dating and core analysis are needed to determine the geomorphological character of the leading study site. This provides a beginning context for interpretation of the results from this study. The discussion of results is summarized here including geophysics in Obelcz (2017), regional stratigraphy in Truong et al. (in review) and Gonzalez et al. (in review), and paleoenvironmental interpretation in Reese et al. (2018) and Harley et al. (in revision).

4.1 Geophysics

Based on previous research (Kindinger 1988, Bartek et al. 2004) and new CHIRP data (Figure 13), the dipping reflectors underlying the entire survey area are interpreted to be bay-head delta deposits, although the geometry could also indicate fluvial lateral accretion deposits. This interpretation was not ground--truthed because no cores penetrated this sequence but is based on sigmoidal reflector geometry and overlying terrestrial facies. These deposits are associated with sea-level transgression, wherein valleys incised across the shelf during sea-level lowstands become deltaic depocenters as the coastal zone (and locus of deposition) moves landward with rising sea level. The steeper-dipping reflectors to the east are logical given the site's location on the western edge of the Mobile paleovalley; steeper gradients would be expected as the axis of the paleovalley (greatest accommodation space) is approached.

Bay-head facies are overlain by terrestrial facies. These include the swamp facies (Late Pleistocene Interbedded Mud and Peat [LPIMP]) in which the drowned forest is situated and paleosol (Late Pleistocene Paleosol [LPP]) in the eastern survey area. There is an erosive unconformity, which forms a reflector of variable amplitude, at the base of the swamp-paleosol strata (LPIMP-LPP) that truncates the bay-head facies; this is interpreted as the transition between marine-estuarine (bay-head delta) and terrestrial (swamp-paleosol) environments. The swamp and paleosol lithofacies (LPIMP-LPP) are stratigraphically coeval; the lateral boundary between them is not apparent in the seismic data.

The penultimate stratigraphic layer is a transitional facies, which is not ubiquitous throughout the survey area. Where it is present, it lies in between swamp-paleosol (LPIMP-LPP) and sand sheet facies (Holocene sand [HS] and Holocene interbedded sand and mud [HISM]) and is lithologically a mix of interbedded muds and sands. The transitional layer is seismically indistinguishable from the underlying terrestrial facies. This layer is interpreted to be a transition between terrestrial or potentially estuarine and marine environments, hence the nomenclature. The bay-head, swamp, paleosol, and transitional facies combine to compose Seismic Unit 1 (Figure 13).

The uppermost layer is the transgressive/marine Mississippi-Alabama-Florida (MAFLA) sand sheet, or Seismic Unit 2. Previous studies have speculated whether the MAFLA sand sheet was entirely formed during and after sea level transgression, or whether bathymetric ridges (Figure 10) are partially or entirely relict Pleistocene barrier island complexes (McBride et al. 1999). Due to the lack of internal stratigraphy (Figure 28), characteristic of barrier islands (washover fans, seaward progradation), the sand sheet in this region is interpreted to be a syn or post-transgressive feature.

Buried tree stumps were not confidently resolvable within the subsurface using CHIRP sub-bottom profiling. This is hypothesized to be due to one of the following two factors, or both: 1) individual tree stumps are at or below the horizontal resolution of the CHIRP sonars used, which is a function of Fresnel zone geometry that is controlled by a number of factors including trace offset, source-receiver geometry, and others; or 2) the acoustic impedance contrast between wood and the sediments they are buried in and between wood-bearing sediments and the surficial sand sheet are similar enough to be indistinguishable.

A sub-bottom system with a smaller ensonifying seafloor footprint, such as an ROV-mounted CHIRP deployed a few meters above the seafloor, would address factor 1. Resolving factor 2, however, would be challenging when using acoustic methods.

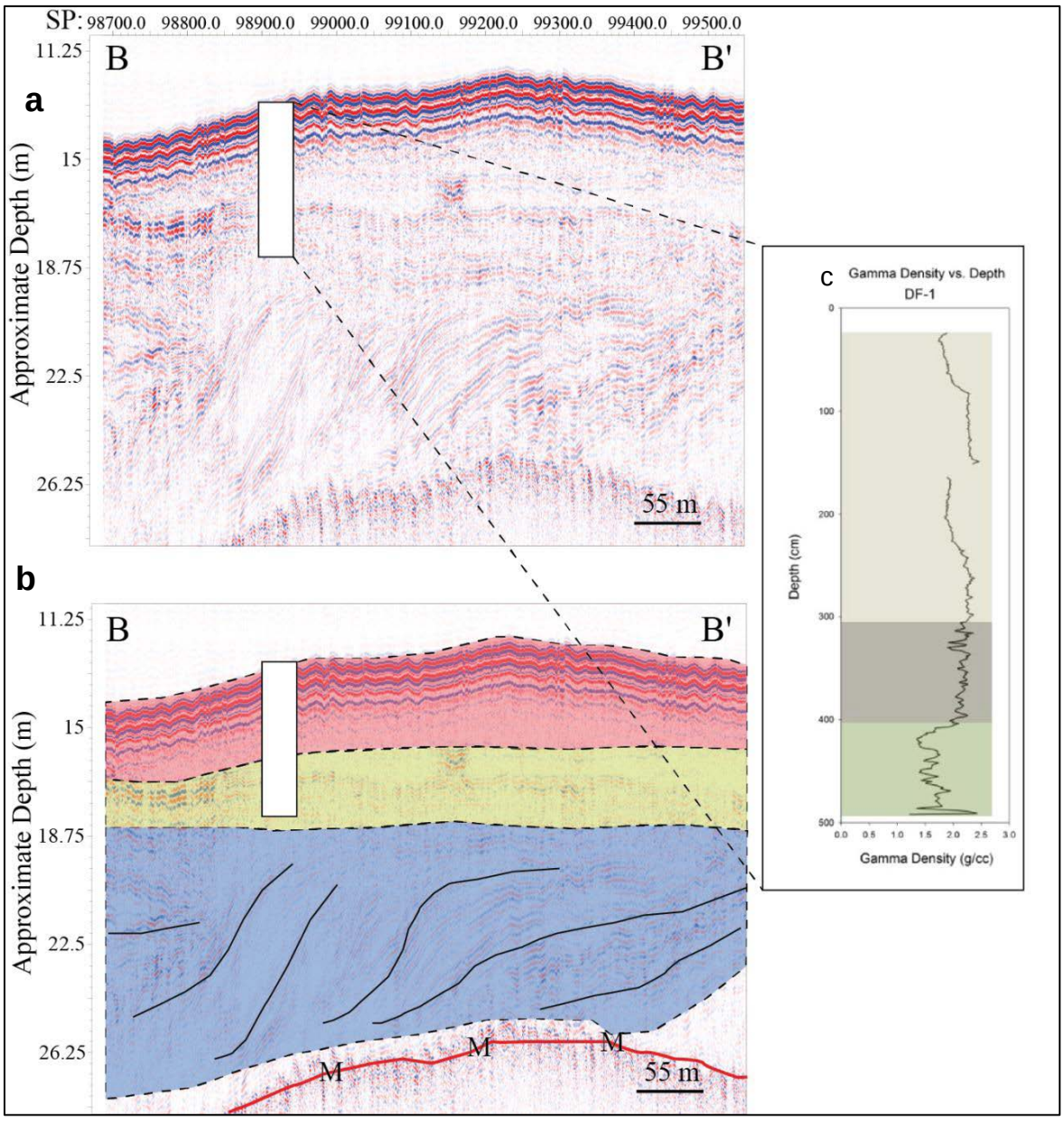

Figure 28. CHIRP sub-bottom profile for B-B′.

Uninterpreted (a) and interpreted (b) strike-oriented CHIRP sub-bottom profile taken across the largest sand ridge in the survey area (see Figure 10). Note the lack of internal stratigraphy within the sand sheet (red), which indicates that these features are entirely reworked during or after transgression, as opposed to relict Pleistocene beach ridges or barrier islands. The yellow layer is undifferentiated terrestrial Pleistocene deposits, which may include swamp, paleosol, or floodplain facies. Below that are bay-head delta facies (blue) with diagnostic clinoform geometry. The red line “M” is a seafloor multiple. (c) Gamma density profile of core 15DF1 acquired in the vicinity of the CHIRP profile where tan indicates sand sheet facies, gray indicates transitional facies, and green indicates swamp facies.

4.2 Paleoenvironmental Interpretation

4.2.1 Pollen

Although a high-resolution chronology for core 15DF1 has not been established, dating places the samples analyzed herein MIS 3–4, during a period of rapid sea-level fluctuations with amplitudes much higher than 10 m (Figure 3). DiMichele and Falcon-Lang (2011) proposed that rapid sea-level rise and corresponding floodplain aggradation are effective methods both to bury and to preserve autochthonous forests. Anderson et al. (2016) documented rapid Pleistocene floodplain aggradation for rivers of the north-western Gulf in a setting similar to the study site, where they found that floodplain aggradation rates tracked sea-level rise 1:1 up to >100 km inland. These observations suggest that the study area was buried deeply, after which glacial sea-level fall and marine transgression removed most of the overburden, allowing the forest strata to be exposed by recent energetic marine processes.

Pollen results from the lowermost section of the mud–peat layer shows a pollen assemblage typical of southeastern US cypress-tupelo backwater (Reese and Liu 2001), with high concentrations of cypress and tupelo and minor components standard in bottomland hardwood environments, which include the sedge family. Typically, bald cypress has biogeographical limits of 50 m in elevation but can occur up to 150 m (Little 1971), which agrees with previously discussed estimates for forest age, global sea level, and pale elevation. These conditions probably existed for some time while the site was exposed and, further inland, separated hydrologically from the littoral zone.

At 4.50 m in core 15DF1 there is a change in the pollen assemblage to a more open, grass-dominated environment. This shift in the pollen assemblage probably corresponds to the impacts of a marine transgression that occurred in later MIS 3 or MIS 4 (Figure 18). It is hypothesized that as sea level rose, floodplain aggradation occurred far inland (Anderson et al. 2016), which may have resulted in an increased water table and an altered flood regime that drove this vegetation change (Schumm 2005, Johnson et al. 2012). The first appearance of both cattail and *Sparganium* (bur-reed), along with the abundance of grass, helps to support this interpretation. However, the establishment of a more open environment was not a static change. In this depth range, from 4.30 to 4.20 m in core 15DF1, results show an interesting change in pollen assemblage. Percentages of grass pollen drop below 10%, while cypress and alder become prominent. This environment may represent a no-modern analog cypress–alder community. However, note that this assemblage has some commonalities to the modern-day Atlantic Coastal Plain Blackwater Levee/Bar Forest (Schafale 2009). This plant association occurs in coastal portions of North and South Carolina along relatively young sand bars or natural levees on blackwater streams. The association is described as having a different structure, with the canopy dominated by *Betula nigra* (river birch), bald cypress, and oaks. Shrubs and herbs are generally sparse, although patches of *Alnus serrulata* (hazel alder), *Cyrilla racemiflora* (swamp titi), and *Vaccinium elliottii* (blueberry) may exist (Schafale 2009).

During this cypress–alder event, *Betula* and oak pollen is still very low, and therefore, this may not be a true analog. However, at the end of this event, as grass pollen begins to increase back to 50–60%, birch pollen does show a slight increase to roughly 10% of the pollen total. It is possible that the formation of bars and new natural levees could have hosted this cypress–alder assemblage, resulting from floodplain aggradation driven by sea-level rise (Gonzalez et al. 2017). In addition, floodplain aggradation and the accompanying sea-level rise may have been the mechanisms that rapidly buried and preserved the terrestrial sediments at this site (DiMichele and Falcon-Lang 2011, Gonzalez et al. 2017). Above 4.20 m, the grass-dominated assemblage returns to the top of the peat section at 4.05 m where the layer of interbedded sand and mud begins.

In summary, pollen assemblages have been determined for core 15DF1 recovered near a unique preserved forest site in the northern Gulf. The peat and mud deposits in this core have been dated to MIS 3–4 during a period of rapid global sea-level variations, providing a glimpse into the response of late Pleistocene plants to climate change and sea-level rise. Based on the radiocarbon dates obtained in the upper section of the peat, the marine transgression that probably caused the final burial of the peat occurred around 40 ka BP near the end of MIS 3. Pollen results within the peat suggest a transition from a cypress-tupelo gum backwater to a more open community dominated by grasses and sedges. During this transition, there may be evidence of a no-modern analog cypress–alder community although additional pollen work is needed, over a wide variety of cores, to enable a more comprehensive explanation of the MIS 3–4 vegetation dynamics at the site.

4.3.2 Wood

The rapid decline in growth towards the end of the chronology (Figure 24) combined with the finding that 8 of 10 samples contained the same outermost partial growth ring inside bark suggests that some event resulted in synchronous tree mortality, at least for most of the individuals included in the submerged forest chronology. Unfortunately, the study design and the nature of the data allow only speculation as to the causal mechanism responsible for such a widespread mortality event. Some of the potential disturbance agents in the region that could have resulted in widespread mortality include fire, insect outbreak, drought, sea-level rise, and tropical cyclone. After careful inspection of the macrofossil wood specimens, no evidence (e.g., insect galleries, fire scars, or mechanical wound scars) was found that provided clues to a mortality agent. Modern bald cypress is not known for being susceptible to pests, and a widespread fire or tropical cyclone would have likely caused immediate mortality of trees, which does not align with the growth trends in the Submerged Forest tree-ring Chronology (SFC) during the last ~140 years of the record. Bald cypress along the Gulf Coast are thought to be a tropical cyclone resilient species along with *Quercus viginiana* (live oak). Certain characteristics such as tree morphology and architecture and rooting structure are considered adaptations to high wind events (Doyle et al. 1995). Studies of coastal bald cypress growth patterns within tidal freshwater swamps show salinity to be a limiting factor (e.g., Thomas et al. 2015). Abrupt climatic shifts known as the Dansgaard Oeschger Event (DO) and Heinrich Event (HE) occurred during the glacial and are characterized by rapid and repeated climate shifts. At only 489 years in length, the SFC time series is too short to analyze for DO and HE events if they are the cause of the tree death. However, additional tree ring samples extending the floating chronology could capture this climate variability. The two most likely disturbances that could have led to the growth trends expressed in the SFC are: (1) long term drought conditions during the period years ~350–430, then a switch to pluvial conditions causing the growth release during the period years ~430–480, or (2) a rapid variation in localized marine transgression and regression.

Mapping the Gini coefficients for the 39 bald cypress tree-ring chronologies distributed throughout its modern geographic range revealed unique patterns concerning tree ring diversity (Figure 29). First, bald cypress individuals located at the southwestern range limit in Texas, the southern range limit in Florida, and the northern latitudinal range limit in North Carolina and Virginia were characterized by the least diversity as shown by the Gini coefficients. Trees that exhibited the highest diversity were located along the Mississippi River Valley, Atlantic Coastal Plain, and the Gulf Coast, which included the Pascagoula River (PASC) chronology. More specifically, the tree ring diversity of the submerged forest chronology (Gini = 0.24) was most similar to a collection from South Carolina (SC006; difference = 0.002), Arkansas (AR052; difference = 0.003), Georgia (GA003; difference = 0.004), North Carolina (NC026; difference = 0.008), and Mississippi (Pascagoula River; difference = 0.01). To investigate the temporal variability of ring width diversity throughout the SFC record, the Gini coefficient was calculated in 100-year intervals. Tree ring diversity (e.g., sensitivity) steadily declines during the first 400 years of the record, then increases sharply from year 400 to the end of the record in year 489. This change in temporal tree ring

diversity is interpreted to represent an event, or series of events, that likely caused physiological stress to individual trees.

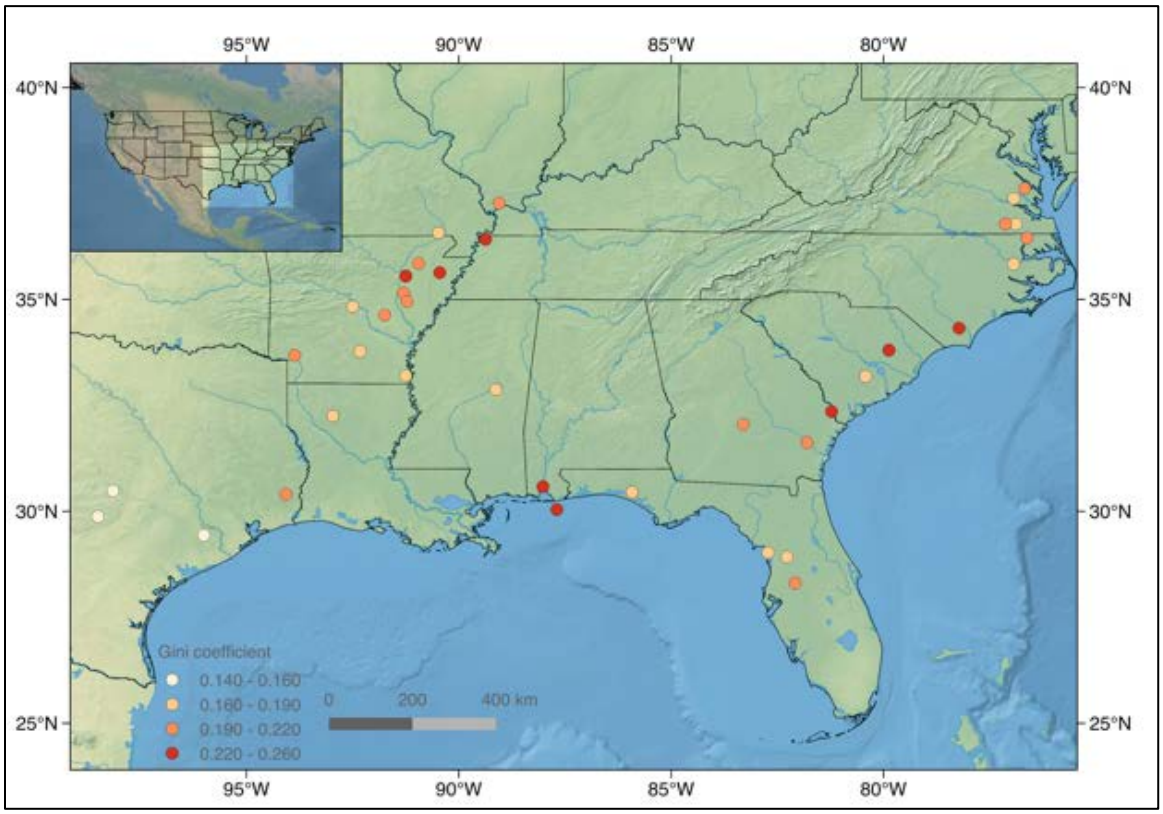

Figure 29. Gini coefficients for the glacial and modern bald cypress tree-ring indices.

Map showing the distributions of Gini coefficients of the available *T. distichum* chronologies throughout its geographic range and locations relative to the submerged forest chronology in the northern Gulf.

Spectral analysis of the SFC over the period year 100–489 identified frequencies in the time series that are significantly different from a red-noise assumption in the interannual (2–3 year; p <0.05–0.01) and at low, multidecadal frequencies (p <0.01) (Figure 30). The same analysis revealed similar frequency patterns for the PASC chronology spanning the period 1466–2014 CE for interannual and lower frequencies (p <0.01). Morlet wavelet analysis indicated that the interannual frequency in the SFC was present throughout most of the time series, from year 100 to year 350 (Figure 30). After year 350, the interannual frequency fades coeval with the gradual decline in growth, most likely associated with growth conditions that were slowly becoming more adverse. The derivative of Gaussian (DOG) wavelet analysis, which is more appropriate for capturing events but not oscillations, reveals single events the span either 16-years, 60-years, and 250-years exist throughout most of the SFC record. Modern-day bald cypress growth rings are known for having a consistent and robust sensitivity to moisture availability and precipitation (e.g., Stahle et al. 1998, Stahle et al. 2012, Cleaveland 2000). The Pascsgoula tree-ring chronology (PASC) reference chronology was found to be strongly correlated with regional precipitation from April to June for the period 1901 to 2014 (r >0.6; p <0.01). The 2–3-year periodicities identified in the spectral analysis fall within the range of variability often associated with El Niño-Southern Oscillation (ENSO), which is known to influence precipitation and river discharge in the southeastern US (Schmidt et al. 2001). However, the correlation between the PASC chronology and (1) a reconstruction of sea surface temperature (SST; HadISST 1º; Rayner et al. 2003) and (2) SST anomalies from the NINO3.4 region masked from the National Oceanic and Atmospheric Administration (NOAA) ERSSTv5 (Huang et al.

2017) was tested and did not yield any significant associations between the PASC chronology and either version of ENSO.

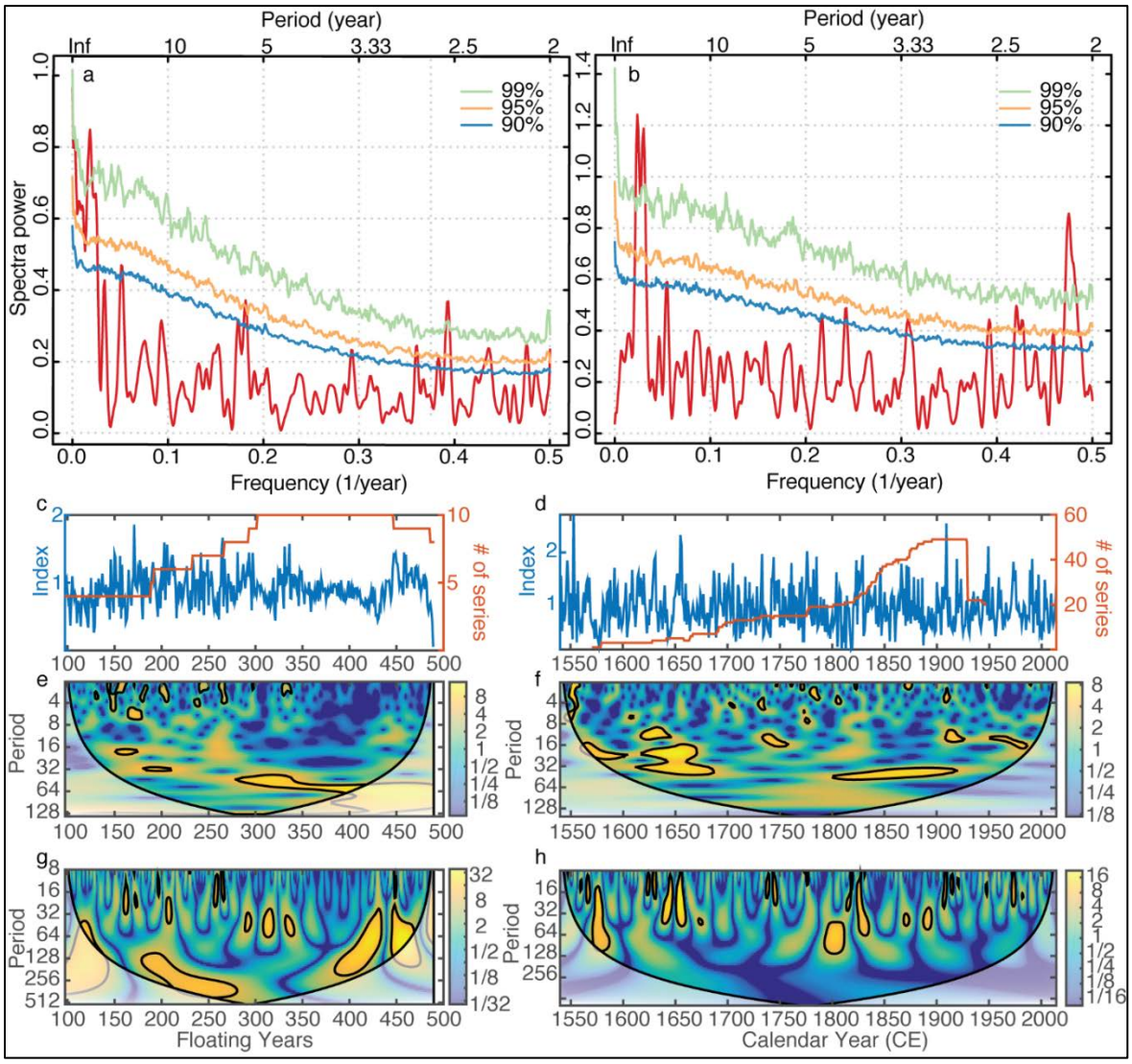

Figure 30. Spectral analyses of tree-ring indices.

Lomb-Scargle spectrum (a–b and wavelet spectra (e–h) of (left) SFC and (right) PASC chronologies. Respective chronologies (c–d) appear above wavelet spectra for reference. The top wavelet is the Morlet mother wavelet (e–f), and the bottom is a DOG mother wavelet (g–h).

The most notable aspect of the SFC record is the changing growth trends from year 350 to the end of the chronology at year 489 marked by synchronous mortality in year 490. Bald cypress is known to have the ability to survive prolonged periods of flooding. In addition, previous research has found the establishment (e.g., Chabreck 1972) and survival of seedlings to be somewhat salt-tolerant. In a controlled experiment, Pezeshki (1990) watered bald cypress seedlings with a saltwater solution for 60 days and found no significant effects on the treatment on height growth, stomatal conductance, or net photosynthetic rate compared to seedlings treated with freshwater. However, Connor (1994) found 100% mortality of seedlings subjected to treatments of regular saltwater flooding. Hence, the combined disturbance of saltwater and flooding (e.g., saltwater inundation) is considered to be detrimental to the survival of bald cypress (e.g., Pezeshki 1990; Javanshir and Ewel 1993; Conner 1994). Coastal wetland

areas along the southeastern coastal plain and more specifically, the northern Gulf have been subjected recently to increases in flooding and saltwater intrusion due to the combined effect of land subsidence and human-induced climate change and sea-level rise (e.g., Krauss et al. 2009; Thomas et al. 2015).

Krauss et al. (2009) found a robust negative relationship between site salinity and tree height, basal area and individual tree basal area increment within bald cypress forests in South Carolina, Georgia, and Louisiana. Given the nature of the submerged forest study site in the Northern Gulf and the subfossil material found there, precisely the causal disturbance mechanism that resulted in synchronous tree mortality and subsequent burial of trees cannot be determined. Yet, study results indicate that based on (1) the previously established relationship between increased salinity and basal area increment and (2) the growth trends during the last ~140 years of the SFC chronology that trees were responding negatively to gradual increase in saltwater intrusion that ultimately leads to the rapid decline in growth and mortality of trees.

Accelerated sea-level rise under current conditions of global climate change continues to impose stress on coastal forests. Along the northern Gulf, the combination of natural processes (e.g., land subsidence) and sea-level rise is causing the progression of saltwater mixing and flooding events upslope and inland. Observations along coastal forest margins report that various tidal freshwater forests of the Gulf and southern Atlantic coasts are undergoing dieback reportedly related to saltwater intrusion and tropical cyclone-induced surge events (Brinson et al. 1985, Brinson et al.1995, Gardner et al. 1991, Ross et al. 1994; Williams et al. 1999, Williams et al. 2003, Williams et al. 2007, Doyle et al. 2003, Doyle et al. 2010, Conner et al. 2007, Krauss et al. 2009, Saha et al. 2011). Despite an increase in research focused on predicting coastal species responses to rising ocean levels, ecological models are needed for regional-scale predictions of how coastal forests will adapt under changing climate and sea-level rise could benefit from dendrochronological data.

Although with this tree-ring study a confident causal mechanism for the synchronous mortality and rapid growth variability at the end of the SFC record could not be identified, the most likely causes were either singular or combined events of drought and saltwater intrusion from sea-level rise or storm surge. The 489-year SFC record presented here provides a baseline on which to build future research at the site. Future work and subsequent sampling trips will be focused on extending the length of the SFC chronology and investigating additional sites with preserved macrofossil wood that were recently discovered at various shallower depths leading inland. These paleoenvironmental records will provide a better understanding of the dynamics of rapid sea-level rise that likely occurred in the past, which can be used to inform coastal communities of what to expect in the near future.

4.3 Regional Stratigraphy

The depositional environments and regional stratigraphy of the study area during the Pleistocene and the Holocene have been greatly impacted by changes in sea level in the northern Gulf. Consequently, events of marine transgression and regression have played a significant role in shaping the stratigraphy observed at this site today. The discussion summarized here is from Gonzalez et al. (in review) and Truong et al. (in review).

4.3.1 Foraminiferal-Environment Interpretation

The surficial sediments in core 15DF1 are dominated by massive, medium-fine sand (Gonzalez et al. 2017) with a relatively homogeneous *Rosalina-Hanzawaia-Elphidium*-miliolid assemblage (Figure 19). *Amphistegina, Archaias, Asterigerina, Nodobaculariella*, Peneroplids, and Soritids, often termed calcareous-bank microfauna (CBF), are present in core 15DF1 (Figure 19, Appendix A). Modern CBF can be found in Cedar Key, Florida (a low-energy siliciclastic coastal setting on the northwest Florida

coast) and on carbonate banks situated on salt domes, and therefore CBF occurrence in modern foraminiferal assemblages are a relict product of shoreface ravinement (Kohl et al. 2004). The surficial foraminiferal assemblages are interpreted as being derived from normal marine conditions (Culver 1988, McBride et al. 1999, Kohl et al. 2004) and deposited in an inner neritic open marine environment similar to the present; this facies is congruent to facies 6 described by McBride et al. (1999). The present seafloor surface will be the future maximum flooding surface marking the boundary between the transgressive systems tract and the highstand systems tract (McBride et al. 1999, Gonzalez et al. in review). A shell bed located from 2.60 to 2.75 m and 3.15 m in core 15DF1 (Figure 9) was produced from shoreface ravinement and continued to be reworked by oceanographic processes (Anderson et al. 1997).

Below the lowermost shell bed (3.15 m), a zone of interbedded sands and muds persists in core 15DF1 (Figures 9, 19). Lithologic variability within the interbedded sand and mud facies is congruent with assemblage variability (Figure 9). Silty sediments correlate with little-to-no preservation of tests (Figure 9). Beds of sandy sediments at 3.60 m and 3.80 m yielded foraminiferal assemblages that are similar to the sand sheet communities with the exception of a sharp decline in miliolids (Figure 9). Foraminifera are present in low abundances and combined with observed test discoloration suggest taphonomic alteration for this core section rather than poor living conditions (Scott et al. 2001, Berkeley et al. 2007). The lack of CBF in the interbedded sand and mud facies provides additional evidence of a pre-shoreface ravinement environment (Anderson et al. 1997). The dark grey interbedded sand, and mud facies (Gonzalez et al. 2017, Gonzalez et al. in review) is lithologically similar to facies four described by McBride et al. (1999) with a slightly different foraminiferal assemblage (Figure 9). McBride et al. (1999)'s facies 4 exhibits an *Elphidium-Haynesina* assemblage that can also be found in many modern bays across the northern Gulf (Bandy 1956, Gangopadhyay et al. 1996, Osterman et al. 2009, Poag 2015), whereas interbedded facies at the study site host more neritic genera (*Rosalina*, *Asterigerina*, *Cibicides*, and *Hanzawaia*) (Figure 9). Radiocarbon dating reveals that sandy portions of the interbedded sand and mud facies were deposited before 3,920 cal BP whereas peaty portions in these facies (e.g., 3.22 m) are older Pleistocene peats reworked in this facies (Figure 9, Table 2). Sea level was ~2 to 4 m lower than present at 3,920 cal BP when sea-level rise started to decline from ~1 to 1.4 mm/year to 0.6 mm/year (Figure 3) (Balsillie and Donoghue 2004). A change in depositional style within Mobile Bay, possibly from rapid retreat of the bay-head delta (4.3–3.0 ka) or from increased storm activity (Twichell et al. 2012), is coeval. Additional evidence for increased storm activity is provided by lithologically similar marine interbedded sand and mud facies, which were preserved as hurricane event horizons in the Mississippi Sound (Bentley et al. 2002, Keen et al. 2004). Alternatively, the possibility exists that the interbedded sand and mud facies is coeval with facies 4 of McBride et al. (1999) but in a more seaward position of the estuary indicating increased marine influence. Sequences of open bay muds overlying pre-Holocene deposits suggest that a barrier island system existed pre-inundation (Mars et al. 1992). This introduces the scenario that these foraminiferal assemblages could be relict barrier island over-wash deposits, and hence, poor preservation. The integration of these results advocates that the interbedded sand and mud facies in core 15DF1 was deposited in a lower shoreface or marine dominated estuarine environment of the Holocene and was not a result of Pleistocene floodplain deposition.

The cessation of foraminiferal assemblages, in combination with pollen (Reese et al. 2018) and sediment core results (Gonzalez et al. in review), suggests the interbedded mud and peat facies as terrestrial in origin and associated with a peat accumulation sequence (Fisk 1960). A floodplain facies sample from core 16DF3A and optically stimulated luminescence (OSL) dating (72 ±8 ka; Table 3) provides an age for the earliest possible forest growth and constrains floodplain deposition to the falling stage systems tract (Figure 3). The succession of cypress assemblages to marsh environments (Figure 31) in the peat layers may be attributed to floodplain aggradation that accompanied pulses of sea-level rise during MIS 3 and 4 (Figure 3).

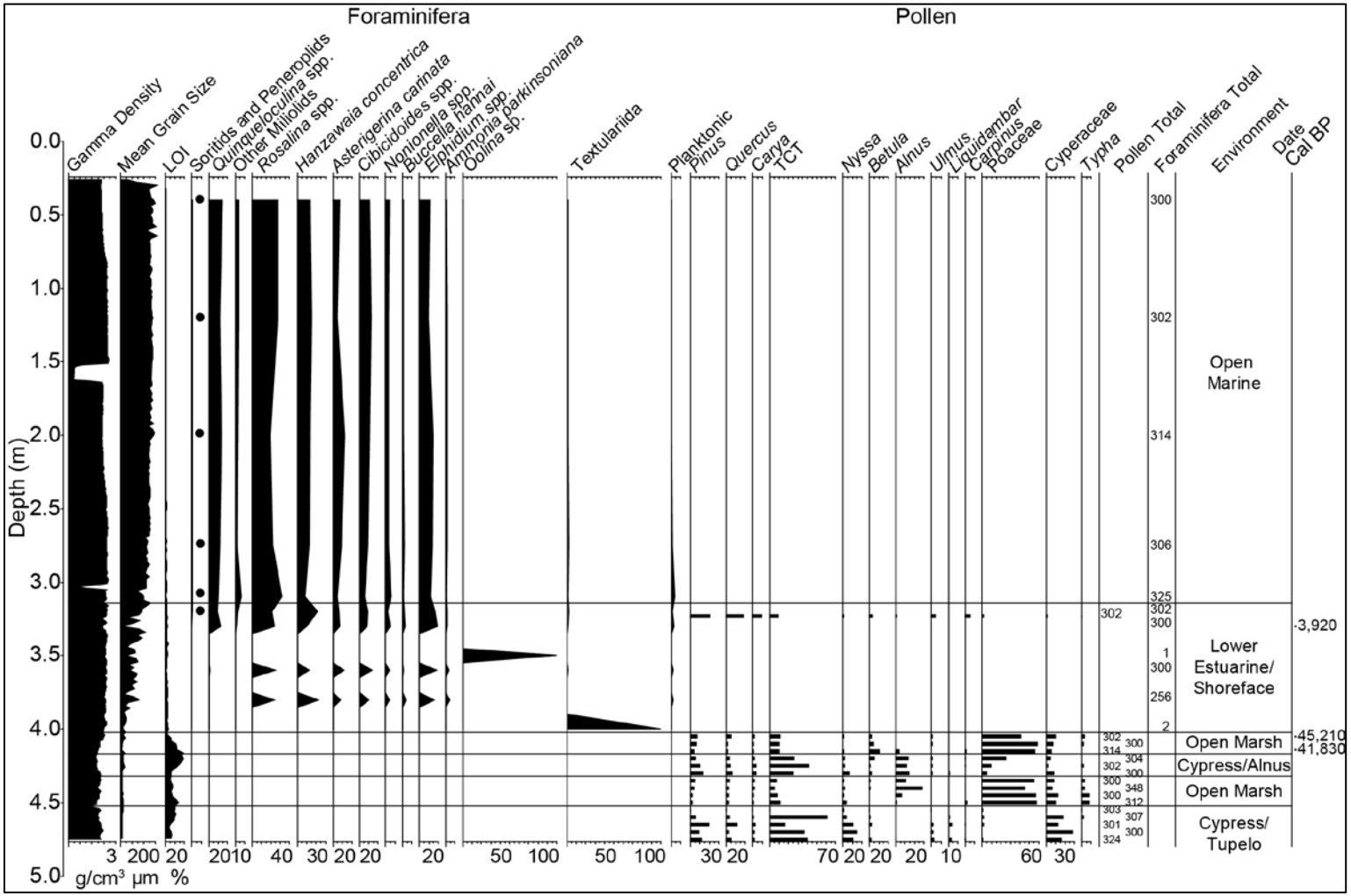

Figure 31. An abbreviated chart of the foraminiferal and pollen assemblages for core 15DF1.

Gamma density, mean grain size, and LOI analysis was completed by Gonzalez et al. (2017). Pollen analysis is summarized in section (4.2.1). TCT (Taxaceae-Cupressaceae-Taxodiaceae) pollen is interpreted as *T. distichum*.

4.3.2 Depth-Age Relations and Lateral Correlation

The stratigraphy and facies of the study area are characterized by substantial geological and chronostratigraphic variability over short lateral and vertical distances (Figure 32). A roughly east-west cross-section (Figure 32) across the trough and ridge shows depth and age relations among facies in cores (all cores are georeferenced to their respective seabed depth and location) and the stratigraphic correlation in the study area. The depth of the Holocene ravinement surface is noted (also shown in Figure 10 but without detailed core data). The cross-section shows that both Holocene interbedded sand and mud and Pleistocene interbedded mud and peat occur in topographic lows and in some core locations have been eroded or are missing from the sedimentary record. Additionally, both of these facies are missing from the topographic high (sand ridge) in the easternmost core locations where the Holocene sand sheet lies directly upon the Pleistocene paleosol and on Pleistocene interbedded mud and sand at slightly deeper depths in cores 16DF9A and 16DF8A. The Holocene interbedded sand and mud is discontinuous, and it is missing from core 15DF6 inside the trough where stumps are exposed.

These observations suggest that paleo-topography (Figure 32) played a role in both the deposition and preservation of the muddy wood-bearing deposits. Holocene interbedded sand and mud were likely deposited in paleo-topographic lows on the Holocene ravinement surface and may have been eroded at the location of core 15DF6 at or near the time the trough was eroded, and the stumps were exposed (Figures 15, 32). Similarly, the Pleistocene interbedded mud and peat appears to have been deposited, or at least preserved, in a topographic low with respect to the elevation of Pleistocene interbedded sand and mud found in cores to the east.

If all of the radiocarbon and OSL dates (Tables 2–3) are reliable, and the actual ages are within the uncertainty estimates (2σ) for each date and are representative of depositional age, then both of the muddy Pleistocene deposits may have been deposited at or near the same time (Figure 3, Figure 32). Concomitant with that deposition scenario, the peaty deposits may have been forming in topographic lows while paleosols were developing on slightly higher ground to the east. These conditions are consistent with the geology and geomorphology of the nearby modern coastal plain where Pleistocene coastal and fluvial deposits (from MIS 5 and earlier) deposited at or uplifted to higher elevations are being eroded, incised, and weathered to form soils, and where many topographic lows are being filled with modern fine-grained sediments and wetland vegetation.

Paleo-topography may have also influenced the time of burial. For example, the bottom of the Pleistocene interbedded sand and mud in core 16DF7B has an OSL age of 73 ±6 ka (Table 3), and it is the deepest core in the study site in terms of absolute elevation (Figure 32). In contrast, the bottom of core 16DF8A has the youngest OSL age of 56 ±5 ka (Table 3), and it is the shallowest core. Generally, older ages are stratigraphically and topographically located below younger ages. This finding is confirmed by the presence of highly oxidized paleosols found in two cores (16DF8A and 16DF8B; Table 6) indicating that the paleo-topographic highs in the study site were subaerially exposed before the Holocene transgression that further eroded and flooded the area (Figures 15, 32).

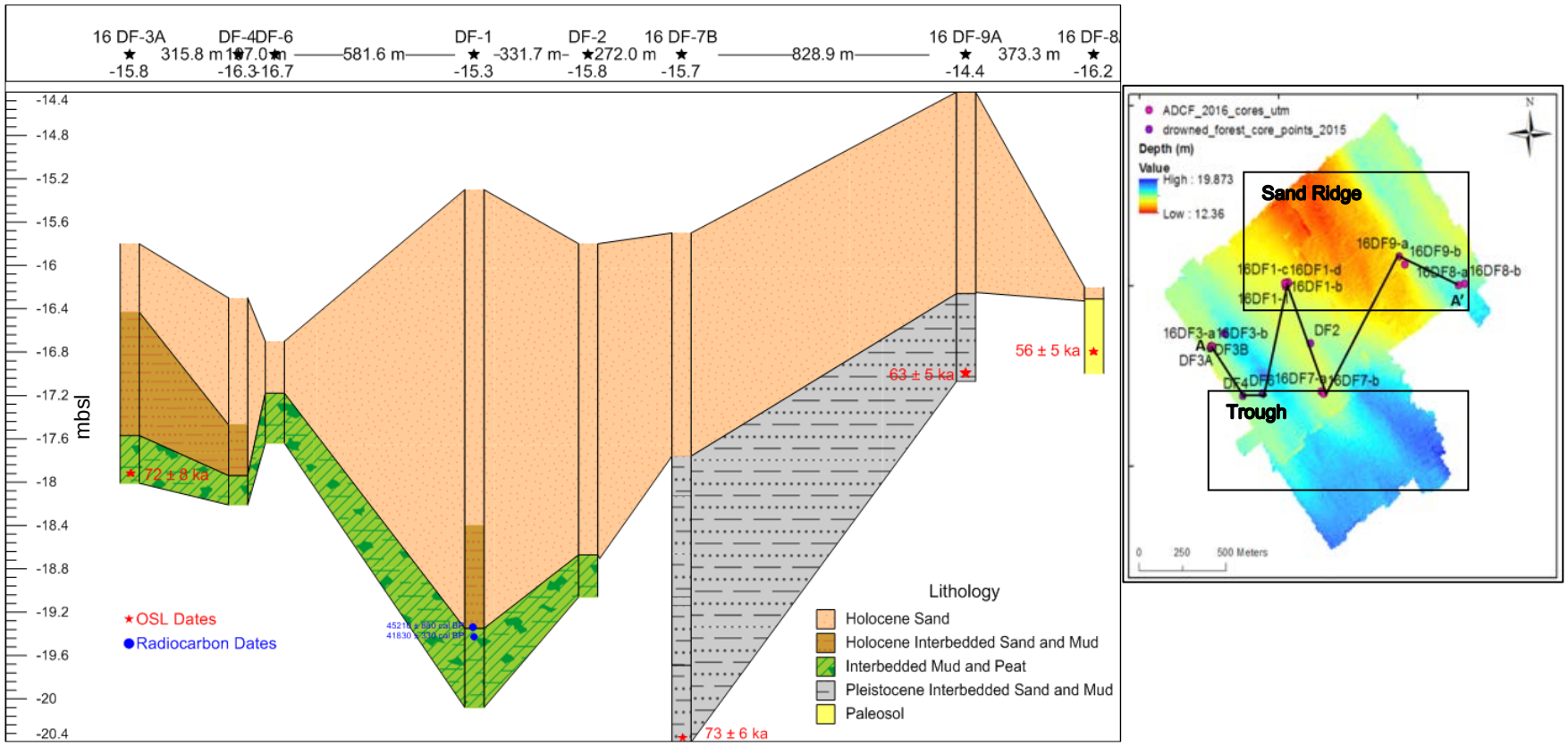

Figure 32. Stratigraphic cross-section and map of study site.

The correlation of facies can be observed with all five units. OSL and radiocarbon dates are also plotted at their respective depths. Cores are georeferenced to their respective depths and locations. Stratigraphic cross-section A-A' shown on map.

One working hypothesis has been developed that could explain forest preservation based on radiocarbon dates in the range of ~42–45 ka cal BP (Table 2), regional stratigraphy and geomorphology (McBride et al. 1999, Bartek et al. 2004) and the published range of sea-level estimates for MIS 1–4 (Waelbroeck et al. 2002). If organic-rich sediments in core 15DF1 were deposited ~42–74 ka cal BP, then elevation and sea level estimates combined with OSL dates (Table 3) suggest that the forest location was well inland from the coast at the time of forest growth ~30 to 50 m above the paleoshoreline (Figure 3), which is consistent with bald cypress biogeographical distribution (Figure 6). A short pulse of sea-level rise (~65 ka, Figure 3) could potentially have caused floodplain aggradation at the forest site, burying and preserving the forest through subsequent sea-level fall, transgression, and ravinement. An alternative hypothesis is that forest burial was not associated with allogenic forcing and was instead caused by an autogenic process such as crevasse splay of the river channel proximal to the forest. This may be evaluated by more detailed stratigraphic analysis, and geomorphological reconstructions from seismic and core data as well as OSL and other dates as those results become available. Results from pollen and microfossil analysis are included to help interpret the evolution of the ancient forest as sea level changed.

4.4 Site Characteristics for Preservation

A consequence of the interbedded sand and mud facies in core 15DF1 being deposited in a coastal environment (Figure 33) constrains the chronology of the site and bounds the Holocene-Pleistocene unconformity (sequence boundary) above by the interbedded sand and mud facies and below by the floodplain facies (Figure 33 and Figure 34). At this location, the sequence boundary and bay-ravinement surfaces become amalgamated (Figure 31, Figure 33, Figure 34). Peat is assumed to mark the base of the sequence boundary, and terminations of coastal foraminifera deposition (Culver 1988, Kohl et al. 2004) are assumed to mark the top of the sequence boundary (Figures 33–34).

Mapping of the sequence boundary reveals an eastern high and a central western low in the study area (Figure 33 and Figure 34) displaying ~1 to 2 m of negative relief dating to MIS 2 (assuming differential compaction is negligible) (Table 2 and Table 3). Evidence of topography before MIS 2 is provided in geophysical data where U2 thins in the northeastern and southeastern extents of the study area (Figure 26 and Figure 27). Geophysical interpretation is supported by the presence of paleosols at the location of paleohighs (Figure 26, Figure 33, Table 6). Peats are preserved in the western portion of the study area (Figure 33) with 15DF3B hosting the longest section of recovered peat (1.57 m). Higher elevation Pleistocene interbedded sands and muds (16DF7 and 16DF9; Figure 34) in the southern extent could have been deposited as part of a fluvial system (Obelcz 2017). Observations are similar to elevation and morphology in modern-day floodplain channel-levee complexes (Lewin and Ashworth 2014).

The accommodation space provided by paleorelief with peats being preserved in the lower-lying areas (Figure 27, Figure 33, Figure 34) is conducive for forest preservation as sediment generally infills the lower-lying areas under the control of gravity first, and higher relief areas are either preferentially eroded or deposited later. Paleosols (56 ±5 (1σ) ka; Table 3) and a low-lying sequence boundary (MIS 2) suggest paleorelief was present and is a contributing factor in forest preservation in the western area of the study site (Figure 26, Figure 27, Figure 33, Figure 34). Core interpretations combined with seismic interpretations and chronology suggest paleorelief was established before 56 ka and existed until Holocene transgression.

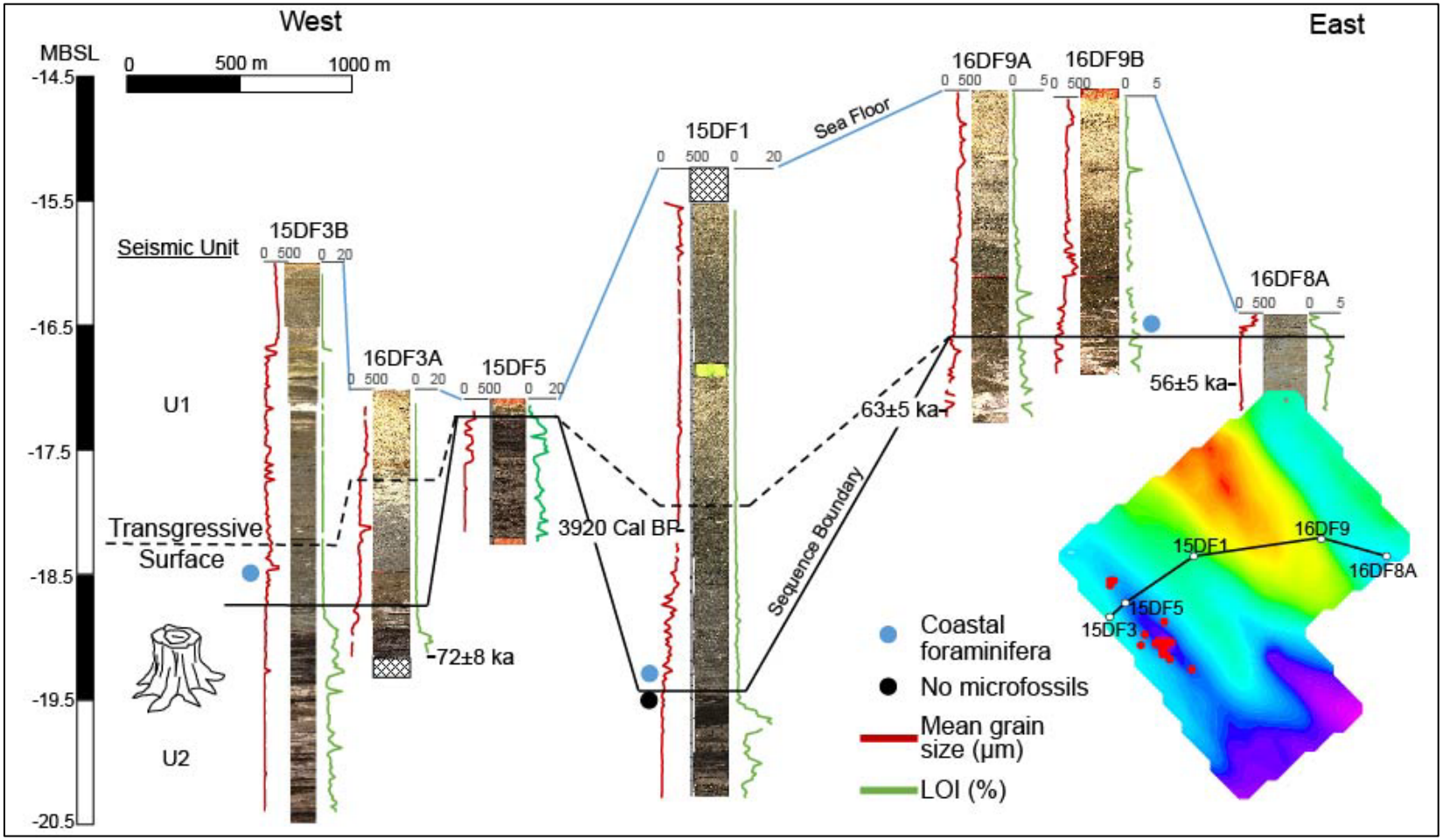

Figure 33. East-West cross-section of the study area.

Core images are shown alongside mean grain size, loss on ignition (LOI) data, and dating results (cal BP are radiocarbon dates and ka are OSL dates) (Tables 2–3). Inset displays site bathymetry (red and yellow are shallow depths, and blue and purple are deep) with cross section and core locations. Red dots indicate possible stump contacts imaged via side-scan sonar (Obelcz 2017). Duplicate cores from the same location (A and B) were collected for OSL dating first and then analyzed for micropaleontological data. The hatched areas in core images are void areas.

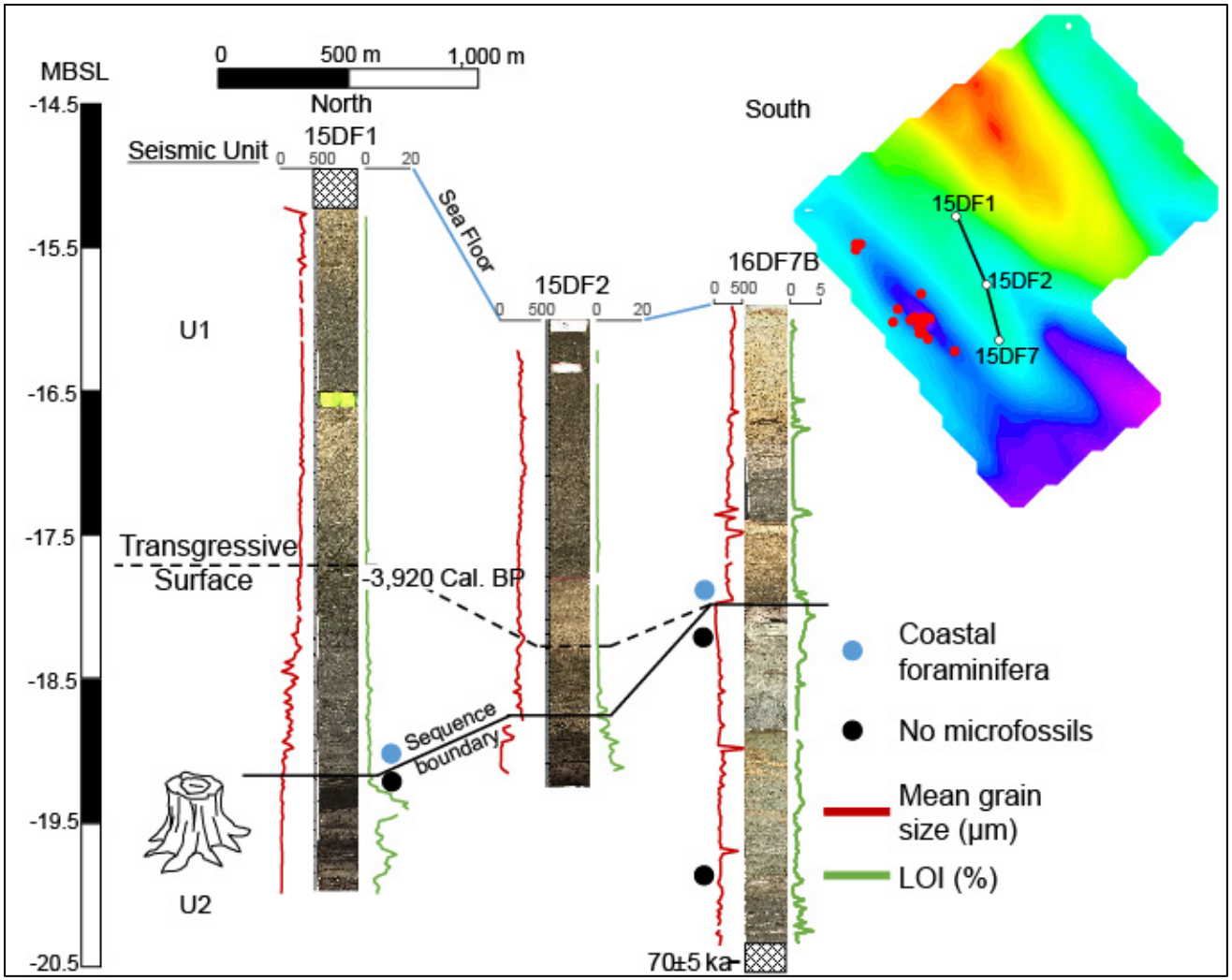

Figure 34. North-South cross-section of the study area.

This figure is similar to Figure 33 with different direction across the study area. Peats are preserved in the north where relief was lower. The southern region did not preserve any peats and was populated instead by interbedded sand and mud, and paleosol facies.

A key requirement for the preservation of organic materials in sediments is anoxic conditions suppressing aerobic decomposition (DiMichele and Falcon-Lang 2011). Swamp environments, such as those in which bald cypress grow, commonly have stagnant waters with a low oxygen content that provide favorable conditions for preservation (Conner and Buford 1998). Ancient kauri (*Agathis australis*) stumps from New Zealand (Lorrey et al. 2018), and bald cypress stumps (early Holocene) of the Trinity-Sabine complex (Pearson et al. 1986) are preserved in similar peaty swamp sediments as the study site. Another possibility is rapid burial of a large volume of sediment from either river overbank flooding or sea-level transgression.

Whereas natural subsidence can account for the stumps being buried, subsidence of the study area is suggested to be minimal for the last glacial interval (Anderson et al. 2004, Bartek et al. 2004). The tree-ring results found dendrochronological evidence that the stumps were buried rapidly. The tree-ring index ends in a single year, suggesting these trees experienced a rapid stress event that resulted in synchronous tree mortality (see section 3.5). These wood specimens provide evidence that the trees were presumably buried rapidly after this stress event because bark is generally shed first while the snag is still standing (Mobley et al. 2013). Such an event could be a hurricane causing tree death from saltwater intrusion (Middleton 2016).

If other locations on northern Gulf had similar geomorphology and environmental conditions, then other sites located within Gulf incised valleys at similar elevations may also contain preserved glacial age forests. Although younger in age, Pearson et al. (1986) demonstrated that the Trinity-Sabine complex on the Texas coast hosts preserved swamp deposits and wood that were possibly preserved in a similar way to the stumps detailed in this study. Pearson et al. (1986) found bald cypress stumps located within the incised valley that were buried and preserved through Holocene transgression. They describe the landforms of the area, and they created a conceptual riverine model to associate landform types and preservation potential of deposits. They found pre-transgressive marsh deposits overlain by estuarine and marine sediments below the marine transgressive zone, in addition to the slopes of the Prairie/Beaumont terrace, such that there is a chance of site preservation due to the powerful wave erosion of the transgressive zone. Pearson et al. (1986) concluded that topography was the most important factor in site preservation, and subsidence and compaction were secondary. The Trinity-Sabine complex provides evidence that preservation processes at the study site are not localized but occur all along the northern Gulf Coast.

This study site provides a unique opportunity to examine changes within a subtropical environment during an interglacial-glacial cycle and the conditions that allowed for wood, pollen, seeds, and other organic materials to be preserved for more than 50,000 years. The forest was located within an area containing paleo-topographic lows that provided accommodation space for forest growth and sediment capping to preserve the forest from erosional processes of eustatic cycles during the last glacial cycle. The highest chance of finding additional stumps is to the west and northwest of the study area where peats are currently preserved based on analysis of reconstructed cross-sections of subseafloor stratigraphy. It is likely that a “bathtub ring” of other sites located within Gulf incised valleys at similar elevations were also preserved. Such locations may contain other well-preserved sediments, wood, and other artifacts that may provide further insights into paleo-oceanographic and paleoenvironmental studies of continental margins around the world.

4.5 Role of Sea Level Change in Forest Preservation

Radiocarbon and OSL results suggest the forest wood-bearing facies are between 74 and 42 ka occurring during MIS 3 and 4 (Table 2, Table 3). The eastern MAFLA has been interpreted as tectonically stable (~2.3 m subsidence/10 ka) (Bartek et al. 2004), but recent studies indicate that the entire northern Gulf margin may deviate from the eustatic sea-level estimates due to continental levering associated with the Laurentide ice sheet (Love et al. 2016). However, these deviations are less than the potential elevation of the bald cypress when they were alive. Based on analogous contemporary environments and core lithology, the forest likely grew in a freshwater swamp within a low-lying river floodplain (Figure 35) (Conner and Toliver 1990). This floodplain could have been adjacent to a tributary river feeding into the main paleo-Mobile River, or the Mobile River itself. Either way, the relatively low elevation of a floodplain and a proximal fluvial source would provide the accommodation space and sediment supply (Figure 26, Figure 27), respectively, necessary for the observed forest preservation state (Damsté et al. 2002).

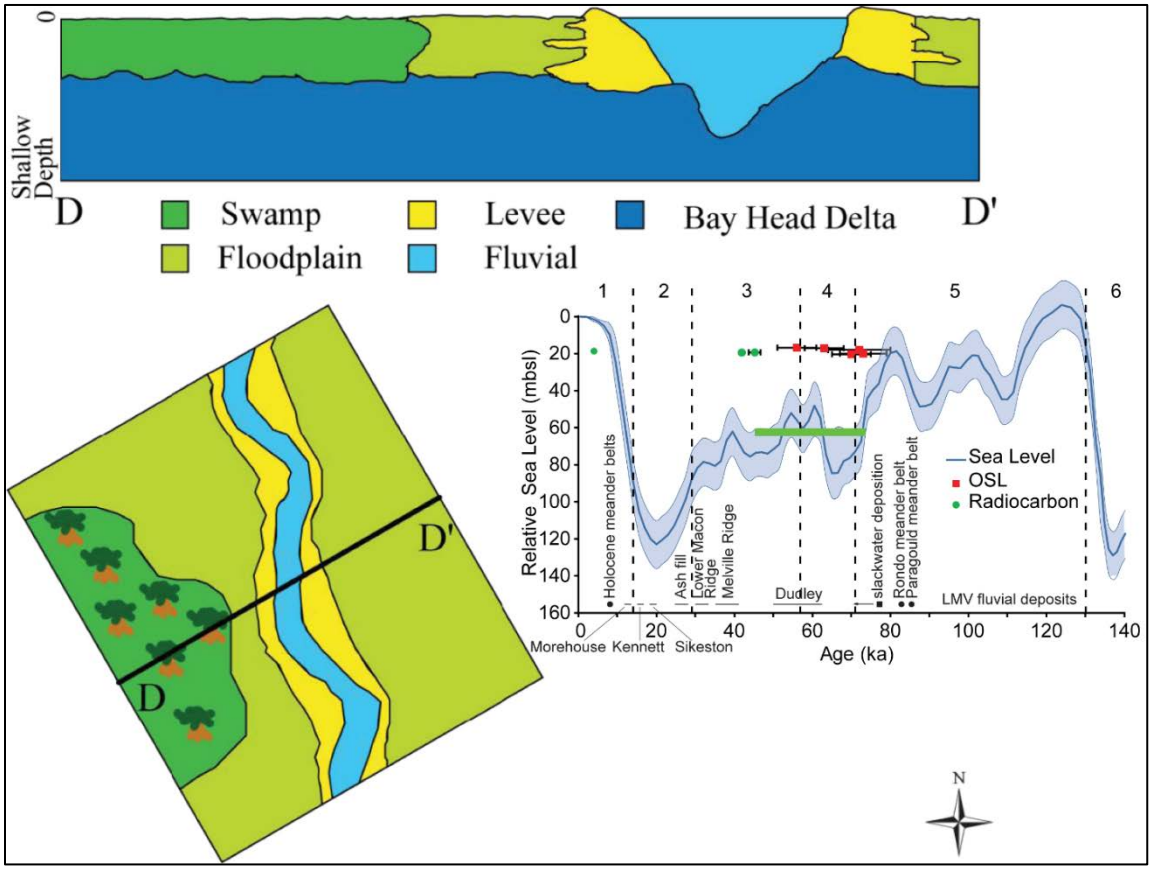

Figure 35. Forest growth conditions.

The approximate time period of forest growth is hypothesized to be 74–45 ka, based on a combination of eustatic sea level (inset modified from Waelbroeck et al. 2002), radiocarbon and OSL dates, cypress biogeography, and stratigraphy derived from cores and seismic data. In this diagram, D-D' represents a vertical cross-section of arbitrary shallow depth, and a plan-view of lateral facies distribution is shown below. The forest is hypothesized to have grown in a relatively low-lying swamp in the floodplain of a Mobile valley tributary river; all of the topmost facies shown are hypothesized to have been deposited on top of bay-head facies formed during an older transgressive phase.

Assuming the postulated growth setting (Figure 35), forest burial could be associated with autogenic or allogenic events. An example of an autogenic burial would be a river crevasse splay that rapidly deposited a large mass of sediment on top of the forest (Shen et al. 2015), preventing degradation through aerobic respiration and/or exposure by erosion. Allogenic burial would involve external forces, such as rapid sea-level rise raising upstream river stage and promoting overbanking and associated floodplain aggradation (Shen Z et al. 2012). The relatively rapid sea-level rise of ~15 m over ~3000 years (~5 mm/year) between 43 and 40 ka is a plausible driver of allogenic burial and is therefore favored in the working hypothesis. Regardless of mechanism, the net outcome is rapid and deep burial of the forest beneath a relatively impermeable sediment cap (Figure 36).

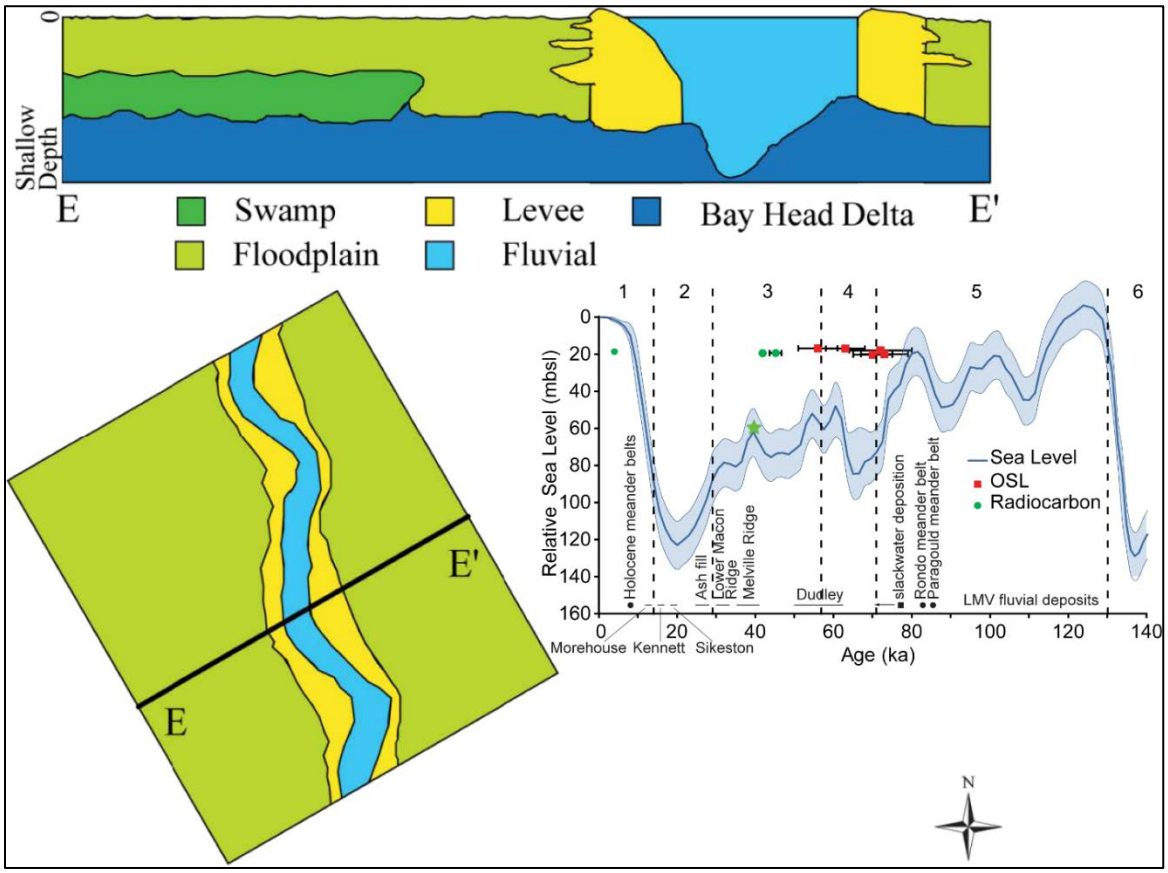

Figure 36. Forest burial conditions.

The approximate time period of forest burial is hypothesized to be 40 ka or 62 ka, based on a combination of eustatic sea level (inset modified from Waelbroeck et al. 2002), radiocarbon and OSL dates, cypress biogeography, and stratigraphy derived from cores and seismic data. In this diagram, E-E' represents a vertical cross-section of arbitrary shallow depth, and a plan-view of lateral facies distribution is shown below. The forest is hypothesized to have been rapidly buried by floodplain aggradation associated with the short sea level rise interval around 40 ka or 62 ka.

The forest survived the falling and lowstand sequence stratigraphic stages that favor the destruction of preexisting sedimentary strata (Van Wagoner et al. 1988). Assuming the forest was buried ~40 ka, the site would have been subaerially exposed for another ~30 ka. This includes the Last Glacial Maximum (LGM) during which the climate was cooler and drier, i.e., conducive to eolian erosion and paleosol formation (Figure 37) (Rutter et al. 2017).

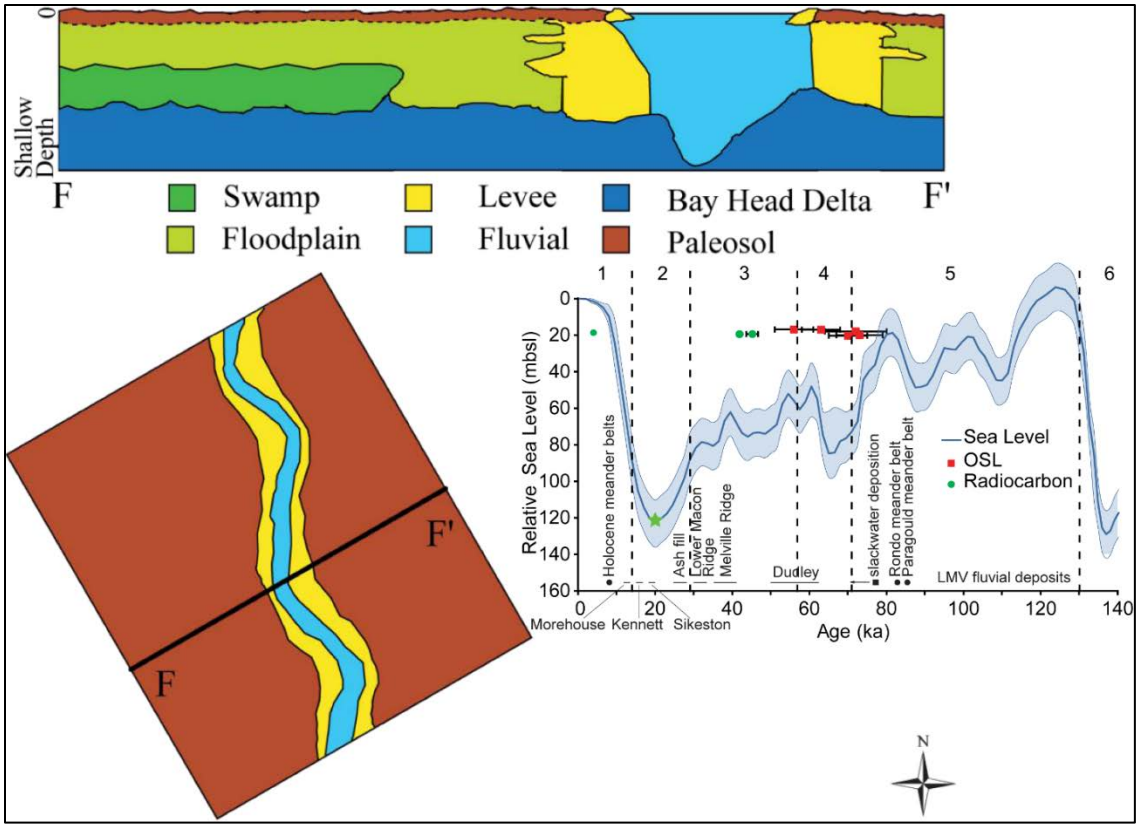

Figure 37. Forest preservation conditions at the Last Glacial Maximum (LGM).

The forest was preserved in the buried sediments during the LGM when sea level was ~120 m below sea level, and the entire continental shelf was subaerially exposed to cooler, drier conditions (inset modified from Waelbroeck et al. 2002) In this diagram, F-F' represents a vertical cross-section of arbitrary shallow depth, and a plan-view of lateral facies distribution is shown below. The forest is hypothesized to have been sufficiently buried so as not to be subaerially exposed during lowstand erosion and paleosol formation.

After the LGM, deglaciation drove sea level rise and marine transgression. Sea level fluctuation is rarely linear, and high-frequency rises and falls in sea level are often superimposed on a larger-scale rising and falling trend (Siddall et al. 2003). This "transgressive belt sander" (D. Swift, pers. comm. 2017) moves the high-energy shoreline environment back and forth across preexisting strata. The MAFLA sand sheet is formed largely by transgressive processes (McBride et al. 1999), and the drowned forest must have been sufficiently buried and/or rapidly bypassed by the nearshore environment to avoid being integrated into the MAFLA sheet (Figure 38). After transitioning to a fully marine environment ~8 ka, the forest was evidently unperturbed until exposure coincident with the passage of Hurricane Ivan in 2004 (Figures 5, 38). Now that the forest is exposed to the water column, degradation is apparent, and preservation is not expected. A synthesis of seismic and lithological data with the forest preservation hypothesis is presented in Figure 39.

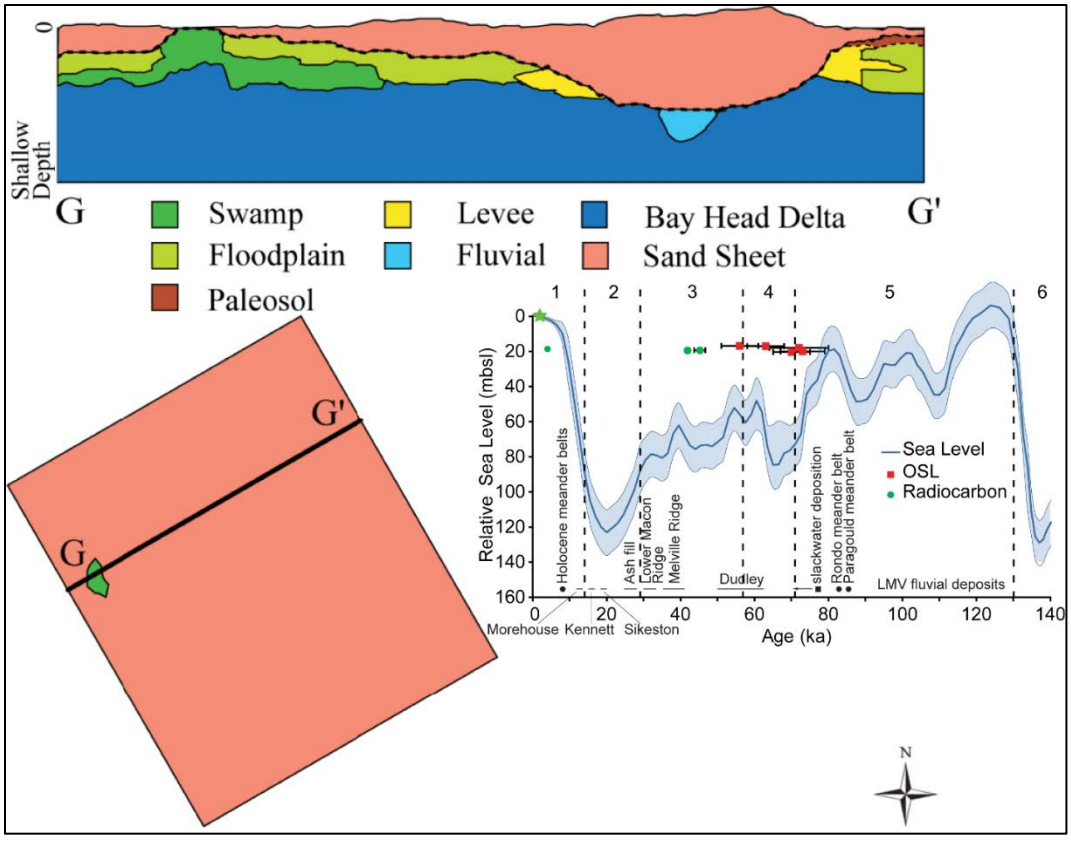

Figure 38. The working hypothesis of drowned forest current conditions.

The forest survived marine transgression and was subaqueously exposed by Hurricane Ivan in 2004. In this diagram, G-G' represents a vertical cross-section of arbitrary shallow depth, and a plan-view of lateral facies distribution is shown below. The modern facies distribution is almost uniform sand sheet, with a small forest section exposed to the water column. Inset modified from Waelbroeck et al. 2002.

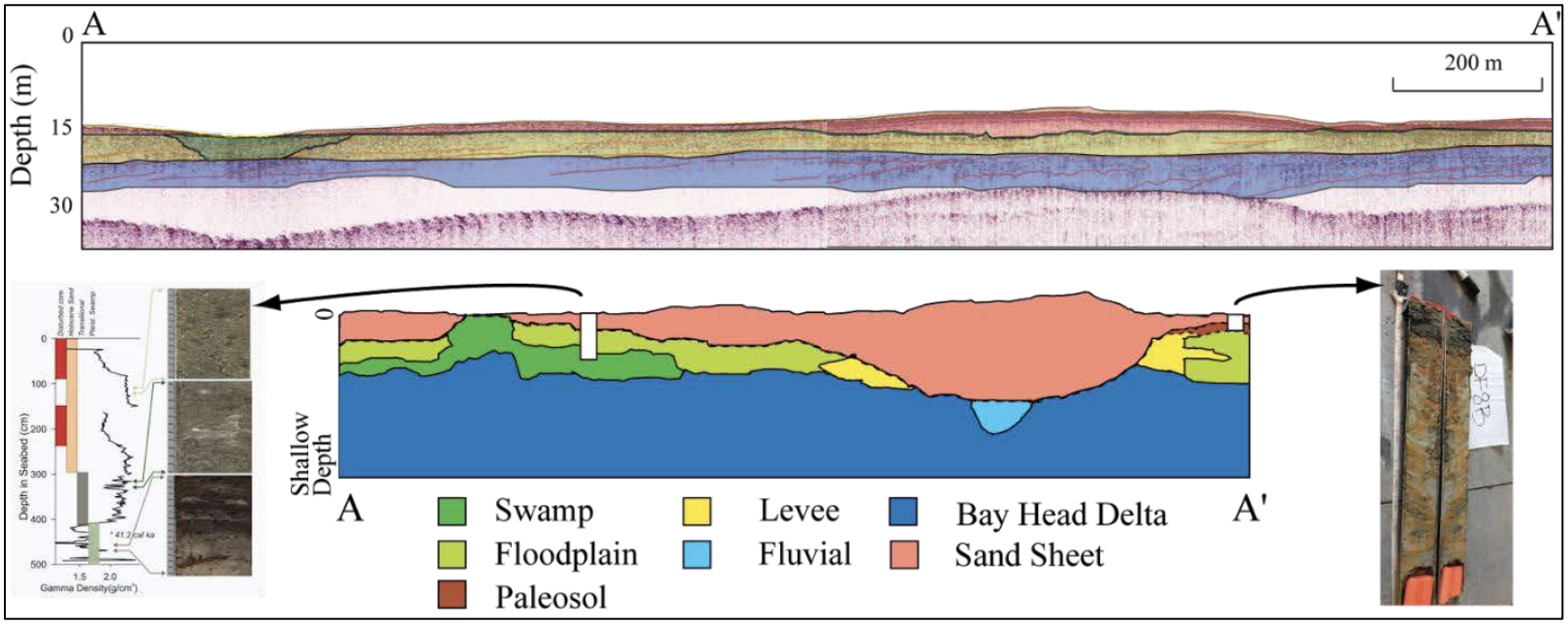

Figure 39. Profile synthesizing CHIRP and core data with forest facies and stratigraphy.

A-A' corresponds to the base map location in Figure 34 through Figure 37. CHIRP profile is shaded to correspond with major conceptual diagram facie groups: pink for Holocene sand sheet, green for Pleistocene swamp, yellow for all other Pleistocene facies, and blue for bayhead delta. White areas are locations of cores. Cores 15DF1 shown to the left with example facies and core gamma density profile (see Figure 17) and a picture core 16DF8B shown to the right with paleosols.

To better evaluate geographic relationships between the study area and the late Pleistocene shoreline locations, simple reconstructions of the coastal plain and continental shelf at various intervals for the dated sediments illustrating sea-level change, shoreline locations, and transgression-regression (Figure 40). First, the time of glacial high and lowstands is identified using the Waelbroeck et al. (2002) global sea level estimates (Figure 3) that bracket the ages of sediments that have been dated. The relevant points in time are 80.0 ka, 65.0 ka, 60.5 ka, 44.0 ka, 39.5 ka, and 4.0 ka (for Holocene facies 2). Then, a regional digital elevation model (Love et al. 2018) was trimmed to highlight study area location and demark the land-sea boundary at each of those time points. This approach ignores topographic change by uplift, subsidence, sedimentation, and erosion from the last glacial to present, and also assumes that the Waelbroeck et al. (2002) global sea level record applies to the northern Gulf for this period, which is not well understood or documented (Donoghue 2011). Nevertheless, these illustrations schematically show the relative magnitudes of distances, elevations, and topographic gradients relating the study area to the location of the coastline for these past periods in time.

From 80 ka (Figure 40a) to 65 ka (Figure 40b), sea level fell from 20 mbsl (close to the study area) to 85 mbsl exposing a new coastal plain >100 km wide measured at the shortest distance from the study area. During this time, the oldest floodplain deposits of facies 4 and the swamp deposits of facies 3, the late Pleistocene interbedded mud and peat, were deposited (Table 6). From 65 ka (Figure 40b) to 60.5 ka (Figure 40c), sea level rose to 48 mbsl, but because of the steep gradient of the outer shelf, the shoreline transgressed <15 km. During this time, the youngest dated deposits of facies 4 accumulated (Table 6). The period of 60.5 ka (Figure 40c) to 44 ka (Figure 40d) encompasses a sea-level rise of ~7 m near 54 ka, falling to ~76 mbsl near 44 ka. This produced an overall coastal regression on the order of 10 km from this elevation model. During this period, the younger (56 ka) paleosol (facies 5) developed and some of the dated swamp deposits of facies 3 accumulated (45 ka) in a topographic low west of the sampled paleosol. From 44 ka (Figure 40d) to 39.5 ka (Figure 40e), sea level rose ~14 m producing a transgression of <10 km during which time the peaty deposits of facies 3 continued to deposit. After 39.5 ka, sea level fell, with a pause near 32 ka, and then continue to fall until the LGM lowstand was attained. During the deglacial interval (18–10 ka), sea levels rose, and marine facies 2 was deposited and then covered by sand of facies 1 during the Holocene, thus preserving the forest remnants.

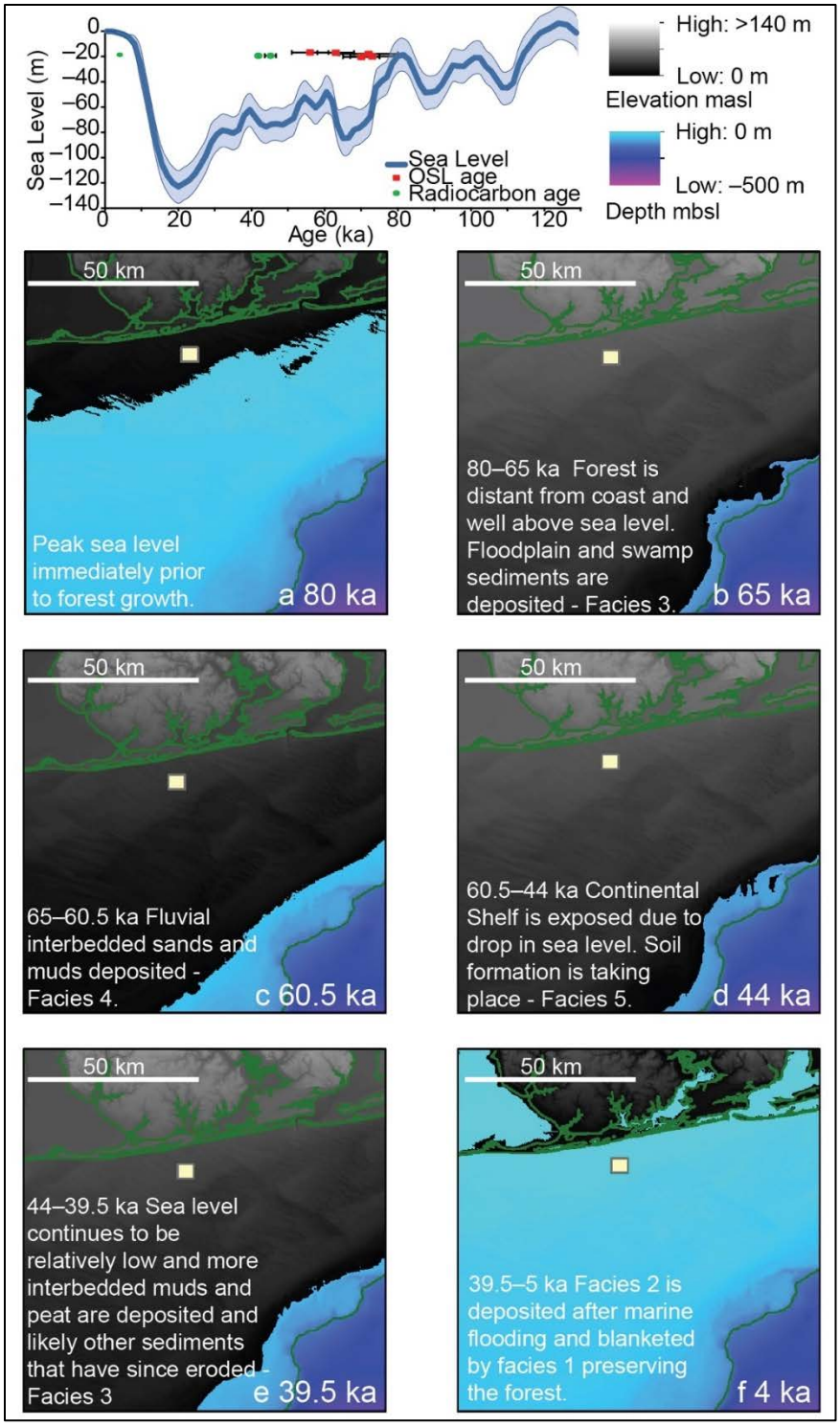

Figure 40. Geographical reconstruction of forest site evolution.

Sea level model reconstructing the coastal plain and continental shelf at times during changes of sea level from the late Pleistocene to the Holocene. Regional data obtained from Love et al. (2018).

These reconstructions suggest that sediment deposition and accumulation in the study area could have occurred during five-time intervals recorded by the site's geochronology. Three depositional intervals coincided with short pulses of sea-level rise at 42 ka, 56 ka, and 63 ka (Figure 3). One depositional interval coincided with a still-stand at 45 ka and one with falling stage 70 ka to 74 ka. The data are insufficient to conclusively identify mechanisms for each case, but previous studies yield some suggestions. The first scenario, where deposition occurred shortly after pulses in sea level rise, has been extensively studied by Anderson et al. (2016) and Shen Z et al. (2012). Those studies showed that such rapid aggradation had been observed many kilometers inland in other coastal-plain alluvial valleys, where rivers aggrade rapidly in order to "keep up" with pulses in sea level rise. During MIS 5, an aggradation event occurred along the northern Gulf (Shen et al. 2015). Anderson et al. (2016) also observed congruent floodplain aggradation to rise in local sea level for small-to-medium-sized rivers along the northwestern Gulf Coast in Texas during the Late Pleistocene (MIS 5–3).

For the second and third scenarios, where deposition occurs during still-stands and falling stages, river avulsion driven by regional gradients (Aslan et al. 2005) could produce autogenic burial, which could have been augmented by subsequent regional aggradation. For the third case, OSL ages clustered (Table 3) at the start of a relatively short period of sea-level fall (late MIS 5 to early MIS 4, between Figure 40a and 40b), which was followed by another pulse of sea-level rise ~60 ka (Figure 3). In this case, floodplain aggradation due to sea-level rise soon after the dated sediments were deposited is not a plausible explanation. If the sediment ages are correct and immediate sediment burial did occur, then another mechanism needs to be involved other than immediate response to sea-level rise. The apparent elevation of the location above sea level ~60 ka (well below the elevation of the study area at that time) suggests that delta progradation is not a likely explanation. Autogenic avulsion driven by local river gradients could also enhance floodplain sedimentation, as occurs in low-gradient river systems (Aslan et al. 2005, Bentley et al. 2016).

Swenson and Muto (2007) examined the response of coastal plain rivers to sea level and found that both degradation and aggradation can occur in one river system simultaneously during sea-level fall. This can occur when and where intrinsic timescale of sediment delivery matches the timescale of sea-level fall. In this case, sediment supply can be sufficient to produce aggradation in upper reaches of a catchment for the duration of the sea-level fall, but the seaward portion of the catchment experiences degradation (Figure 41). The rates of sea-level change addressed by Swenson and Muto (2007) (<1 mm/year) are much lower than rates evident in Figure 3 around the time of MIS 4 (rises and falls at rates of 4–5 mm/year), but the relatively small spatial size of rivers feeding the study area suggests that they should have rapid response times as described by Swenson and Muto (2007). One final consideration is that the actual record of northern Gulf sea level change could differ from that of Waelbroeck et al. (2002) or the authors' age models are incorrect or uncertainty too large, in which case the mechanisms for forest burial and preservation remain unknown.

Another key component of this hypothesis is that some accommodation spaces had to exist in order for thick packages of sediments to be deposited and therefore allow for forest preservation. This assumption is supported by the integrative digital elevation model (DEM) developed for the study site and the two underlying surfaces (Figure 26) where an accommodation surface is being created by the bottom surface dipping southwest.

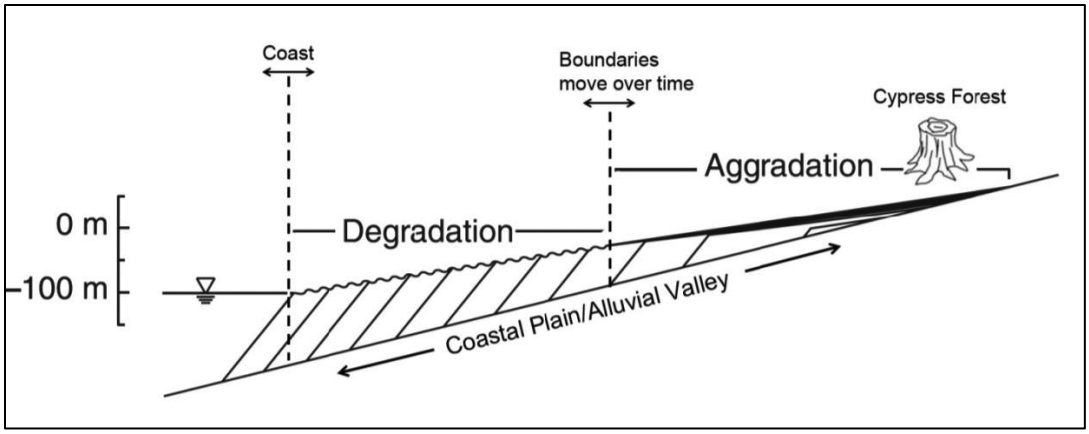

Figure 41. Patterns of floodplain aggradation and degradation.

Patterns identified by Swenson and Muto (2007) if the timescale of sediment supply approaches the timescale of sea-level change in a fluvial system, producing aggradation in upper reaches of the catchment, and degradation in seaward reaches of the catchment. Adapted from Swenson and Muto (2007).

In summary, the swamp sediments found in cores 15DF1, 15DF2, 15DF3B, 15DF4, 15DF4, 15DF5, 15DF6, 16DF1D, and 16DF3A that are located in topographic lows are hypothesized to have been preserved and buried by fluvial/floodplain sediment accumulation. Accommodation for this sediment accumulation and preservation is indicated in the local divergence of the two lower seismic surfaces in Figure 26. Finally, as sea level rose and transgression occurred during the Late Pleistocene, sediments within the incised valleys were first eroded by transgression of the coastline and associated wave energy and later covered by Holocene shelf sands as sea level rose, thus causing the coastline position to retreat. Coastal wave erosion during transgression likely eroded high ground, but enough sediment layers remained to keep the cypress forest blanketed, therefore fortuitously favoring preservation.

4.6 Implications of Forest Model for Analogous Sites

This unique scenario where cypress tree stumps have been preserved for up to 70 ka represents a puzzling geologic setting that is possibly explained by relatively rapid and deep burial by floodplain aggradation that occurred for different reasons at different times. In three plausible cases, aggradation likely occurred as rivers responded to the pulsed sea level rise. In two additional cases, floodplain aggradation may have been out of phase with sea-level rise, and local sediment supply likely played a role in burying floodplains in inland portions of the coastal plain, while seaward portions of river valleys incised. Overall, these mechanisms for fluvial sediment accumulation prevented exposure by channel incision and coastal erosion during the latest Pleistocene regression and Pleistocene-Holocene transgression, thus preserving the tree stumps and wood debris.

Partial preservation of forests following sea-level transgression via wood debris, seeds, and pollen is fairly common and can provide paleoenvironmental and climatic information including species assemblage, aridity, temperature, and radiocarbon age (Hautevelle et al. 2006). However, preservation of an entire forest in growth position post-transgression is rare and provides information that fragments, seeds, and pollen cannot, such as dendrochronological records of interseasonal climate variation (Schongart et al. 2006). The hypothesis of forest growth setting, burial, and preservation conditions can serve as a model for discovering analogous environments, both along the northern Gulf and on other passive margins around the world.

The conjecture that the forest grew in a floodplain setting proximal to a river is based on analogous contemporary environments (Conner and Toliver 1990). Major river paleochannels are resolvable in seismic data, and well-mapped for many passive continental margins (Shaw and Courtney 1997, Schwab et al. 2014, van Heteren et al. 2014), therefore potential forest growth locations can be identified in many cases with preexisting maps. The other two major factors expected to dictate the abundance of analogous preserved forests are burial and post-burial erosion and disturbance.

If the forest detailed in this study was buried by widespread overbank flooding associated with eustatic sea-level rise, other still-buried preserved forests might exist as a "bathtub ring" proximal to paleochannels. If an autogenic process with smaller spatial extent, such as a river crevasse splay, buried the forest, the number of analogous sites may be lower.

Regardless of autogenic or allogenic forcing leading to forest burial, the existence of similar sites is also heavily dependent on surviving conditions unfavorable for stratigraphic preservation, including sea-level lowstand and transgression (Figure 37, Figure 38). The proximity of the drowned forest to the current shoreline may have aided its preservation, since sea-level rise rapidly accelerated 11,000 years before present (Love et al. 2016), reducing the amount of time the forest area was exposed to the "transgressive band saw." For this reason, high-resolution constraints on sea-level fluctuation history should assist in identifying areas conducive to forest preservation.

This research suggests an approach that could help identify locations of other similar preserved forests of contemporaneous age around the Gulf. Due to the depth range of such forest preservation caused by the regional impact of sea-level rise and associated floodplain transgression, similar to the study area, a sort of "bathtub ring" could have formed around the Gulf at common age and depth. If this hypothesis is correct, each time a pulse in sea-level rise occurs there should be a backwater effect and floodplain aggradation event that occurs in response to that rise in sea level. These preserved sites should be concentrated offshore of modern river systems that would have incised the shelf at lower sea levels and deposited sediments during the phases of floodplain aggradation, such as the sediment accumulation that likely preserved the glacial-age forest.

5. Future Plans

The study used an Edgetech 4600 swath bathymetry and side-scan sonar system. The seabed bathymetry was measured, and large exposed tree stumps were identified by side-scan at the seabed surface. However, the CHIRP sub-bottom acoustic data collected using both Edgetech 0512i and 216 systems proved that neither the exposed nor buried tree features could be uniquely resolved using these systems. These instruments, operating in the range of 0.5 to 16 kHz, are capable of imaging largely buried structures, but they collapse responses from a 3-D environment into 2-D vertical slices and therefore provide no cross-dip information. To resolve this issue, the use of a 3-D CHIRP system is proposed for future work to resolve the tree stumps still buried at the site. Furthermore, this study recovered several cores with ~1 m of Pleistocene terrestrial sediments with peat that contain wood yet the digital elevation model (Figure 26) suggests there is more accommodation space that could contain more of these sediments, possibly up to 9 m in thickness. The recovery of long cores from the site would allow a better characterization of the paleoenvironment and provide a basement age control for the peat and woody sediments. Lastly, collection of seismic data from the northern Gulf region is proposed for marine isotope stage (MIS) 2 and 6 surfaces along with core data where wood was found. This information would be used to develop a prediction model of encountering wood at any depth within a core at a given location to quantitatively test the hypothesis that forest location is related to paleo-relief. This site represents a rare opportunity to study an easily accessible Pleistocene landform and develop a model to identify other possible outer continental shelf (OCS) locations with still buried forests.

Future fieldwork would enhance seabed survey methods and provide recommendations on survey tools and methods that might increase the chances of detecting such features. This information could be used by Bureau of Ocean Energy Management (BOEM) to (1) develop more effective survey methods for detecting and characterizing such seabed features, and (2) determine if environmental impact statements are necessary for such sites when relevant to proposed oil, gas, and dredging activities, or if categorical exclusion reviews are more appropriate.

Additionally, other sites have been identified in the northern Gulf. Buried wood was found in sediment cores south of Petit Bois, Mississippi. Stumps were found by Florida Fish and Wildlife south of Mexico Beach, Florida near one of the sites they monitor on a regular basis after Hurricane Michael made landfall in 2018. Pearson et al. (1986) examined the Trinity-Sabine complex on the Texas coast and found preserved swamp deposits and bald cypress wood similar to this study but were Holocene in age. Investigating these other sites is the next logical step towards developing a research program focused on finding, identifying, and modeling where similar sites may occur on the OCS.

Obelcz is currently developing a geospatial prediction model for subsurface wood-bearing sediments using machine learning. (Figure 42). He is focusing on the Mississippi Sound area where he is cataloging seismic and core data with Rob Hollis of the US Naval Research Laboratory and Davin Wallace of the University of Southern Mississippi (USM) Department of Marine Science. They developed isopach maps of the MIS 2 and MIS 6 surfaces underneath Mississippi Sound. They have the locations of other cores collected by USM and others that they analyzed for presence or absence of wood. The predictions made over the entire area shown in Figure 42 were trained and validated using observations in a relatively small area. Obelcz predicted encountering wood at any depth within a core at a given location, with the assumption that wood in core equals a higher probability for the preservation of buried forests. The predictors were depth to MIS 2 and MIS 6 surfaces, which is a way of quantitatively testing the study's hypothesis that forest location is related to paleo-relief. The prediction probability increases in areas of deeper MIS 2 and 6 surfaces as could be expected. The prediction is very inaccurate; it only made a correct prediction on 1 out of every 10 observations during 10-fold cross-validation, but he found the predictions that are inaccurate in bulk can still have instructive spatial trends. Overall, preliminary results are: 1) Different machine learning algorithms predict similar spatial trends, but differ in

generalization/magnitude; 2) The probability of encountering wood is highest around fringes of paleo-river channels—this matches the location of the only preserved forest found in the northern Gulf to date; and 3) Paleo-slope curvature better correlates with wood presence than paleo-topography.

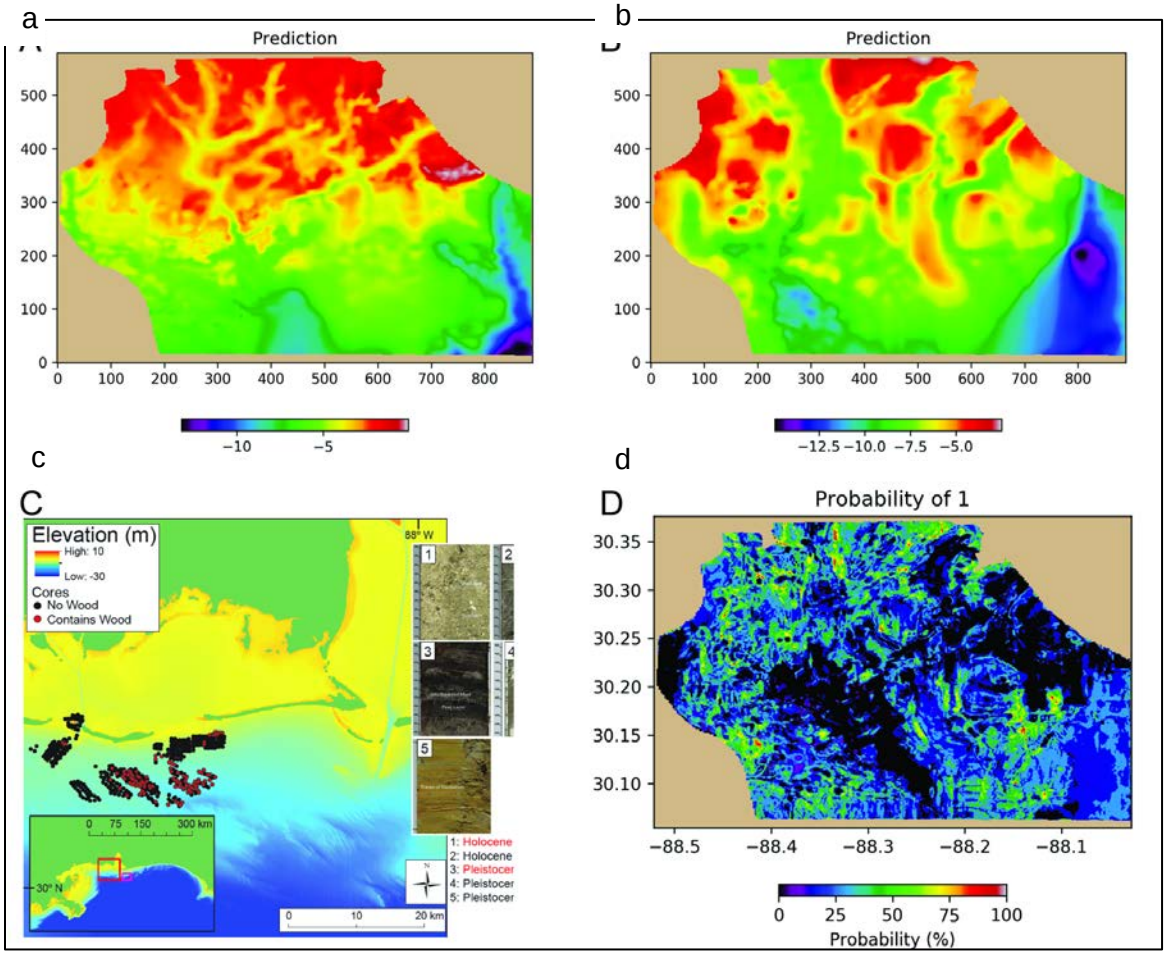

Figure 42. Preliminary predictions of other locations with wood bearing sediments.

a) Isopach map of the MIS 2 surface and b) isopach map of MIS 6 surface for the Mississippi Sound area. c) Locations of the cores analyzed for the presence or absence of wood. d) Prediction of encountering wood at any depth within a core at a given location.

The primary objectives of a "phase 2" project are to refine the characterization of the study area located just off the coast of Alabama that contains well-preserved glacial-age bald cypress stumps in order to generate more precise information about its geological, geophysical, ecological, and paleoenvironmental characteristics. By placing the cypress forest site within the sedimentological context of the northern Gulf, this continued research would (1) determine the characteristics of the site that led to preservation, (2) provide a better understanding of depositional and geomorphic layout of the site, and (3) provide the opportunity to develop a model to predict other paleo-forest sites within the northern Gulf.

Hypothesis 1: High-resolution 3-D CHIRP geophysical surveys will be able to resolve exposed and buried tree stumps and logs not previously revealed in earlier surveys using different acoustic systems.

Hypothesis 2: Well-preserved woody remains in the sediments at the site suggest that similar depositional environments may contain potential archaeological sites even though this

site is too old to contain archaeological materials. In the current study, the environment during the time when the trees were alive is hypothesized to have been slow to still waters with anoxic sediments that prevented decomposition thus preserving organic material.

Hypothesis 3: Previous pollen-based studies suggest the southeastern US was colder and drier during the glacial intervals yet none of these studies were conducted in regions that were coastal during the glacial intervals. Bald cypress stands can grow in swamps with slow-moving water thus lessening the potential transportation of pollen from other locations. In the current study, the northern Gulf Coast supported a robust subtropical bald cypress forest during the early glacial interval since the last interglacial.

Objective 1: Refine the methodology for identifying buried tree stumps and logs in the sediments.

Objective 2: Ground-truth geophysical survey targets using divers.

Objective 3: Collect cores at locations in the main site to obtain a deeper, continuous sedimentary record of Pleistocene sediments than was previously obtained and for new sites.

Objective 4: Expand the geophysical survey area to other known nearby buried tree sites.

Objective 5: Use established dating methods to compare the age of sediments and the subsequent sedimentation rates to estimate the ages of the in situ tree stumps.

Objective 6: Refine the paleoenvironmental setting of the preserved Pleistocene wetland forest using microfossils, pollen, seed, and wood analysis.

Objective 7: Develop a model to predict other buried forest sites on the northern Gulf OCS.

An additional project on shipworms in the exposed wood is planned by Dan Distel of the Marine Science Center at Northeastern University. Distel studies wood-associated marine organisms and their symbiotic bacteria. Distel was funded by the National Oceanic and Atmospheric Administration (NOAA) in September 2019 to conduct research on the wood and the shipworms. The project title is “Bioprospecting for industrial enzymes and drug lead compounds in an ancient submarine forest.” This study has the potential to inform this ongoing project on how long the wood has been exposed to the marine environment and if it has been previously exposed in the past ~15,000 years. DeLong will work with on the NOAA project as an advisor.

Works Cited

Aitken MJ. 1985. Thermoluminescence dating. London (England): Academic Press.

Allard G, Roy M, Ghaleb B, Richard PJH, Larouche AC, Veillette JJ, Parent M. 2012. Constraining the age of the last interglacial-glacial transition in the Hudson Bay lowlands (Canada) using U-Th dating of buried wood. Quat Geochrol. 7:37–47. doi:10.1016/j.quageo.2011.09.004.

Andersen HV. 1961. Genesis and paleontology of the Mississippi River mudlumps. Part 2, Foraminifera of the mudlumps, lower Mississippi River delta. Baton Rouge (LA): Louisiana Geological Survey.

Anderson JB, Rodriguez AB, Abdulah KC, Fillon RH, Banfield LA,et al. 2004. Late Quaternary stratigraphic evolution of the northern Gulf of Mexico margin: a synthesis. In: Anderson JB, Fillon RH, eds. Late Quaternary stratigraphic evolution of the northern Gulf of Mexico margin. Tulsa (OK): SEPM (Society for Sedimentary Geology). p. 1–23. doi.org/10.2110/pec.04.79

Anderson JB, Wallace DJ, Simms AR, Rodriguez AB, Weight RWR, et al. 2016. Recycling sediments between source and sink during a eustatic cycle: Systems of late Quaternary northwestern Gulf of Mexico basin. Earth-Sci. 153:111–138. doi:10.1016/j.earscirev.2015.10.014.

Anderson LC, Sen Gupta BK, McBride RA, Byrnes MR. 1997. Reduced seasonality of Holocene climate and pervasive mixing of Holocene marine section: northeastern Gulf of Mexico shelf. Geology. 25(2):127–130. doi:10.1130/0091-7613(1997)025<0127:RSOHCA>2.3.CO;2.

Aslan A, Autin WJ, Blum MD. 2005. Causes of river avulsion: Insights from the Late Holocene avulsion history of the Mississippi River, U.S.A.. J Sediment Res. 75(4):650–664. doi:10.2110/jsr.2005.053.

Balsillie JH, Donoghue JF. 2004. High-resolution sea-level history for the Gulf of Mexico since the Last Glacial Maximum. Tallahassee (FL): Florida Geological Survey.

Ballarini M, Wallinga J, Wintle AG, Bos AJJ. 2007. A modified SAR protocol for optical dating of individual grains from young quartz samples. Radiat Meas. 42(3):360–369. doi:10.1016/j.radmeas.2006.12.016.

Bandy OL. 1954. Distribution of some shallow-water Foraminifera in the Gulf of Mexico. Geological Survey professional paper 254-F. 39 p. Washington (DC): US Department of the Interior, US Geological Survey. https://pubs.usgs.gov/pp/0254f/report.pdf.

Bandy OL. 1956. Ecology of foraminifera in northeastern Gulf of Mexico. Geological Survey professional paper 274-G. Washington (DC): US Department of the Interior, US Geological Survey.

Bartek LR, Cabote BS, Young T, Schroeder W. 2004. Sequence stratigraphy of a continental margin subjected to low-energy and low-sediment-supply environmental boundary conditions; Late Pleistocene-Holocene deposition offshore Alabama, U.S.A. In: Anderson JB, Fillon RH, eds. Late Quaternary stratigraphic evolution of the northern Gulf of Mexico margin. Special Publication 79. Tulsa (OK): SEPM (Society for Sedimentary Geology). p. 85–109.

Bentley SJ Sr, Keen TR, Blain CA, Vaughan WC. 2002. The origin and preservation of a major hurricane event bed in the northern Gulf of Mexico: Hurricane Camille, 1969. Mar Geol. 186(3):423–446. doi:10.1016/S0025-3227(02)00297-9.

Bentley SJ, Blum MD, Maloney J, Pond L, Paulsell R. 2016. The Mississippi River source-to-sink system: Perspectives on tectonic, climatic, and anthropogenic influences, Miocene to Anthropocene. 2016. Earth Sci Rev. 153:139–174. doi:10.1016/j.earscirev.2015.11.001.

Berkeley A, Perry CT, Smithers SG, Horton BP, Taylor KG. 2007. A review of the ecological and taphonomic controls on foraminiferal assemblage development in intertidal environments. Earth Sci Rev. 83(3–4):205–230. doi:10.1016/j.earscirev.2007.04.003.

Biondi F, Qeadan F. 2008. Inequality in paleorecords. Ecology. 89(4):1056–1067. doi:10.1890/07-0783.1.

Blum MD, Tomkin JH, Purcell A, Lancaster RR. 2008. Ups and downs of the Mississippi delta. Geology. 36(9):675–678. doi:10.1130/g24728a.1.

Brennan ML, Ballard RD, Croff Bell KL, Piechota D. 2011. Archaeological oceanography and environmental characterization of shipwrecks in the Black Sea. In: Buynevich IV, Yanko-Hombach V, Gilbert AS, Martin RE, eds. Geology and ceoarchaeology of the Black Sea region: beyond the flood hypothesis. Special Paper 473. Boulder (CO): Geological Society of America. 196 p.

Brinson MM, Bradshaw HD, Jones MN. 1985. Transitions in forested wetlands along gradients of salinity and hydroperiod. J Elisha Mitchell Sci Soc. 101(2):76–94.

Brinson MM, Christian RR, Blum LK. 1995. Multiple states in the sea-level induced transition from terrestrial forest to estuary. Estuaries. 18(4): 648–659. doi:10.2307/1352383.

Bunn, AG. 2008. A dendrochronology program library in R (dplR). Dendrochronol. 26(2):115–124.

Chabreck RH. 1972. Vegetation, water and soil characteristics of the Louisiana coastal region. Baton Rouge (LA): Louisiana State University Agricultural Experiment Station Reports No 147. Bulletin No. 664. 72 p.

Cheng H, Edwards LR, Shen C-C, Polyak VJ, Asmerom Y, et al. 2013. Improvements in ^{230}Th dating, ^{230}Th and ^{234}U half-life values, and U–Th isotopic measurements by multi-collector inductively coupled plasma mass spectrometry. Earth Planet Sci Lett. 371–372:82–91. doi:10.1016/j.epsl.2013.04.006.

Cleaveland MK. 2000. A 963-year reconstruction of summer (JJA) stream flow in the White River, Arkansas, USA, from tree-rings. Holocene. 10(1): 33–41. doi:10.1191/095968300666157027.

Conner WH, Toliver JR. 1990. Long-term trends in the bald-cypress (*Taxodium distichum*) resource in Louisiana (U.S.A.). For Ecol Manage. 33–34:543–557. doi:10.1016/0378-1127(90)90217-Y.

Conner WH. 1994. The effect of salinity and waterlogging on growth and survival of baldcypress and Chinese tallow seedlings. J Coast Res. 10(4):1045–1049.

Conner WH, Buford MA. 1998. Southern deepwater swamps. In: Messina MG, Conner WH, eds. Southern forested wetlands ecology and management. Boca Raton (FL): CRC Press. p. 261–287.

Conner WH, Doyle TW, Krauss KW. 2007. Ecology of tidal freshwater forested wetlands of the southeastern United States. Dordrecht (NL): Springer.

Culver SJ. 1988. New foraminiferal depth zonation of the northwestern Gulf of Mexico. Palaios. 3(1):69–85. doi:10.1007/s10584-011-0082-0.

Damsté JSS, Rijpstra WIC, Reichart GJ. 2002. The influence of oxic degradation on the sedimentary biomarker record ii. Evidence from arabian sea sediments. Geochim Cosmochim Acta. 66:2737–2754.

Dansgaard W, Johnsen SJ, Clausen HB, Dahl-Jensen D, Gundestrup NS, et al. 1993. Evidence for general instability of past climate from a 250-kyr ice-core record. Nature. 364(6434):218–220. doi:10.1038./364218a0.

DiMichele WA, Falcon-Lang HJ. 2011. Pennsylvanian 'fossil forests' in growth position (T^0 assemblages): origin, taphonomic bias and palaeoecological insights. J Geol Soc [London]. 168(2):585–605. doi:10.1144/0016-76492010-103.

Donders TH, de Boer HJ, Finsinger W, Grimm EC, Dekker SC, et al. 2011. Impact of the Atlantic warm pool on precipitation and temperature in Florida during north Atlantic cold spells. Clim Dyn. 36(1–2):109–118. doi:10.1007/s00382-009-0702-9.

Donoghue J. 2011. Sea level history of the northern Gulf of Mexico coast and sea level rise scenarios for the near future. Clim Change. 107(1):17–33. doi:10.1007/s10584-011-0077-x.

Doyle LJ, Sparks TN. 1980. Sediments of the Mississippi, Alabama, and Florida (MAFLA) continental shelf. J Sediment Res. 50(3):905–915. doi:10.1306/212F7B1C-2B24-11D7-8648000102C1865D.

Doyle TW, Keeland BD, Gorham LE, Johnson DJ. 1995. Structural impact of Hurricane Andrew on the forested wetlands of the Atchafalaya Basin in south Louisiana. J Coast Res. Special issue 21: Impacts of Hurricane Andrew on the coastal zones of Florida and Louisiana. (Spring 1995):354–364.

Doyle TW, Girod GF, Books MA. 2003. Modeling mangrove forest migration along the southwest coast of Florida under climate change. In: Ning ZH, Turner RE, Doyle T, Abdollahi KK, eds. Preparing for a changing climate: potential consequences of climate variability and change–Gulf coast region. Baton Rouge (LA): Gulf Coast Climate Change Assessment Council (GCRCC). p. 211–222.

Doyle TW, Krauss KW, Conner WH, From AS. 2010. Redicting the retreat and migration of tidal forests long the northeren Gulf of Mexico under sea-level rise. For Ecol Manage. 259(4): 770–777. doi:10.1016/j.foreco.2009.10.023.

Doyle TW, Chivoiu B, Enwright NM. 2015. Sea-level rise modeling handbook: resource guide for coastal land managers, engineers, and scientists. Reston (VA): US Department of the Interior, US Geological Survey. 76 p. Report No.: US Geological Survey Professional Paper 1815. doi:10.3133/pp1815.

Dufrene TA, Bentley SJ, Allen YC. 2003. Geologic and geoscoustic study of surficial deposits, north-central Gulf of Mexico continental shelf. Trans Gulf Coast Assoc Geol Soc. 53:210–216.

Edmands JD, Brabander DJ, Coleman DS. 2001. Uptake and mobility of uranium in black oaks: Implications for biomonitoring depleted uranium-contaminated groundwater. Chemosphere. 44(4):789–795.

Faegri K, Iversen J. 1989. Textbook of pollen analysis. New York (NY): John Wiley & Sons.

Fisk HN. 1960. Recent Mississippi River sedimentation and peat accumulation. In: van der Waals, L ed. Quatrieme congress pour l'avancement des etudes de stratigraphic et de geologie du Carbonifere; Heerlen, the Netherlands. Mastriche (NL): Ernest van Aelst.

Flocks JG, Ferina NF, Kindinger JL. 2011. Recent geologic framework and geomorphology of the Mississippi-Alabama shelf, northern Gulf of Mexico. In: Buster NA, ed. Gulf of Mexico origin, waters, and biota: vol. 3, geology. College Station (TX): Texas A&M University Press. p. 157–174.

Flora of North America Editorial Committee. 1982. Flora of North America. Volume 2. Oxford (GB): Oxford University Press.

Fojutowski A, Wróblewska H, Komorowicz M, Kropacz A, Noskowiak A, et al. 2014. Changes in the properties of English oak wood (*Quercus robur L.*) as a result of remaining submerged in Baltic Sea waters for two years. Int Biodeter Biodegrad. 86:122–128. doi:10.1016/j.ibiod.2013.06.029.

Frohlich C, Hornbach MJ, Taylor FW, Shen C-C, Moala A, et al. 2009. Huge erratic boulders in Tonga deposited by a prehistoric tsunami. Geology. 37:131–134. doi:10.1130/G25277A.1.

Gangopadhyay T, Anderson LC, Jones MH, McBride RA. 1996. Mollusca and benthic foraminifera of the Pensacola Bay and Perdido Bay estuarine systems, Florida and Alabama. Gulf Coast Assoc Geol Soc Trans. 46:133–147.

Gardner WS, Seitzinger SP, Malczyk JM. 1991. The effects of sea salts on the forms of nitrogen released from estuarine and freshwater sediments: does ion pairing affect ammonium flux? Estuaries. 14(2):157–166. doi:10.2307/1351689.

Gonzalez S. 2017. Facies reconstruction and stratigraphy of a Late Pleistocene bald cypress forest discovered on the northern Gulf of Mexico continental shelf [thesis]. Baton Rouge (LA): Louisiana State University.

Gonzalez S, Bentley SJ Sr, DeLong KL, Xu K, Obelcz J, et al. 2017. Facies reconstruction of a Late Pleistocene cypress forest discovered on the northern Gulf of Mexico continental shelf. Gulf Coast Assoc Geol Soc Trans. 67:133–146.

Gonzalez S. 2018. 4719: Stratigraphic reconstruction of a late paleistocene bald cypress forest discovered on the northern Gulf of Mexico continenetal shelf [thesis]. Baton Rouge (LA): Louisiana State University.

Guérin G, Mercier N, Admiec G. 2011. Dose-rate conversion factors: update. Anc TL. 29(1): 5–8**.**

Grimm EC. 1991. Tilia and Tiliagraph [software]. Springfield (IL): Illinois State Museum.

Hautevelle Y, Michels R, Malartre F, Trouiller A. 2006. Vascular plant biomarkers as proxies for palaeoflora and palaeoclimatic changes at the dogger/malm transition of the paris basin (France). Org Geochem. 37(5):610–625.

Hays JD, Imbrie J, Shackleton NJ. 1976. Variations in the Earth's orbit: pacemaker of the ice ages. Science. 194(4270):1121–1132.

Heinrich H. 1988. Origin and consequences of cyclic ice rafting in the northeast Atlantic ocean during the past 130,000 years. Quat Res. 29(2):142–152.

Heiri O, Lotter AF, Lemcke G. 2001. Loss on ignition as a method for estimating organic and carbonate content in sediments: reproducibility and comparability of results. J Paleolimnol. 25(1):101–110. doi:10.1023/a:1008119611481.

Heitmuller FT, Hudson PF, Kesel RH. 2017. Overbank sedimentation from the historic A.D. 2011 flood along the lower Mississippi River, USA. Geology. 45(2):107–110. doi:10.1130/g38546.1.

Hiess J, Condon DJ, McLean N, Noble SR. 2012. $^{238}U/^{235}U$ systematics in terrestrial uranium-bearing minerals. Science. 335(6076):1610-1614. doi:10.1126/science.1215507.

Hook DD. 1984. Waterlogging tolerance of lowland tree species of the south. South J Appl For. 8(3):136–149. doi:10.1093/sjaf/8.3.136.

Huang B, Thorne PW, Banzon VF, Boyer T, Chepurin G, et al. 2017. Extended reconstructed sea surface temperature, version 5 (ERSSTv5): upgrades, validations, and intercomparisons. J Clim. 30(20):8179–8205. doi:10.1175/JCLI-D-16-0836.1.

Hülse P, Bentley SJ Sr. 2012. A ^{210}Pb sediment budget and granulometric record of sediment fluxes in a subarctic deltaic system: The Great Whale River, Canada. Estuarine Coast Shelf Sci. 109:41–52. doi:10.1016/j.ecss.2012.05.019.

Jaffey AH, Flynn KF, Glendenin LE, Bentley WC, Essling AM. 1971. Precision measurement of half-lives and specific activities of ^{235}U and ^{238}U. Phys Rev C: Nucl Phys. 4(5):1889–1906. doi:10.1103/PhysRevC.4.1889.

Javanshir K, Ewell K. 1993. Salt resistance of bald cypress. In: Lieth H, Al Masoom AA, eds. Towards the rational use of high salinity tolerant plants. Tasks for vegetation science. Dordrecht (NL): Springer. p. 285–291.

Johnson WC, Dixon MD, Scott ML, Rabbe L, Larson G, Volke M, Werner B. 2012. Forty years of vegetation change on the Missouri river floodplain. BioScience. 62(2):123–135. doi:10.1525/bio.2012.62.2.6.

Keen TR, Bentley SJ Sr, Chad Vaughan W, Blain CA. 2004. The generation and preservation of multiple hurricane beds in the northern Gulf of Mexico. Mar Geo. 210(1–4):79–105. doi:10.1016/j.margeo.2004.05.022.

Keim RF, Amos JB. 2012. Dendrochronological analysis of baldcypress (*Taxodium distichum*) responses to climate and contrasting flood regimes. Can J For Res. 42(3):423–436. doi:10.1139/x2012-001.

Kennedy HE Jr. 1972. Baldcypress (*Taxodium distichum*). Washington (DC): US Department of Agriculture Forest Service. 5 p. Publication No. FS-218.

Kindinger JL. 1988. Seismic stratigraphy of the Mississppi-Alabama shelf and upper continental slope. Mar Geo. 83(1–4):79–94.

Kindinger JL, Balson PS, Flocks JG. 1994. Stratigraphy of the Mississippi-Alabama shelf and the Mobile River inclised valley systems. In: Dalrymple RW, Boyd R, Zaitlin B, eds. Incised-valley systems: origin and sedimentary sequences. Special publication 51. Tulsa (OK): Society of Sedimentary Geology (SEPM). p. 83–95.

Kohl B, Fillon RH, Roberts HH. 2004. Foraminiferal biostratigraphy and paleoenvironments of the Pleistocene lagniappe delta and related section, northeastern Gulf of Mexico. In: Anderson JB,

Fillon RH, eds. Late Quaternary stratigraphic evolution of the northern Gulf of Mexico margin. Tulsa (OK): Society for Sedimentary Geology (SEPM). p. 189–216.

Krauss KW, Duberstein JA, Doyle TW, Conner WH, Day RH, et al. 2009. Site condition, structure, and growth of baldcypress along tidal/non-tidal salinity gradients. Wetlands. 29(2):505–519. doi:10.1672/08-77.1.

Landsea CW, Franklin JL. 2013. Atlantic hurricane database uncertainty and presentation of a new database format. Mon Weather Rev. 141(10):3576–3592. doi:10.1175/mwr-d-12-00254.1.

Lewin J, Ashworth PJ. 2014. The negative relief of large river floodplains. Earth Sci Rev. 129:1–23. doi:10.1016/j.earscirev.2013.10.014.

Lisiecki LE, Raymo ME. 2005. A pliocene-pleistocene stack of 57 globally distributed benthic $\delta^{18}O$ records. Paleoceanogr. 20(1):PA1003. doi:10.1029/2004PA001071.

Little EL. 1971. Atlas of United States trees. Volume 1. Conifers and important hardwoods. Washington (DC): US Deptartment of Agriculture, Forest Service. Publication No. 1146.

Lobo FJ, Ridente D. 2014. Stratigraphic architecture and spatio-temporal variability of high-frequency (Milankovitch) depositional cycles on modern continental margins: an overview. Mar Geol. 352:215–247. doi:10.1016/j.margeo.2013.10.009.

Loeblich AR, Tappan HN. 1988. Foraminiferal genera and their classification. New York (NY): Van Nostrand Reinhold.

Lofverstrom M, Caballero R, Nilsson J, Kleman J. 2014. Evolution of the large-scale atmospheric circulation in response to changing ice sheets over the last glacial cycle. Clim Past. 10(4):1453–1471. doi:10.5194/cp-10-1453-2014.

Lorrey AM, Boswijk G, Hogg A, Palmer JG, Turney CS, et al. 2018. The scientific value and potential of New Zealand swamp kauri. Quat Sci Rev. 183:124–139. doi:10.1016/j.quascirev.2017.12.019.

Love R, Milne GA, Tarasov L, Engelhart SE, Hijma MP, et al. 2016. The contribution of glacial isostatic adjustment to projections of sea-level change along the Atlantic and gulf coasts of North America. Earth's Future. 4(10):440–464.

Ma R, Bellis D, McLeod CW. 2000. Isotopic analysis of uranium in tree bark by ICP mass spectrometry: a strategy for assessment of airborne contamination. Anal Chem. 72(20):4878–4881. doi:10.1021/ac000545b.

Maksimov F, Kuznetsov V, Laukhin S, Kuksa K, Levchenko S, et al. 2015. Comparative $^{230}Th/U$ and ^{14}C dating of a buried stump layer (western Siberia). Geochronometria. 42(1):139–147. doi:10.1515/geochr-2015-0016.

Mars JC, Shultz AW, Schroeder WW. 1992. Stratigraphy and Holocene evolution of Mobile Bay in southwestern Alabama. Gulf Coast Assoc Geol Soc Trans. 42:529–542.

Mauz B, Packman S, Lang A. 2006. The alpha effectiveness in silt-sized quartz: new data obtained by single and multiple aliquot protocols. Anc TL. 24(2):47–52.

Mazzullo J, Peterson M. 1989. Sources and dispersal of Late Quaternary silt on the northern Gulf of Mexico continental shelf. Mar Geo. 86(1):15–26. doi:10.1016/0025-3227(89)90015-7.

McAndrews JH, Berti A, Norris J. 1973. Key to the Quaternary pollen and spores of the Great Lakes region. Royal Ontario Museum life Sci Miscellaneous Publication. Toronto (CA): University of Toronto Press.

McAndrews JH, King JE. 1976. Pollen of the North American Quaternary: the top twenty. Geosci Man [sic]. 15:41–49. doi:10.1080/00721395.1976.9989772.

McBride RA, Anderson LC, Tudoran A, Roberts HH. 1999. Holocene stratigraphic architecture of a sand-rich shelf and the origin of linear shoals; northeastern Gulf of Mexico. In: Bergman KM, Snedden JW, eds. Isolated shallow marine sand bodies: sequence stratigraphic analysis and sedimentologic interpretation. Society for Sedimentary Geology (SEPM) Special Publication. 64:95–126.

McBride RA, Byrnes MR, Anderson LC, Gupta BKS. 1996. Holocene and late Pleistocene sedimentary facies of a sand rich continental shelf: a standard section for the northeastern Gulf of Mexico. Gulf Coast Assoc Geol Soc Trans. 46:287–299.

McBride RA, Byrnes MR. 1995. Surficial sediments and morphology of the southwestern Alabama western Florida panhandle coast and shelf. Gulf Coast Assoc Geol Soc Trans. 45:392–404.

Mejdahl V. 1979. Thermoluminescence dating: beta-dose attenuation in quartz grains. Archaeometry. 21:61–72. doi:10.1111/j.1475-4754.1979.tb00241.x.

Middleton BA, McKee KL. 2004. Use of a latitudinal gradient in bald cypress (*Taxodium distichum*) production to examine physiological controls of biotic boundaries and potential responses to environmental change. Glob Ecol Biogeogr. 13(3):247–258. doi:10.1111/j.1466-822X.2004.00088.x.

Middleton BA. 2016. Differences in impacts of Hurricane Sandy on freshwater swamps on the Delmarva Peninsula, Mid-Atlantic coast, USA. Ecol Eng. 87:62–70. doi:10.1016/j.ecoleng.2015.11.035.

Mobley ML, Richter Dd, Heine PR. 2013. Accumulation and decay of woody detritus in a humid subtropical secondary pine forest. Can J For Res. 43(2):109–118. doi:10.1139/cjfr-2012-0222.

Montero-Serrano JC, Bout-Roumazeilles V, Carlson AE, Tribovillard N, Bory A, et al. 2011. Contrasting rainfall patterns over North America during the Holocene and last interglacial as recorded by sediments of the northern Gulf of Mexico. Geophys Res Lett. 38(14):L14709. doi:10.1029/2011GL048194.

Murray JW. 1991. Ecology and palaeoecology of benthic foraminifera. London (GB): Routledge. doi:10.4324/9781315846101.

Murray AS, Wintle AG. 2003. The single aliquot regenerative dose protocol: potential for improvements in reliability. Radiat Meas. 37(4–5):377–381. doi:10.1016/S1350-4487(03)00053-2.

North American Commission on Stratigraphic Nomenclature. 2005. North American stratigraphic code: Am Assoc Petrol Geol Bull. 89:1547–1591, doi:10.1306/07050504129

Nürnberg D, Ziegler M, Karas C, Tiedemann R, Schmidt M. 2008. Interacting loop current variability and Mississippi river discharge over the past 400 kyr. Earth Planet Sci Lett. 272(1–2):278–289. doi:10.1016/j.epsl.2008.04.051.

Obelcz JB. 2017. 4293: Sediment transport and slope stability in the northern Gulf of Mexico [dissertation]. Baton Rouge (LA): Louisiana State University.

Osterman LE, Smith CG. 2012. Over 100 years of environmental change recorded by foraminifers and sediments in Mobile bay, Alabama, Gulf of Mexico, USA. Estuarine Coast Shelf Sci. 115:345–358.

Osterman LE, Poore RZ, Swarzenski PW, Senn DB, DiMarco SF. 2009. The 20th-century development and expansion of Louisiana shelf hypoxia, Gulf of Mexico. Geo-Mar Lett. 29(6):405–414. doi:10.1007/s00367-009-0158-2.

Otvos EG. 1985. Coastal evolution - Louisiana to northwest Florida: guidebook, American Association of Petroleum Geologists annual meeting, New Orleans, Louisiana field trip, 27–29 March 1995. Goldthwaite D, Wiltenmuth KS, eds. New Orleans (LA): New Orleans Geological Society.

Pearson CE, Kelley DB, Weinstein RA, Gagliano SM (Coastal Environments, Inc., Metairie, LA). 1986. Archaeological investigations on the outer continental shelf; a study within the sabine river valley, offshore Louisiana and Texas. New Orleans (LA): US Department of the Interior, Minerals Management Service.

Pezeshki SR, DeLaune RD, Patrick WH Jr. 1990. Flooding and saltwater intrusion: potential effects on survival and productivity of wetland forests along the US Gulf Coast. Forest Ecol Manage. 33–34:287–301. doi:10.1016/0378-1127(90)90199-L.

Phleger FB, Parker FL. 1951. Ecology of Foraminifera, northwest Gulf of Mexico: part II. Foraminifera species. New York (NY): Geological Society of America.

Plets RMK, Dix JK, Adams JR, Bull JM, Henstock TJ, et al. 2009. The use of a high-resolution 3D CHIRP sub-bottom profiler for the reconstruction of the shallow water archaeological site of the Grace Dieu (1439), River Hamble, UK. J Archaeol Sci. 36(2):408–418. doi:10.1016/j.jas.2008.09.026.

Poag CW. 2015. Benthic foraminifera of the Gulf of Mexico. Distribution, ecology, paleoecology. College Station (TX): Texas A&M University Press.

Puckett TM. 1992. Distribution and ecology of foraminifera from Mobile Bay, Mississippi Sound, and costal Alabama. Geological Survey of Alabama Circular 166. Tuscaloosa (AL): Geological Survey of Alabama. 35 p.

Ramil-Rego P, Muñoz-Sobrino C, Rodríguez-Guitián M, Gómez-Orellana L. 1998. Differences in the vegetation of the north Iberian peninsula during the last 16,000 years. Plant Ecol. 138(1):41–62. doi:10.1023/A:1009736432739.

Rayner NA, Parker DE, Horton EB, Folland CK, Alexander LV, et al. 2003. Global analyses of sea surface temperature, sea ice, and night marine air temperature since the late nineteenth century. J Geophys Res. 108(D14). doi:10.1029/2002JD002670.

Reese CA, Harley GL, DeLong KL, Bentley SJ Sr, Xu K, et al. 2018. Stratigraphic pollen analysis performed on a Late Pleistocene cypress forest preserved on the northern Gulf of Mexico continental shelf. J Quat Sci. 33(8):865–870. doi:10.1002/jqs.3074.

Reese CA, Liu K-B. 2001. Late-Holocene vegetation changes at Bluff Swamp, Louisiana. Southeast Geogr. 41(1):20–35. doi:10.1353/sgo.2001.0022.

Reimer PJ, Bard E, Bayliss A, Beck JW, Blackwell PG, , et al. 2013. Intcal13 and marine13 radiocarbon age calibration curves 0–50,000 years cal BP. Radiocarbon. 55(4):1869–1887. doi:10.2458/azu_js_rc.55.16947.

Research Planning Inc., Tidewater Atlantic Research, Inc., WF Baird & Associates Ltd. 2004. Archaeological damage from offshore dredging: recommendations for pre-operational surveys and mitigation during dredging to avoid adverse impacts. Herndon (VA): US Department of Interior, Minerals Management Service. 98 p. Contract No.: 01-02-CT-85139. Report No.: MMS 2004-005.

Rhodes EJ. 2011. Optically stimulated luminescence dating of sediments over the past 200,000 years. Annu Rev Earth Planet Sci. 39:461–488. doi:10.1146/annurev-earth-040610-133425.

Roberts HH, Walker N, Cunningham R, Kemp GP, Majersky S. 1997. Evolution of sedimentary architecture and surface morphology: Atchafalaya and Wax Lake deltas, Louisiana (1973–1994). Gulf Coast Assoc Geol Soc Trans. 47:477–484.

Ross MS, O'Brien JJ, Sternberg LdSL. 1994. Sea-level rise and the reduction in pine forests in the Florida Keys. Ecol Soc Am. 4(1):144–156. doi:10.2307/1942124.

Rutter NW, Rokosh D, Evans ME, Little EC, Chlachula J, et al. 2017. Correlation and interpretation of paleosols and loess across European Russia and Asia over the last interglacial–glacial cycle. Quat Res. 60:101–109. doi:10.1016/S0033-5894(03)00069-3.

Saha AK, Saha S, Sadle J, Jiang J, Ross MS, et al. 2011. Sea level rise and south Florida coastal forests. Clim Change. 107(1–2):81–108. doi:10.1007/s10584-011-0082-0.

Sanford JM, Harrison AS, Wiese DS, Flocks JG. 2016. Archive of digitized analog boomer seismic reflection data collected from the Mississippi-Alabama-Florida Shelf during cruises onboard the R/V *Kit Jones*, June 1990 and July 1991. US Geological Survey Data Series 429. Washington (DC): US Geological Survey.

Schafale MP. 2009. Atlantic coastal plain blackwater levee/bar forest. Washington (DC): United States National Vegetation Classification. Federal Geographic Data Committee.

Schmidt N, Lipp EK, Rose JB, Luther ME. 2001. ENSO influences on seasonal rainfall and river discharge in Florida. J Clim. 14(4):615–628. doi:10.1175/1520-0442(2001)014<0615:EIOSRA>2.0.CO;2.

Schongart J, Orthmann B, Hennenberg KJ, Porembski S, Worbes M. 2006. Climate-growth relationships of tropical tree species in west Africa and their potential for climate reconstruction. Global Change Biol. 12(7):1139–1150.

Schumm SA. 2005. River variability and complexity. New York (NY): Cambridge University Press.

Schwab WC, Baldwin WE, Denny JF, Hapke CJ, Gayes PT, List JH, Warner JC. 2014. Modification of the Quaternary stratigraphic framework of the inner-continental shelf by Holocene marine transgression: an example offshore of fire island, New York. Mar Geol. 355:346–360. doi:10.1016/j.margeo.2014.06.011.

Scott DB, Medioli FS, Schafer CT. 2001. Monitoring in coastal environments using foraminifera and thecamoebian indicators. Cambridge (GB) : Cambridge University Press.

Shaw J, Courtney RC. 1997. Multibeam bathymetry of glaciated terrain off southwest Newfoundland. Mar Geol. 143:125–135. doi:10.1016/S0025-3227(97)00093-5.

Shen C-C, Cheng H, Edwards RL, Moran SB, Edmonds HN, et al. 2003. Measurement of attogram quantities of ^{231}Pa in dissolved and particulate fractions of seawater by isotope dilution thermal ionization mass spectroscopy. Anal Chem. 75(5):1075–1079. doi:10.1021/ac026247r.

Shen C-C, Li K-S, Sieh K, Natawidjaja D, Cheng H, et al. 2008. Variation of initial ^{230}Th/^{232}Th and limits of high precision U–Th dating of shallow-water corals. Geochim Cosmochim Acta. 72(17):4201–4223. doi:10.1016/j.gca.2008.06.011.

Shen C-C, Wu C-C, Cheng H, Edwards RL, Hsieh Y-T, , et al. 2012. High-precision and high-resolution carbonate ^{230}Th dating by MC-ICP-MS with SEM protocols. Geochim Cosmochim Acta. 99(0):7186. doi:10.1016/j.gca.2012.09.018.

Shen Z, Tornqvist TE, Autin WJ, Mateo ZRP, Straub KM, et al. 2012. Rapid and widespread response of the lower Mississippi River to eustatic forcing during the last glacial-interglacial cycle. Geol Soc Am Bull. 124:690–704. doi:10.1130/B30449.1.

Shen Z, Törnqvist TE, Mauz B, Chamberlain EL, Nijhuis AG, et al. 2015. Episodic overbank deposition as a dominant mechanism of floodplain and delta-plain aggradation. Geology. 43(10):875–878. doi:10.1130/G36847.1.

Siddall M, Rohling EJ, Almogi-Labin A, Hemleben C, Meischner D, et al. 2003. Sea-level fluctuations during the last glacial cycle. Nature. 423:853–858. doi:10.1038/nature01690.

Smith M, Bentley SJ Sr. 2015. Sediment capture in flood plains of the Mississippi River: a case study in Cat Island National Wildlife Refuge, Louisiana. In: Xu, YJ, Allison MA, Bentley SJ, Collins AL, Erskine WD, et al., eds. Sediment Dynamics from the Summit to the Sea. International Symposium on Sediment Dynamics. International Commission on Continental Erosion 2014, IAHS [International Association of Hydrological Sciences]; New Orleans, Louisiana; 11–14 December. Oxfordshire (UK): IAHS Press. IAHS Publication 367. p. 442–446. doi:10.5194/piahs-367-442-2015

Speer JH. 2010. Fundamentals of tree-ring research. Tucson (AZ): University of Arizona Press.

Stahle DW, Cleaveland MK, Blanton DB, Therrell MD, Gay DA. 1998. The lost colony and Jamestown droughts. Science. 280(5363): 64–567. doi:10.1126/science.280.5363.564.

Stahle DW, Burnette DJ, Villanueva J, Cerano J, Fye FK, et al. 2012. Tree-ring analysis of ancient baldcypress trees and subfossil wood. Quat Sci Rev. 34:1–15. doi:10.1016/j.quascirev.2011.11.005.

Stahle DW, Edmondson JR, Howard IM, Robbins CR, Griffin RD, et al. 2019. Longevity, climate sensitivity, and conservation status of wetland trees at Black River, North Carolina. Environ Res Commun. 1(4):041002. doi:10.1088/2515-7620/ab0c4a.

Stockmarr J. 1971. Tablets with spores used in absolute pollen analysis. Pollen et Spores. 13:615–621.

Stokes MA, Smiley TL. 1968. An introduction to tree-ring dating. Tucson (AZ): University of Arizona Press.

Stoll P, Weiner J, Schmid B. 1994. Growth variation in a naturally established population of pinus sylvestris. Ecology. 75(3):660–670. doi:10.2307/1941724.

Stuiver M, Polach HA. 1977. Reporting of C-14 data. Radiocarbon. 19(3):355–363.

Swenson JB, Muto T. 2007. Response of coastal plain rivers to falling relative sea-level: allogenic controls on the aggradational phase. Sedimentology. 54(1):207–221.

Sydow J, Roberts HH. 1994. Stratigraphic framework of a Late Pleistocene shelf-edge delta, northeast Gulf of Mexico. Am Assoc Pet Geol Bull. 78(8):1276–1312.

Szumigalski AR, Bayley SE. 1996. Decomposition along a bog to rich fen gradient in central Alberta, Canada. Can J Bot. 74(4):573–581. doi:10.1139/b96-073.

Teague WJ, Jarosz E, Keen TR, Wang DW, Hulbert MS. 2006. Bottom scour observed under Hurricane Ivan. Geophysical Research Letters. 33(7):L07607. doi:10.1029/2005GL025281.

The Underwater Forest [Documentary Film]. This is Alabama. Alabama Media Group. 2017 June 23, 27:27 minutes. [accessed 2017 June 23]. https://www.youtube.com/watch?v=PKm0eRfFFfo

Thomas BL, Doyle T, Krauss K. 2015. Annual growth patterns of baldcypress (*Taxodium distichum*) along salinity gradients. Wetlands. 35:831. doi:10.1007/s13157-015-0659-x.

Torrence C, Compo GP. 1998. A practical guide to wavelet analysis. Bull Am Meteorol Soc. 79(1):61–78. doi:10.1175/1520-0477(1998)079<0061:APGTWA>2.0.CO;2

Truong, J. 2018. Micropaleontological record of a preserved, Late Pleistocene bald cypress forest on the Northern Gulf of Mexico Inner Shelf [thesis]. Baton Rouge (LA): Louisiana State University.

Twichell D, Kelso K, Pendleton E. 2012. Evidence for mid-Holocene shift in depositional style in Mobile bay, Alabama. Report No. 01961497. Reston (VA): US Geological Survey.

van Heteren S, Meekes JAC, Bakker MAJ, Gaffney V, Fitch S, et al. 2014. Reconstructing North Sea palaeolandscapes from 3D and high-density 2D seismic data: an overview. Neth J Geosci. 93(1–2):31–42.

Van Wagoner JC, Posamentier HW, Mitchum RM, Vail PR, Sarg JF, Loutit TS, Hardenbol J. 1988. An overview of the fundamentals of sequence stratigraphy and key definitions In: Wilgus CK, Hastings BS, Posamentier H, Wagoner JV, Ross CA, et al, eds. Sea-level changes: An integrated approach. SEPM Special Publication 42. Tulsa (OK): SEPM Society for Sedimentary Geology.

Waelbroeck C, Labeyrie L, Michel E, Duplessy JC, McManus JF, et al. 2002. Sea-level and deep water temperature changes derived from benthic foraminifera isotopic records. Quat Sci Rev. 21(1–3):295–305. doi:10.1016/S0277-3791(01)00101-9.

Wang DW, Mitchell DA, Teague WJ, Jarosz E, Hulbert MS. 2005. Extreme waves under Hurricane Ivan. Science. 309(5736):896–896. doi:10.1126/science.1112509.

Watson, FD. 1985. The nomenclature of pondcypress and baldcypress (Taxodiaceae). Taxon. 34(3): 506-509.

Webb T III, Anderson KH, Bartlein PJ, Webb RS. 1998. Late quaternary climate change in eastern north america: a comparison of pollen-derived estimates with climate model results. Quat Sci Rev. 17(6–7):587–606. doi:10.1016/S0277-3791(98)00013-4.

Wheeler BD, Proctor MCF. 2000. Ecological gradients, subdivisions and terminology of north-west European mires. J Ecol. 88(2):187–203. doi:10.2307/2648523.

Wilhite LP, Toliver JR. 1990. Baldcypress. In: Burns RM, Honkala BH, eds. Silvics of North America: volume 1 conifers. Washington (DC): US Department of Agriculture, Forest Service. 683 p.

Williams K, Ewel KC, Stumpf RP, Putz FE, Workman TW. 1999. Sea-level rise and coastal forest retreat on the west coast of Florida, USA. Ecology. 80(6):2045–2063. doi:10.1890/0012-9658(1999)080[2045:SLRACF]2.0.CO;2.

Williams K, MacDonald M, McPherson K, Mirti TH. 2003. Interactions of storm, drought, and sea-level rise on coastal forest: a case study. J Coast Res. 19(4):1116–1121.

Williams K, MacDonald M, McPherson K, Mirti TH. 2007. Ecology of the coastal edge of hydric hammocks on the gulf coast of Florida. In: Conner WH, Doyle TW, Krauss KW, eds. Ecology of tidal freshwater forested wetlands of the southeastern United States. Dordrecht (NL): Springer. p. 255–289.

Witrock RB, Nixon LD, Post PJ, Ross KM. 2003. Biostratigraphic chart of the Gulf of Mexico offshore region, Jurassic to Quaternary. New Orleans (LA): US Department of the Interior, Bureau of Ocean Energy Management, Regulation and Enforcement.

Ziegler M, Nürnberg D, Karas C, Tiedemann R, Lourens LJ. 2008. Persistent summer expansion of the Atlantic warm pool during glacial abrupt cold events. Nat Geosci. 1(9):601–605.

Appendix A: Full foraminiferal counts from core 15DF1

Depth (m)	0.40	1.20	2.00	2.75	3.10	3.20	3.30	3.35	3.40	3.45
Soritids and Peneroplids	Present	Present	Present	Present	Present	Present	0	0	0	0
Quinqueloculina spp.	43	36	43	36	33	28	37	0	0	0
Other Miliolids	11	12	11	8	22	8	4	0	0	0
Rosalina spp.	83	83	60	67	103	63	70	0	0	0
Hanzawaia concentrica	41	47	43	39	27	64	30	0	0	0
Asterigerina carinata	21	13	39	27	15	18	23	0	0	0
Cibicidoides spp.	33	37	33	29	18	27	24	0	0	0
Nonionella spp.	11	10	11	11	19	7	16	0	0	0
Guttulina sp.	3	2	2	8	6	5	4	0	0	0
Bulimina spp.	1	0	2	2	13	1	2	0	0	0
Reussella atlantica	1	0	1	4	0	1	1	0	0	0
Buccella hannai	4	4	3	6	4	6	9	0	0	0
Haynesina germanica	6	10	1	3	1	3	3	0	0	0
Elphidium spp.	33	28	47	43	39	49	56	0	0	0
Ammonia parkinsoniana	3	6	5	6	4	5	5	0	0	0
Indeterminate	1	6	3	3	3	5	2	0	0	0
Textulariida	3	4	4	6	4	6	5	0	0	0
Planktonic	0	0	1	4	12	4	9	0	0	0
Planulina sp.	0	1	0	1	0	0	0	0	0	0
Fursenkoina sp.	0	1	0	0	1	0	0	0	0	0
Bolivina sp.	0	0	0	0	0	0	0	0	0	0
Oolina sp.	0	0	0	1	0	1	0	0	0	0
Cassidulina sp.	0	0	0	0	0	0	0	0	0	0
Eponides sp.	0	1	0	0	0	0	0	0	0	0
Amphistegina gibbosa	0	0	1	0	0	0	0	0	0	0

Depth (m)	0.40	1.20	2.00	2.75	3.10	3.20	3.30	3.35	3.40	3.45
Virgulina sp.	0	0	1	0	0	0	0	0	0	0
Islandiella sp.	1	0	0	0	0	0	0	0	0	0
Uvigerina sp.	0	0	2	1	0	0	0	0	0	0
Total	300	302	314	306	325	302	300	0	0	0
Abundance (individuals/g)	134.35	136.47	138.39	284.92	1625.00	144.15	185.30	0.00	0.00	0.00
Depth (m)	3.50	3.55	3.60	3.65	3.70	3.75	3.80	3.85	3.90	4.00
Soritids and Peneroplids	0	0	0	0	0	0	0	0	0	0
Quinqueloculina spp.	0	0	4	0	0	0	1	0	0	0
Other Miliolids	0	0	2	0	0	0	0	0	0	0
Rosalina spp.	0	0	73	0	0	0	61	0	0	0
Hanzawaia concentrica	0	0	39	0	0	0	58	0	0	0
Asterigerina carinata	0	0	34	0	0	0	21	0	0	0
Cibicidoides spp.	0	0	41	0	0	0	26	0	0	0
Nonionella spp.	0	0	13	0	0	0	11	0	0	0
Guttulina sp.	0	0	5	0	0	0	4	0	0	0
Bulimina spp.	0	0	2	0	0	0	1	0	0	0
Reussella atlantica	0	0	2	0	0	0	3	0	0	0
Buccella hannai	0	0	4	0	0	0	9	0	0	0
Haynesina germanica	0	0	0	0	0	0	0	0	0	0
Elphidium spp.	0	0	55	0	0	0	41	0	0	0
Ammonia parkinsoniana	0	0	10	0	0	0	11	0	0	0
Indeterminate	0	0	2	0	0	0	3	0	0	0
Textulariida	0	0	5	0	0	0	0	0	0	2
Planktonic	0	0	7	0	0	0	5	0	0	0
Planulina sp.	0	0	0	0	0	0	0	0	0	0
Fursenkoina sp.	0	0	0	0	0	0	1	0	0	0
Bolivina sp.	0	0	0	0	0	0	0	0	0	0
Oolina sp.	1	0	1	0	0	0	0	0	0	0
Cassidulina sp.	0	0	1	0	0	0	0	0	0	0

Depth (m)	0.40	1.20	2.00	2.75	3.10	3.20	3.30	3.35	3.40	3.45
Eponides sp.	0	0	0	0	0	0	0	0	0	0
Amphistegina gibbosa	0	0	0	0	0	0	0	0	0	0
Virgulina sp.	0	0	0	0	0	0	0	0	0	0
Islandiella sp.	0	0	0	0	0	0	0	0	0	0
Uvigerina sp.	0	0	0	0	0	0	0	0	0	0
Total	1	0	300	0	0	0	256	0	0	2
Abundance (individuals/g)	0.70	0.00	73.10	0.00	0.00	0.00	44.82	0.00	0.00	3.05

Department of the Interior (DOI)

The Department of the Interior protects and manages the Nation's natural resources and cultural heritage; provides scientific and other information about those resources; and honors the Nation’s trust responsibilities or special commitments to American Indians, Alaska Natives, and affiliated island communities.

BOEM
Bureau of Ocean Energy Management

Bureau of Ocean Energy Management (BOEM)

The mission of the Bureau of Ocean Energy Management is to manage development of U.S. Outer Continental Shelf energy and mineral resources in an environmentally and economically responsible way.

BOEM Environmental Studies Program

The mission of the Environmental Studies Program is to provide the information needed to predict, assess, and manage impacts from offshore energy and marine mineral exploration, development, and production activities on human, marine, and coastal environments. The proposal, selection, research, review, collaboration, production, and dissemination of each of BOEM’s Environmental Studies follows the DOI Code of Scientific and Scholarly Conduct, in support of a culture of scientific and professional integrity, as set out in the DOI Departmental Manual (305 DM 3).